Unfolding and Aggregation of Monoclonal Antibodies during Cation Exchange Chromatography

---

A Dissertation

Presented to

the faculty of the School of Engineering and Applied Science

University of Virginia

---

in partial fulfillment

of the requirements for the degree

Doctor of Philosophy

by

Jing Guo

December

2016

APPROVAL SHEET

The dissertation

is submitted in partial fulfillment of the requirements

for the degree of

Doctor of Philosophy

AUTHOR

The dissertation has been read and approved by the examining committee:

Giorgio Carta

Advisor

Kyle Lampe

Geoffrey Geise

Gaurav Giri

Jill Venton

Accepted for the School of Engineering and Applied Science:

Craig H. Benson, Dean, School of Engineering and Applied Science

December

2016

Abstract

This work elucidates the molecular interactions that are responsible for protein unfolding and aggregation on the surface of certain cation exchanger resins. The chromatographic behavior of a monoclonal antibody (mAb) that exhibits a two-peak elution behavior is studied for a range of strong cation exchange resins and with varying load buffer pH and composition. The two-peak elution behavior is very pronounced for the tentacle and polymer-grafted resins, but is essentially absent for hydrophilic macroporous resins. Confocal Laser Scanning Microscopy (CLSM) shows that this behavior is related to the unique kinetics of protein binding in the tentacle-type resin Fractogel. Hydrogen-Deuterium Exchange Mass Spectrometry (HXMS) proves that the two-peak elution behavior is tied to conformational changes that occur when the mAb binds. Circular dichroism suggests that the propensity of different mAbs to form stabilizing intermolecular structures can be related to their chromatographic behaviors. Another mAb exhibiting a three-peak elution behavior on the CEX resin POROS XS was also investigated. Dynamic Light Scattering (DLS) shows that the third peak contains significant levels of aggregates formed in the column that only slowly revert to monomeric species after elution. Circular dichroism and HXMS analyses of the eluted fraction, in-line fluorescence detection, and bound-state HXMS analysis indicate that the aggregates are generated by a destabilized, unfolded intermediate that is slowly formed on the resin. The two early eluting peaks observed regardless of hold time are shown to comprise exclusively monomeric species and form as a result of the presence of weak and strong binding sites on the resin having, respectively, fast and slow binding kinetics. This work has important practical implications in downstream processing for the industrial production of biopharmaceuticals as well as broad scientific value from a biomolecular perspective.

Acknowledgements

I would like to give my deepest gratitude to my academic advisor, Professor Giorgio Carta, for his guidance and support during my PhD study. I will never forget the many hours we spent together discussing my research results, drawing sketches of protein aggregation mechanisms, and fixing all sorts of experimental equipment.

I would also like to thank my advisory committee members: Professor Kyle Lampe, Professor Geoffrey Geise, Professor Gaurav Giri and Professor Jill Venton for their valuable inputs and inspiring discussions.

I would like to also give my special thanks to Professor Erik Fernandez, who was my advisor at the beginning of my PhD study. He initiated my PhD project, stimulated my interest in research and set a good example for me as a researcher and lecturer. I also want to thank Professor John O'Connell, who gave me valuable suggestions in the starting period of my project.

I would also like to thank all the former and current graduate students from Fernandez and Carta lab, especially Joe Costanzo, Yige Wu, Shaojie Zhang, Joe Basconi, Mimi Zhu, Arch Creasy, Jason Reck, Yiran Wang, Andreas Alberti and Preston Fuks, for their help and companion. I want to give a special acknowledgment to Adrian Gospodarek, who spent so much time and effort teaching me how to use the Mass Spectrometer.

I also appreciate the help from Vickie, Teresa, Jennifer and Ricky, for smoothing things out in registration, purchasing, and moving the lab instruments.

Finally, I want to thank my parents for their continuous love. Although you were far away in China during the five years of my PhD study, I have shared all the good and bad moments with you and have continuously received your encouragement and support.

Table of contents

List of Figures

List of Tables

List of Symbols

N_m	Number of monomer units in the aggregates
r_h	Hydrodynamic radius (nm)
q_m	Maximum adsorption capacity in Langmuir model (mg/mL)
q	Adsorbed protein concentration (mg/mL)
C	Protein solution concentration (mg/mL)
K	Adsorption constant in Langmuir model (mL/mg)
D_0	Free solution diffusivity (cm^2/s)
D_e	Effective diffusivity (cm^2/s)
ρ_s	Normalized position of the adsorption front in the particle
r_p	Resin particle radius (μm)
$\overline{q}$	Average adsorbed protein concentration (mg/mL)
$C^E_{Na^+}$	Na^+ concentration at peak maximum (mM)
z	Effective protein binding charge
A	Equilibrium constant in the mass action law model ($(mM)^z$)
k	Binding rate constant (s^{-1})
ε	Extra-particle porosity

ε_p	Intra-particle porosity

Chapter 1

Motivations and Background

Monoclonal antibodies (mAbs) have gained widespread recognition as biopharmaceuticals as a result of their safety, efficacy, and consistent quality [1]. Although mAbs are generally more stable compared to other proteins, they can still undergo a variety of chemical and physical transformations both within the bioreactor and during downstream processing, including deamination, oxidation, fragmentation and unfolding [2]. The latter is a special concern as unfolding is often a key precursor to aggregation, which has been recognized as a major potential safety concern and as a critical factor in the storage stability of mAb formulations ([3][4]). As a result, understanding the factors that control the stability or lack thereof of mAbs during downstream processes is an important concern [5].

Ion-exchange chromatography (IEX) plays a major role in mAb purification. Although initial capture is most commonly carried out with high selective protein A-based adsorbents, increasing product titers and a desire to reduce costs are stimulating increasing interest in using IEX and, particularly, cation exchange chromatography (CEX) as an alternative for capture. Although the selectivity is lower, the protein binding capacity and chemical stability of CEX resins are much higher compared to that of protein A adsorbents resulting in more manageable column sizes and lower costs [6]. Additionally, unlike protein A adsorbents, CEX affords the ability to separate charge variants and other isoforms and to resolve soluble aggregates from monomeric species [7].

An important advantage often attributed to CEX resins is that they tend not to significantly affect protein conformation [8]. In contrast, quite different results are generally obtained for adsorbents that rely on hydrophobic interactions such as reverse phase (RPC) and hydrophobic interaction chromatography (HIC) resins. In this case, interaction with hydrophobic residues has been shown to cause unfolding leading to the appearance of multiple elution peaks in step or gradient elution processes. Karger and Blanco [9], for example, demonstrated that protein-surface interactions were responsible for conformational changes of β-lactoglobulin A, which resulted in multiple peaks during gradient elution from an HIC column. McNay and Fernandez [10] demonstrated, using hydrogen-exchange NMR, that hen egg white lysozyme (HEWL) unfolds on RPC surfaces. Jungbauer et al. [11] showed that resin-induced unfolding results in a larger hydrophobic surface area, which, in turn, facilitates stronger binding, suggesting that binding and unfolding are inherently connected in these systems. Several models have also been proposed to describe protein adsorption and unfolding on HIC resins. For instance, Xiao et al. [12] proposed a four state model where native and unfolded species can adsorb to and desorb from the surface. Muca et al. [13] and Marek et al. [14] used a three-state model to describe a band splitting behavior of model proteins on HIC resin Butyl Sepharose 4FF. Accordingly, they postulated the existence of an unfolded species on the surface of the HIC resin that is strongly bound and elutes only at low concentration of kosmotrope. More recently, molecular simulation has been used to predict protein unfolding on hydrophobic chromatography surfaces. Zhang et al. [15], for instance, predicted, using molecular dynamic simulation, conformational transitions of a 46-bead β-barrel model protein on a hydrophobic charge induction chromatography resin. Their simulation showed that strong hydrophobic interaction strengthened adsorption, but caused protein unfolding. On the other hand, weak hydrophobic

interactions were able to maintain native protein conformation, while still resulting in relatively strong binding.

Although, as noted earlier, IEX is inherently less likely to cause unfolding, a few recent studies suggest that protein conformational changes can also occur as a result of protein-surface interactions on these resins. Even though the underlying mechanisms are likely to be quite different from those involved in hydrophobic adsorption, their empirical manifestations are analogous, in some cases, to those observed for hydrophobic adsorption, including the appearance of multiple peaks during elution and the on-column formation of aggregates. Voitl el al. [16], for example, reported a two-peak behavior when pure human serum albumin was loaded and then eluted from the two strong CEX resins Fractogel EMD SO3- and Fractogel EMD SE Hicap. Since the same species was found in both early and late eluting peaks, these authors hypothesized that the transition from one orientation of the protein relative to the chromatography surface to another resulted in two different binding states that required different salt concentrations for elution.

Gillespie el al. [17] showed that a two-peak elution behavior could also be observed with CEX resins, including Fractogel EMD SO3-, when an aglycosylated IgG1 antibody was loaded on the column and then eluted with a salt gradient. However, unlike the results of Voitl et al. [16], in this case while the early eluting peak was comprised of monomer only, the late eluting peak was a mixture of monomer and aggregated species. Using hydrogen-deuterium exchange and Fourier transform infrared spectroscopy (FTIR), Gillespie et al. showed that conformational changes resulting in greater exposure of the protein to the solvent occurred during the binding step. These changes, characteristic of an unfolding behavior, resulted in the formation of the late-

eluting, strongly bound aggregated species together with a fraction of co-eluting monomeric species.

Although glycosylated mAbs are expected to be more stable than their aglycosylated counterparts [2], recent work has shown that conformational changes upon binding to CEX resins can also occur for these molecules. Luo and co-workers [18][19] showed the occurrence of distinct two-peak elution behaviors for two different glycosylated mAbs. For the first of these mAbs [18], the two-peak elution behavior occurred on both strong and weak CEX resins and was attributed to a resin-induced reversible self-association which resulted in aggregate formation. For the second mAb [19], no aggregates were formed in the column and the two-peak elution behavior was attributed to the slow protonation of a histidine residue, which, in turn, resulted in un-protonated and protonated forms with different binding strength on the CEX surface.

In a recent study, Marek et al. [20] considered the isolation of a mAb from cell culture supernatant using a process that integrates HIC and CEX. These authors noted that, dependent on conditions, a fraction of the loaded mAb could not be desorbed from the CEX column. Recovery was strongly affected by pH, salt type and concentration, and by the duration of the adsorption period and attributed these effects to the formation of a hypothesized unfolded mAb species formed on the chromatographic surface. A three-state model, comprising the native protein in solution, the bound native protein, and a more strongly bound unfolded species, was used by these authors to describe incomplete recovery of the mAb. The model provided accurate description of the mAb elution behavior using equilibrium and rate parameters obtained by data fitting for the inter-conversion of the protein between the three states.

The overall goal for this project is to understand unfolding and aggregation mechanisms of mAbs on various CEX resins. Chapter 2 will explore the elution behavior of a pure glycosylated antibody on the CEX resin Fractogel EMD SO3-, including characterizing the nature of the aggregates and investigating a connection between unfolding/aggregation behavior and the tentacle architecture of the Fractogel resin. Chapter 3 will seek a molecular level understanding of the unfolding/aggregation behavior using hydrogen-deuterium exchange mass spectrometry (HX-MS) to determine peptide-level conformational changes caused by binding and/or elution on the Fractogel resin. Chapter 4 will expand the previous studies into a broader range of CEX resins with different types of surface extenders and different pores sizes, and will determine whether a correlation exists between the intrinsic stability of the protein and protein unfolding/aggregation behavior on CEX columns using two additional mAbs as model systems. Chapter 5 will investigate the three-peak elution behavior of a fourth mAb on the CEX resin POROS XS including using a number of biophysical measurements to characterize the system and elucidate the molecular mechanisms and protein-surface interactions that are responsible for this complex elution behavior.

Chapter 2

Chromatography elution and batch adsorption behavior

2.1. Introduction

This chapter has three principal objectives. The first is to explore the elution behavior of a pure glycosylated antibody on the CEX resin Fractogel EMD SO3- in a direct follow-up to the study of Gillespie et al. [17]. Glycosylation is expected to improve stability of the mAb ([21][22]). Since many commercially relevant mAbs are glycosylated, it is important to determine if on-column aggregation is also observed for these proteins and under what conditions. The second objective is to characterize the nature of the aggregates formed using Size Exclusion Chromatography (SEC) and Dynamic Light Scattering (DLS) and to determine how their formation depends on buffer pH, hold time before elution, loading salt concentration, loading flow rate, and protein mass load. The third is to investigate a potential connection between unfolding/aggregation behavior and the tentacle architecture of the Fractogel resin, particularly with respect to the very high binding capacities and unique diffusional mass transfer kinetics that are often associated with polymer-functionalized ion exchangers ([23][24][25]). For this purpose, confocal laser scanning microscopy (CLSM) is used to determine the evolution of intraparticle protein concentration profiles during the load, hold, and elution steps. For comparison purposes similar experiments are conducted for a CEX resin with backbone similar to that of the Fractogel resin but with an open-pore structure and without grafted polymers. In Chapter 3 we seek a molecular level understanding of the unfolding/aggregation behavior using hydrogen-deuterium exchange mass spectrometry (HDX-MS) to determine peptide-level conformational changes caused by binding and/or elution on the Fractogel resin.

2.2. Materials and Methods

2.2.1. Materials

The cation exchange resin Fractogel EMD SO3 (M) used in this work was obtained from EMD Millipore (Darmstad, Germany). According to the manufacturer, the resin is based on a polyacrylate backbone functionalized with charged polymers, called "tentacles", designed to facilitate interaction with the protein. The resin is a strong cation exchanger with sulfonic acid groups. The particle size distribution of the sample used in this work was obtained from microphotographs and spanned the range 40-110 μm with a volume-average particle diameter of 74 μm. Another strong cation exchange resin also with sulfonic acid groups, UNOsphere Rapid S, was obtained from Bio-Rad Laboratories (Hercules, CA, USA) and used for comparison. According to its manufacturer, this resin is based on acrylic and vinyl polymers. However, unlike the Fractogel resin, UNOsphere Rapid S has an open pore structure without any grafted polymers or tentacles. The backbone chemistry and internal structure of UNOsphere Rapid S are similar to those of UNOsphere S as reported in Refs. [25][26], but contains only a small amount of weak acid groups [27][28]. The antibody binding capacity of UNOsphere S has been reported to be around 120 mg/mL of resin particle [25][26].

The monoclonal antibody principally used in this work was provided by Amgen (Seattle, WA, USA) and is a glycosylated IgG2 antibody with molecular mass ~150 kDa and a pI of 8.7 theoretically calculated based on its amino acid sequence. Porcine pepsin, sodium acetate, sodium sulfate, ethanolamine were purchased from Sigma-Aldrich (St. Louis, MO, USA). Acetic acid, sodium chloride, potassium phosphate, ammonium sulfate, sodium citrate, sodium cyanoborohydride, ethylenediaminetetraacetic acid (EDTA), citric acid, formic acid, and trifluoroacetic acid (TFA) were purchased from Fisher Scientific (Houston, TX, USA).

Guanidine hydrochloride (GdnHCl) was purchased from MP Biomedicals (Solon, OH, USA). Tris(2-carboxyethyl)phosphine hydrochloride (TCEP) was purchased from Thermo Scientific (Rockford, IL, USA). Deuterium oxide was purchased from Cambridge Isotope Laboratories, Inc. (Andover, MA, USA). All experiments were conducted at room temperature (22±2 ℃) unless otherwise indicated.

2.2.2. Methods

2.2.2.1. Chromatographic experiments

All chromatography runs were conducted on an AKTA Explorer 10 unit from GE Healthcare (Piscatawy, NJ, USA). The resin samples were packed into 0.5 cm × 5 cm Tricorn columns from GE Healthcare (Piscataway, NJ, USA) with actual packed bed volume of 0.982 and 1.07 mL for the Fractogel and UNOsphere resins, respectively. Table 2.1 shows the baseline conditions for the column chromatography experiments. In all cases, the column was first equilibrated with 5 column volumes of loading buffer (40 mM $NaCH_3COO$ adjusted to pH 4.9 to 5.1 with acetic acid) and then loaded with 0.5 mL of 2 mg/mL mAb. After loading, the flow was stopped and the column was held idle for different time periods. Two column volumes of loading buffer were then supplied followed by a 20 CV gradient to 1 M sodium chloride in 40 mM $NaCH_3COO$ at the same pH. Step-wise elution experiments were also conducted comprising first a step to 0.33 M NaCl, also in 40 mM $NaCH_3COO$, followed by a second step to 1 M NaCl. UV absorbance at 280 nm and conductivity were monitored and 1 to 2-mL effluent samples collected for offline analyses using a model Frac-900 fraction collector from GE Healthcare (Piscataway, NJ, USA). All chromatograms were normalized to a total peak area proportional to the amount of protein injected per unit of column volume in order to account for small changes in actual protein feed concentration and thus facilitate comparisons between runs.

Table 2.1. Baseline conditions for CEX column chromatography experiments.

Step	Duration (min)	Buffer	Flow rate (mL/min)	Protein mass load (mg/mL)[(a)]
Load	0.5	40 mM $NaCH_3COO$ at pH 5.0	1	1
Hold	1000	Same as load	0	-
Wash	2	Same as load	1	0
Elution	20	0 to 1 M NaCl in 40 mM $NaCH_3COO$ at pH 5.0 in 20 CV	1	0

[(a)] obtained by loading 0.5 mL of 2 mg/mL mAb. The mass load is expressed in mg of protein loaded per mL of column volume.

2.2.2.2. Size exclusion chromatography

Size exclusion chromatography (SEC) was performed with a 30 cm × 0.78 cm Yarra 3u 3000 column obtained from Phenomenex (Torrance, CA, USA) using a AKTA Explorer 10 unit from GE Healthcare (Piscataway, NJ, USA). 0.5 mL samples from fractions obtained from CEX chromatography run were injected into the SEC column and eluted at a flow rate of 1 mL/min in 40 mM $NaCH_3COO$ at pH 5.0.

2.2.2.3. Dynamic light scattering

Dynamic light scattering (DLS) measurements were conducted on a Dynapro Nanostar instrument from Wyatt (Santa Barbara, CA, USA) in batch mode at 20 °C. For this purpose, fractions from the CEX column runs were filtered through a 0.22-μm syringe filter directly into the instrument cell for analysis. Mean hydrodynamic radii were determined as z-averages using a cumulant fit of the autocorrelation function, which corresponds to a single exponential decay [29]. Attempts to determine the molecular size distribution of the components in these fractions

provided inconclusive results since the difference between fitting the data with either a single exponential decay or multiple ones was not statistically significant.

2.2.2.4. Batch experiments

Adsorption isotherms were obtained by mixing known amounts of resin samples and protein solutions at different initial concentrations. The resin samples pre-equilibrated with the load buffer were centrifuged at 5000 rpm for 20 min in a filter centrifuge tube to remove the extraparticle liquid. Different amounts of resins, estimated to yield a 50% drop in protein concentration between initial and final values, were dosed gravimetrically and added to the protein solutions in 1.5 mL tubes which were slowly rotating end-over-end for 24 h. The supernatant protein concentration was then measured by UV absorbance at 280 nm with a Nanovue spectrophotometer (GE Healthcare, Piscataway, NJ) and the amount of protein bound was determined by mass balance. Finally, the resin mass was converted to resin volume using a hydrated resin particle density of 1.11 g/mL determined with a pycnometer in order to express the adsorbed protein concentration, q, as mg of protein bound per mL of resin bead volume.

Transient batch uptake experiments were performed as described in Ref. [30] to determine the mAb binding kinetics. For this purpose a known amount of hydrated particles (99 mg), centrifuged to remove the extraparticle liquid, was added to a glass vessel containing 20 mL to 2 g/L protein solution agitated with a paddle stirrer at about 300 rpm. A stream of the solution was rapidly recirculated through a UV detector to determine the residual protein concentration in solution from the UV absorbance at 280 nm. The adsorbed protein concentration as a function of time was then calculated by mass balance.

Batch experiments were also conducted to determine the effects of protein load on the formation of late eluting species. Unlike the chromatographic runs where the protein load was varied only over a limited range, these experiments explored a broad range of loads all the way to complete saturation of the binding capacity. Moreover, unlike the chromatography experiments where, as a result of slow binding kinetics, the local protein load likely varied from particle to particle along the column length, these experiments provided data for particles having all the same protein load. For this purpose, 10 mg samples of hydrated resin were mixed with 200 μL of protein solution with initial protein concentration in the range between 0.5 and 15 mg/ml (corresponding to 10 to 300 mg per g of hydrated resin) in 2 mL centrifuge filter tubes. The tubes were agitated at 300 rpm for 1000 min on an orbital shaker and then centrifuged at 5000 rpm for 1 min to remove the extraparticle liquid and the resin washed three times with 0.5 mL of the load buffer (40 mM $NaCH_3COO$ at pH 5). After washing, each resin sample was eluted batch wise by first adding 0.33 M NaCl in 40 mM $NaCH_3COO$ at pH 5 and equilibrating for 45 min and then, after removing the 0.33 M buffer, adding 1 M NaCl also in 40 mM $NaCH_3COO$ at pH 5 and equilibrating for another 45 min. The protein concentration in solution was measured at the end of each step with the Nanovue spectrophotometer to determine, by material balance, the amount of protein initially bound and the amounts of protein desorbed in the first and second elution buffers.

2.2.2.5. Confocal microscopy

Confocal laser scanning microscopy (CLSM) was used to determine the distribution of the bound protein within the particles at the end of the batch loading and desorption steps with protocol and equipment described in refs. [26][31]. For this purpose, the mAb was conjugated with Rhodamine RedTM-X dye by incubating a mixture of the two with a dye-to-protein molar

ratio of 1:3 in a pH 8.5 sodium bicarbonate buffer for 1 h at room temperature. A PD 10 desalting column from GE Healthcare (Piscataway, NJ, USA) was then used to separate the unreacted dye from the protein. An average labeling ratio of 0.15 was determined using UV-Vis spectrophotometry. In order to test if conjugation with the dye affect protein binding to the resin, the labeled mAb mixture was injected in a 0.5 cm diameter x 5 cm long Fractogel column and eluted in 40 mM $NaCH_3COO$ at pH 5.0 with a linear gradient form 0 to 1 M NaCl and detection at both 280 nm and 570 nm, which are absorbance maxima of the mAb and dye-conjugated mAb, respectively. The results showed essentially identical retention for the unlabeled mAb, the unconjugated mAb in the labled mAb mixture, and the dye-conjugated mAb, confirming that, for these conditions, the dye does not significantly affect interactions of the mAb with the resin. Similar results have been obtained previously for the same dye with different mAbs [26][31].

CLSM was carried out using a Zeiss LSM 510 microscope with a Plan-Apochromat 63×/1.4 NA oil objective (Carl Zeiss MicroImaging, LLC, Thornwood, NY, USA). All measurements were made in batch mode. In order to follow the evolution of intraparticle protein concentration during batch adsorption, the labeled protein mixture was first diluted with unlabeled protein in a 1 to 40 ratio to produce a solution containing 2 g/L of total protein. A small sample of the resin particles was then incubated in 10 mL of this solution in a test tube rotated end-over-end on a rotator. At different times, 300 μL samples were taken from the tube and rapidly centrifuged to separate particles from protein solution at time intervals. The separated particles were then placed in a drop of 40% sucrose prepared in the load buffer and imaged by CLSM. As shown in refs. [26][31], the sucrose reduces the refractive index difference between particles and solution making the particles nearly transparent and allowing collection of images with little or no attenuation of fluorescence intensity.

A similar procedure was used to image the distribution of protein in the resin beads at the end of the hold step and after the desorption steps. In the first case, a 2 mg sample of the resin was mixed with 500 μL of the 2 g/L protein solution containing the labeled mAb for 1 min in a 2 mL filter centrifuge tube. The protein solution was then removed and the resin sample washed with the load buffer for three times, after which the protein loaded resin sample was held in protein-free load buffer for different times and finally imaged by CLSM. In the second case, after holding the protein-loaded resin for 1000 min in the protein-free load buffer, the particles were desorbed in a two-step process, first with an excess volume of 40 mM $NaCH_3COO$ at pH 5 containing 0.33 M NaCl for 45 min and then with 40 mM $NaCH_3COO$ at pH 5 containing 1 M NaCl for another 45 min, imaging the intraparticle protein concentration profile after each step by CLSM.

2.3. Results

2.3.1. Chromatographic behavior

Fig. 2.1 shows the gradient elution chromatographic behavior of the mAb on the Fractogel column at different pH values as a function of the hold time. A single peak is obtained at all three pH values with a zero hold time. The position of this peak shifts slightly to lower conductivities as the pH increases indicating that the binding strength becomes slightly weaker. As the hold time is increased from 0 to 1000 min, an increasingly pronounced two-peak elution behavior is observed. The trends with regards to hold time are qualitatively the same at each pH value, but a much greater fraction of the protein elutes at high conductivity at lower pH values. In each case, the second peak becomes increasingly broader with the peak maximum shifting to higher conductivities as the hold time is increased. All along, however, the early eluting peak retains both the same retention time and breadth. Since pH appears to affect the magnitude of the

two-peak behavior but not its general trends, the mechanisms leading to these effects are likely the same. Thus, the remainder of the experiments was conducted at pH 5.0. For these conditions the hold times that result in a large second peak are relatively long, which allows us to gain insight on the independent effects of protein load and elution.

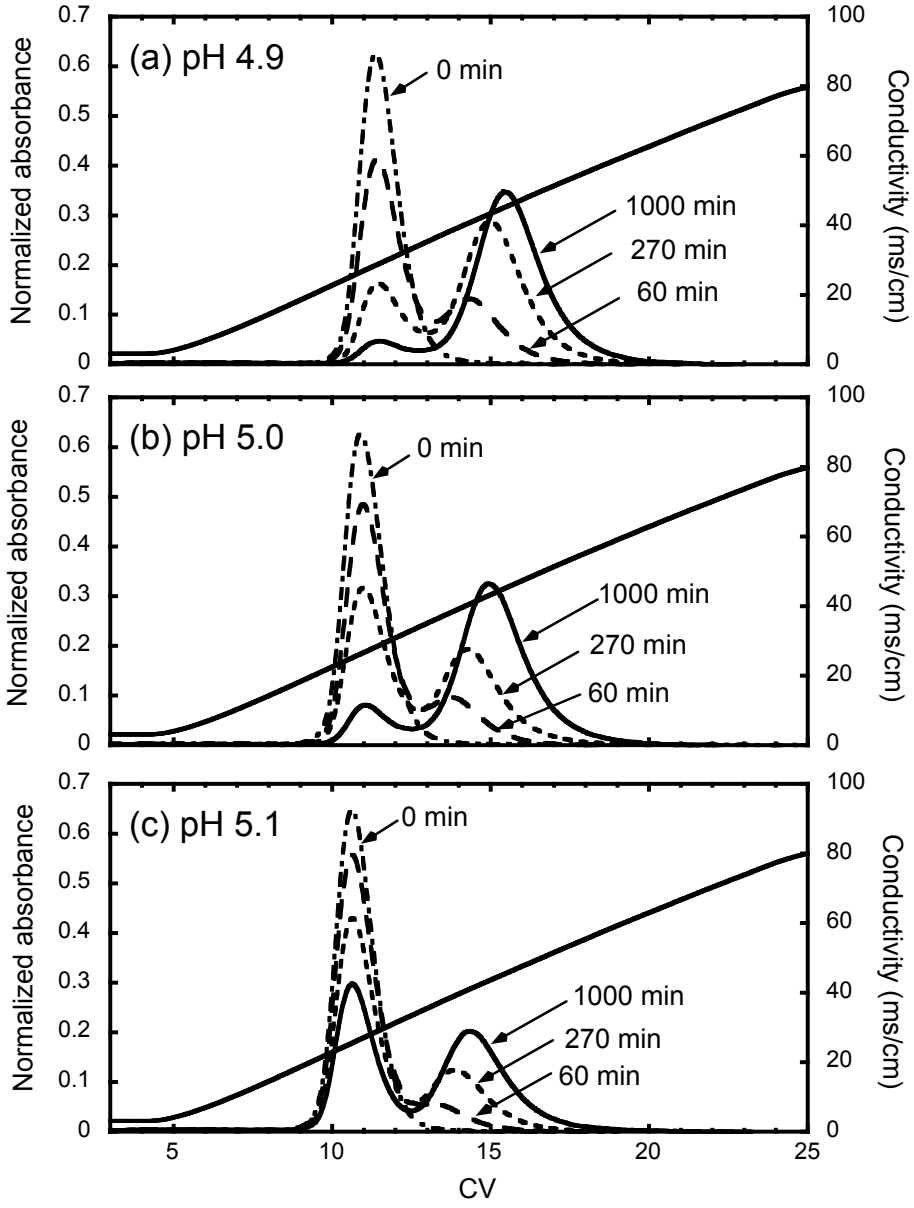

Figure 2.1. Effects of pH and hold time on elution profile of the mAb on the Fractogel column (a) pH 4.9, (b) pH 5.0, (c) pH 5.1. Other conditions are as given in Table 2.1. The percentages of protein eluting in the second peak were 0, 31, 72, and 92% for 0, 60, 270, 1000 min hold times in (a), 0, 18, 48, and 87% in (b), and 0, 11, 30, 53% in (c) for hold times of 0, 60, 270, 1000 min, respectively.

Fig. 2.2 illustrates the chromatographic behavior of the mAb on the Fractogel column for the following conditions: (a) at pH 5.0 with two different Na^+ concentrations in the load buffer and a 270 min hold time; (b) for gradient elution from 0 to 1 M NaCl (top) and for two-step elution with the first step at 0.33 M NaCl and the second at 1 M NaCl (bottom); (c) for different protein mass loads; and (d) for different flow rates in the load step. All other conditions were kept constant in each experiment according to Table 2.1. As seen in Fig. 2.2a, increasing the Na^+ concentration in the load buffer dramatically reduces the fraction of protein eluting in the second peak while, as seen in Fig. 2.2b, nearly identical results are obtained for the fraction eluted in the second peak whether linear gradient elution or a two-step elution protocol is implemented. These results, taken together, suggest that the two-peak behavior is caused by the load conditions and is not affected substantially by the way elution is carried out. Further evidence suggests that this is the case is given by Fig. 2.2c, which shows that the fraction of protein eluting in the second peak is nearly independent of the protein mass load, and by Fig. 2.2d, which shows that the load flow rate has a large effect on the fraction eluted in the second peak. It should be noted that the mass loads used for the experiments in Fig. 2.2c were quite low, approximately 75 to 300 times lower than the column equilibrium binding capacity, which, as shown below is on the order of 200 mg/mL. Thus, for any of these experiments most of the resin particles were far from saturation. In this range of operating conditions, a much more important effect is that of the load flow rate. Since the load volume was fixed at 0.5 mL, both the residence time during the load step and the load time varied in inverse proportion to the flow rate, spanning the ranges 1 to 200 min and 0.5 to 100 min for the residence time and load time, respectively.

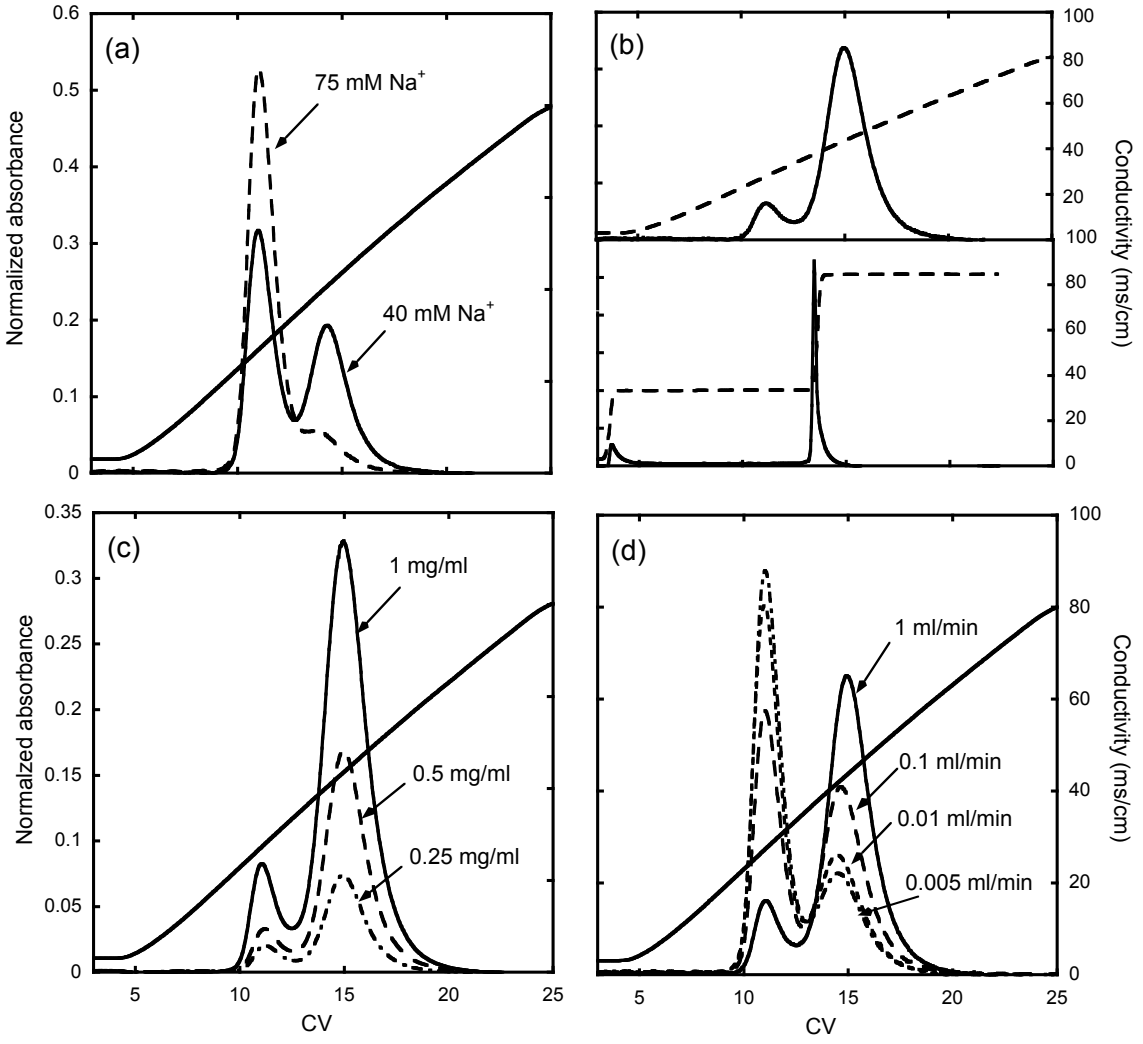

Figure 2.2. Chromatographic behavior of the mAb on the Fractogel column at pH 5.0. (a) Effect of Na^+ concentration in load buffer with a hold time of 270 min. (b) Comparison of linear gradient elution and two-step elution at 0.33 M followed by 1 M NaCl with 1000 min hold time. (c) Effect of protein mass load with 1000 min hold time. (d) Effect of load flow rate with a 2 mg/ml protein mass load and 1000 min hold time. Other conditions are as given in Table 2.1. The percentage of protein eluted in the second peak was 48 and 13% for 40 and 75 mM Na^+, respectively, in (a), 88 and 86% for LGE and two-step elution, respectively, in (b), 87, 88, and

84% for 1, 0.5, and 0.25 mg/mL protein mass loads, respectively, in (c), and 87, 53, 35, and 31% for 1, 0.1, 0.01, and 0.005 mL/min load flow rates, respectively, in (d).

Fig. 2.3 shows the percentage of high molecular mass species, obtained by SEC, and the mean hydrodynamic radius, obtained by DLS, for fractions collected from a gradient elution run with the Fractogel column for the conditions in Table 2.1 but with a hold time of 270 min. For these conditions, the mAb elutes in two distinct peaks with peak maximum at about 11 and 14.5 CVs, respectively. The SEC results show that the early eluting peak contains little or no high molecular mass species. However, the percentage of these species increases dramatically for the late eluting peak. Representative SEC chromatograms are given in Fig. 2.4a and show that the late eluting peak consists of a mixture of monomeric species, eluting about 8.8 mL from the SEC column, and a range of high molecular mass species eluting between 6 and 8.3 mL. The percentage of these species increases along the late peak eluting from the CEX column. The DLS results shown in Fig. 2.3 indicate that the mean hydrodynamic radius, r_h, increases along the CEX gradient together with the percentage of high molecular mass species, from a minimum of about 5 nm, which is characteristic of monomeric IgG [32][33][34] to a maximum slightly above 10 nm, which corresponds to aggregated IgG [33]. Assuming that the aggregates are fractal objects, the number of monomer units in the aggregates formed can be estimated as $N_m \approx \left(r_{h,a}/r_{h,m}\right)^d$ where $r_{h,a}$ and $r_{h,m}$ are the radii of the aggregates and of the monomer, respectively, and *d* is the fractal dimension [35][36][37]. Values of *d* for protein aggregates have been reported to be in the range 1.7 to 2.7 with a value of 2.5 typical for antibodies [35][37]. A value of 2.5 yields N_m between 1.4 and 5.2 for the fractions collected between 13.4 and 17.4 CV, which corresponds to the late eluting peak, indicating that the aggregates in these fractions are relatively small oligomers. The r_h-values measured for these fractions at different times after

their collection are shown in Figure 2.4b. As seen in this figure, there is no change in r_h for the monomer species collected from the early eluting peak. Conversely, r_h decreases slowly with time, apparently leveling off after about 300 min. This slow decrease suggests that aggregation is at least partially reversible.

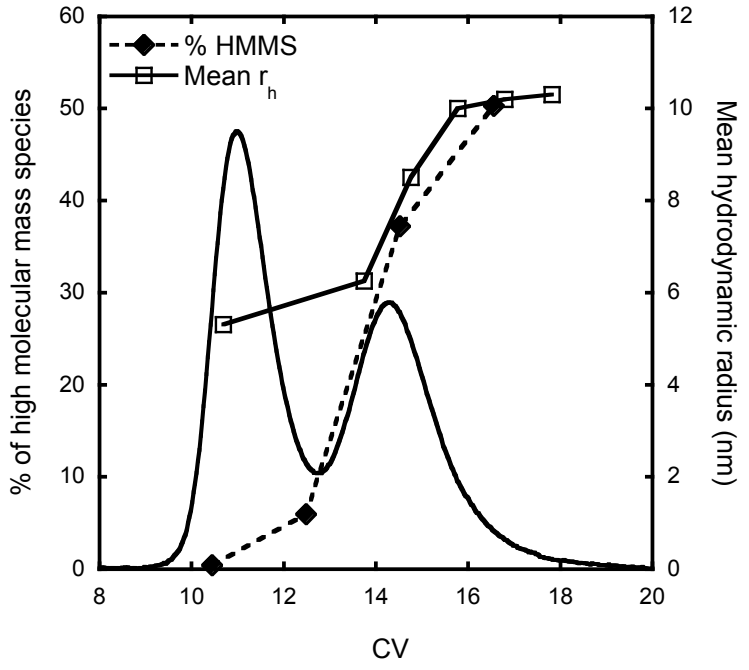

Figure 2.3. Percentage of high molecular mass species and mean hydrodynamic radius for fraction collected during elution from the Fractogel column following a 270 min hold time for the baseline conditions summarized in Table 2.1. The conductivity profile is omitted from the figure but is as in Fig. 2.1b.

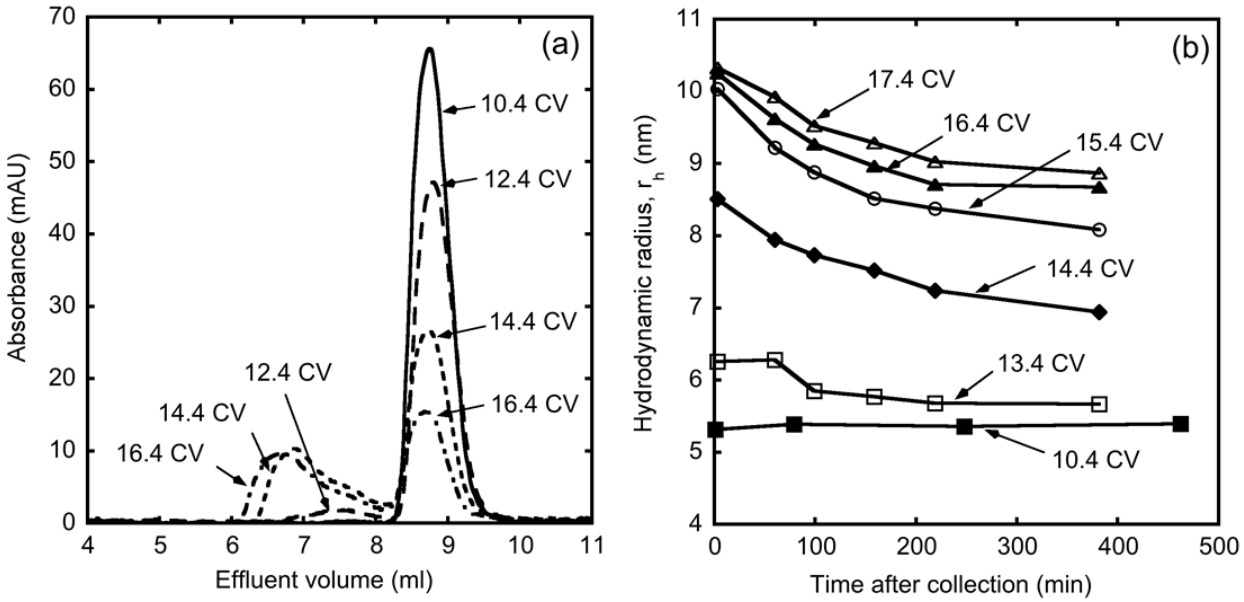

Figure 2.4. SEC (a) and DLS (b) analyses of fractions collected during elution from the Fractogel column following a 270 min hold time for the baseline conditions summarized in Table 2.1. The CV-labels in both (a) and (b) correspond to the CV-values at which fractions were collected for the run in Fig. 2.3; (b) shows the mean hydrodynamic radius for these fractions as a function of the time elapsed after collection.

Fig. 2.5 shows a comparison of the mAb elution behavior for the Fractogel column with that observed for the UNOsphere column with 0 and 1000 min hold times. With a zero hold time, both columns give a single, early eluting peak with essentially 100% recovery. Although this peak is somewhat broader for the UNOsphere column compared to the Fractogel column likely as a result of the larger mean particle diameter of the latter (100 μm for UNOsphere vs. 74 μm for Fractogel), the elution times are similar for the two columns suggesting that for these low protein loads, protein-surface interactions are similar during elution for the two resins. However, with 1000 min hold time the late eluting peak is seen only with the Fractogel column. A possible explanation is that the tentacle structure of the Fractogel resin, which is absent in UNOsphere,

affects the protein behavior. Another is that the binding strength at the load conditions is actually different for the two resins even though the salt concentration required for elution is nearly the same.

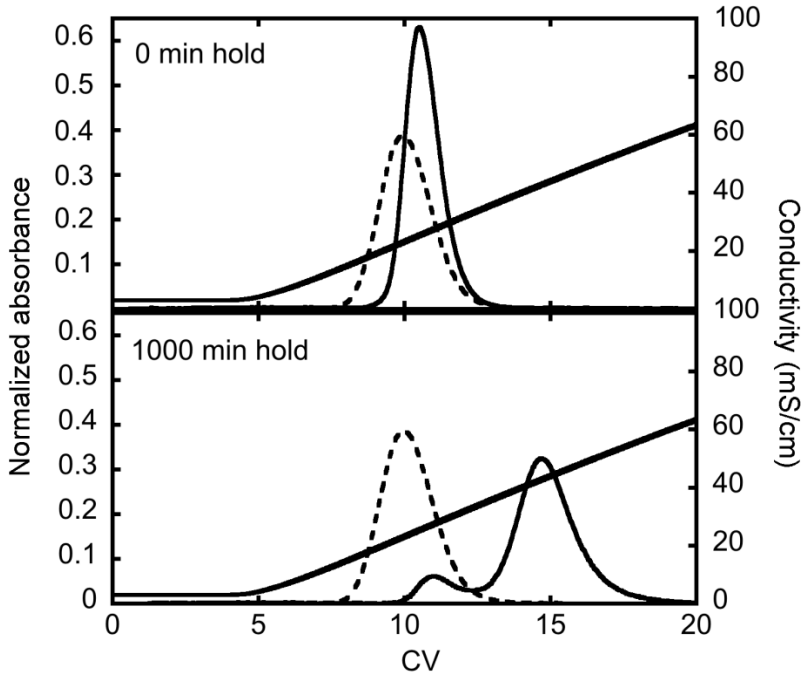

Figure 2.5. Comparison of mAb elution behavior in Fractogel (solid line) and UNOsphere (dashed line) columns for the baseline conditions summarized in Table 2.1 with 0 and 1000 min hold times. The elution peaks at 0 and 1000 min hold times for the UNOsphere column are virtually coincident. The percentages of protein eluting in the second peak with 1000 min hold time were 88 and 0% for the Fractogel and UNOsphere column, respectively.

2.3.2. Batch adsorption behavior

Batch adsorption experiments were conducted with the Fractogel resin to determine the mAb equilibrium binding capacity and kinetics and to study the two-peak elution behavior at protein loadings much higher than those used in the chromatographic experiments. An important consideration is the fact that, because of mass transfer limitations, protein loading in the column

(prior to hold and elution steps) was likely not uniform along the column length. As a result, the chromatographic results averaged out the contributions of different particles along the column length. Batch experiments remove this concern, as all particles will have the same protein load prior to hold and desorption steps.

Fig. 2.6 shows the 24 hour binding capacity and batch adsorption kinetics of the mAb on the Fractogel resin. As seen in Fig. 2.6a, the binding capacity achieved in 24 hours is 215±9 mg/mL of resin particle volume and is essentially independent of protein solution concentration in the range 0.2-2.3 mg/mL. As seen in Fig. 2.6a, the relationship between adsorbed protein concentrations, q, and solution protein concentrations, C, can be represented by the Langmuir isotherm, $q = q_m KC/(1+KC)$ with q_m=215 mg/mL and K=150 mL/mg. In practice, the isotherm can be treated as rectangular for these conditions. As seen in Fig. 2.6b for the same conditions, the adsorption kinetics is relatively slow. Only about 85% of the 24 hour binding capacity is achieved in 200 min. An apparent effective diffusivity, D_e, was determined from these data by fitting the pore diffusion model with a rectangular isotherm based on eqs. A16-A18 in ref. [38], which account for the particle size distribution of the resin. Since the binding kinetics is slow, external mass transfer resistances were neglected in these calculations. A value of D_e = (1.7±0.2)x10^{-8} cm^2/s was obtained by matching data and numerically computed model results. This value corresponds to a ratio D_e/D_0 ~ 0.04, where D_0 = 4x10^{-7} cm^2/s is the free solution diffusivity of the mAb obtained by DLS, indicating that mAb transport in the Fractogel resin is severely hindered for these conditions. As seen in Fig. 2.6b, although not perfect, the pore diffusion model provides a reasonable description of the batch uptake data.

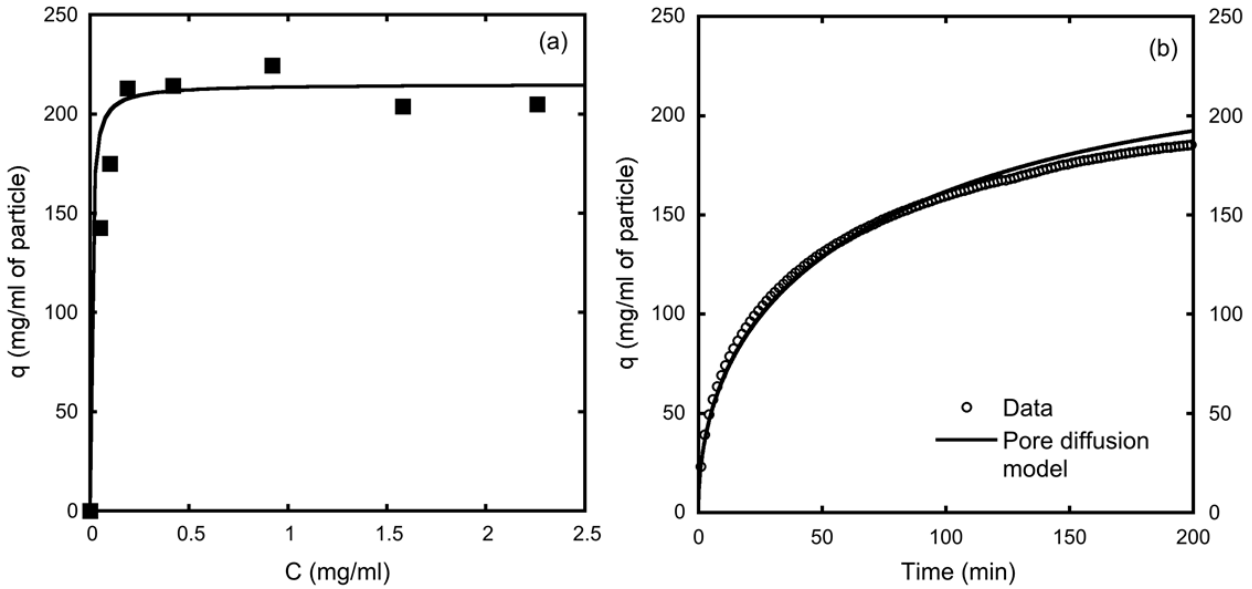

Figure 2.6. Batch adsorption behavior of Fractogel resin in 40 mM $NaCH_3COO$ buffer at pH 5.0. (a) amount of mAb adsorbed at 24 h; (b) batch uptake curve for 2 mg/mL initial mAb concentration. The solid lines are based on the Langmuir isotherm model fitted to the data with q_m = 215 mg/mL and K=150 mL/mg in (a) and the pore diffusion model with $D_e = 1.7 \times 10^{-8}$ cm^2/s in (b).

Fig. 2.7 shows the mAb batch desorption behavior for Fractogel resin that was loaded with different amounts of protein in batch mode and held for 1000 min followed by a two-step desorption process, first in 0.33 M NaCl and then 1 M NaCl. The data, spanning fractional loadings between about 0.05 to 1 relative to the binding capacity, q_m, show that the percentage of protein desorbed in the second step decreased as the fractional protein load increased. In fact, for completely saturated beads, virtually all the protein (> 98%) was desorbed in 0.33 M NaCl. This result suggests that the molecular interactions that are responsible for the two-peak chromatographic elution behavior are strongly influenced by the protein load in the particles. Fogle et al. [39] observed analogous behavior of model proteins on HIC media, showing that

increasing mass load decreased the extent of surface-induced unfolding. They concluded that crowding on the surface and protein-protein repulsive interactions helped prevent unfolding at high protein loads. Haimer et al. [40] also observed that increasing protein loads resulted in a reduced two-peak elution behavior of β-lactoglobulin on a butyl-type HIC resin and explained this behavior using the surface spreading model of Lundstrom [41]. Accordingly, the protein is hypothesized to undergo a conformational change that causes spreading on the surface, which is lessened at higher protein loads. The spreading model also was used by McCue et al. [42] to explain irreversible binding on HIC surfaces and by Yang and Etzel [43] to explain the tailing behavior of breakthrough curves observed for proteins on ion-exchange membranes. On the other hand, Sane et al. [44] observed the opposite behavior for lysozyme on reversed phase resins, with higher protein loads causing more conformational change of the protein. Thus, it is evident that these effects cannot be generalized and are both, likely, protein and surface structure specific.

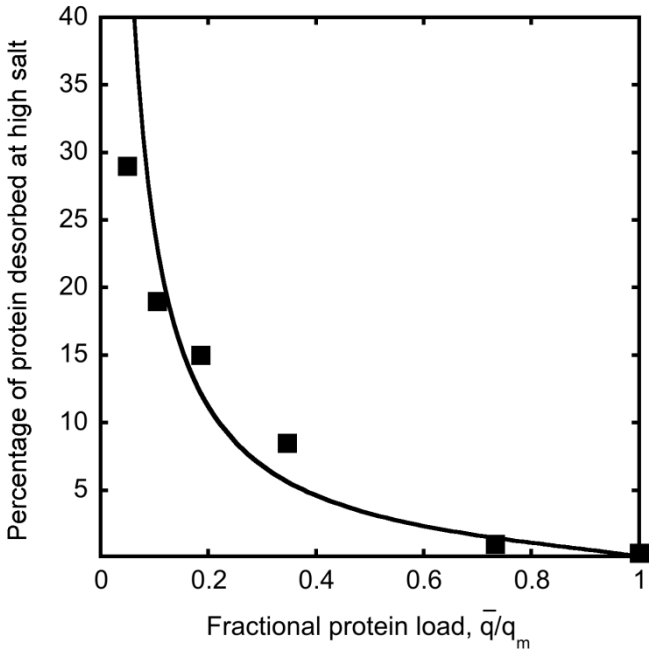

Figure 2.7. Percentage of mAb desorbed in 1 M NaCl following desorption in 0.33 M NaCl plotted as a function of the initial average adsorbed concentration $\bar{q}$ normalized by the binding capacity q_m = 215 mg/mL. All data are in 40 mM $NaCH_3COO$ buffer at pH 5.0.

2.3.3. Confocal microscopy results

CLSM was used to determine the distribution of the mAb in the Fractogel resin beads during batch adsorption, hold, and desorption steps. Fig. 2.8 shows representative images of the intraparticle protein concentration for batch adsorption from a 2 mg/mL mAb solution in 40 mM $NaCH_3COO$ at pH 5. As seen in the images, a fairly sharp adsorption front is established in the particles at very short times and progresses slowly toward the center of the particle. Note that because of the need to place the particles in the sucrose refractive index matching solution, each image is for a different particle. Particles of similar sizes are thus shown in order to facilitate their comparison. The sharp front behavior observed suggests that the pore diffusion model with a rectangular isotherm can also be used to describe these data. Accordingly, the dimensionless

front position in the particles, $\rho_s = r_s / r_p$, where r_s is the radial position of the adsorption front and r_p is the particle radius, is given by [45]:

$$2\rho_s^3 - 3\rho_s^2 + 1 = \frac{6D_e C}{q_m}\frac{t}{r_p^2} \tag{2.1}$$

Fig. 2.8 also shows a plot of both the ρ_s values determined from the CLSM images and of the corresponding values of the function $f(\rho_s) = 2\rho_s^3 - 3\rho_s^2 + 1$ vs. t/r_p^2 . As seen from this graph, the $f(\rho_s)$ plot is linear (R = 0.987), indicating conformance with eq. 2.1. Its slope gives D_e = (1.9±0.1)x10^{-8} cm^2/s, which is in approximate agreement with the value obtained by fitting the batch uptake data.

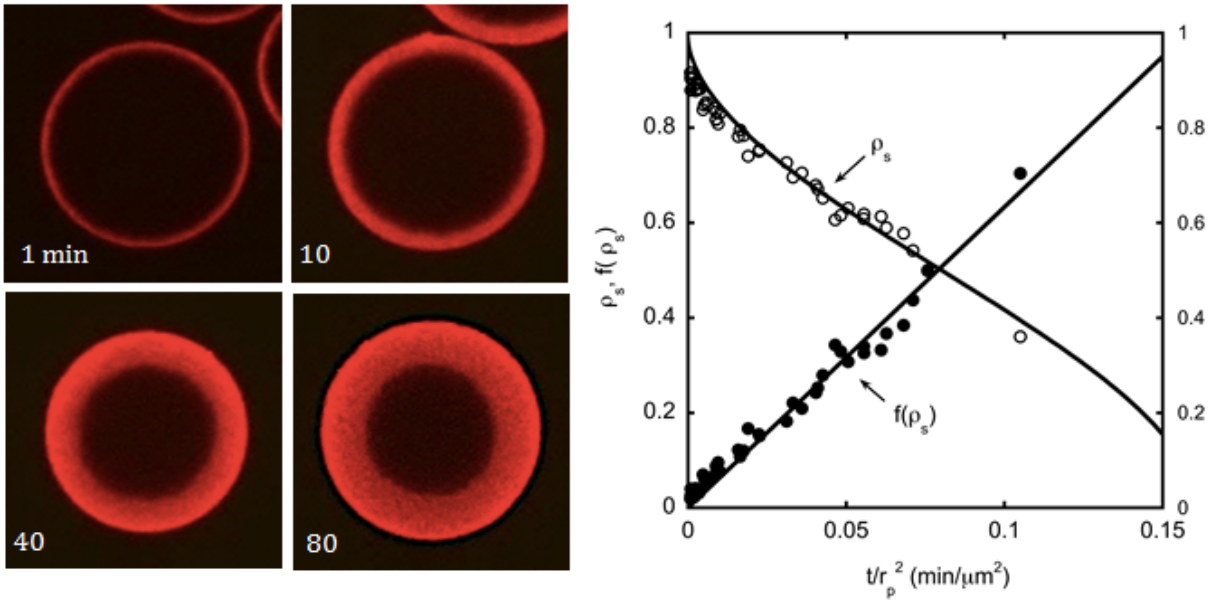

Figure 2.8. CLSM images of Fractogel particles during transient adsorption of 2 mg/mL mAb in 40 mM $NaCH_3COO$ at pH 5 at 1, 10, 40 and 80 min. Actual particle diameters are 65, 63, 63, and 69 μm from top left to bottom right. The graph on the right hand side shows plots of the dimensionless position of the adsorption front, ρ_s, and the function $f(\rho_s)$ vs. the reduced time t/r_p^2.

Fig. 2.9 shows the intraparticle mAb concentration profiles at different hold times shown for each image, following adsorption of the mAb from a 2 mg/mL solution for 1 min. Results are shown for both the Fractogel resin (top) and for the UNOsphere resin (bottom). In both cases, after the 1-min adsorption time, the particles were placed in the protein-free load buffer and held there at room temperature. The results are dramatically different for the two resins. In both cases, we start with a thin protein-saturated layer near the particle surface. This layer remains unchanged for the UNOsphere resin (b) even after 1000 min. However, in the case of Fractogel, the layer spreads toward the center of the particles becoming increasingly diffuse. Because of the highly favorable nature of the binding isotherm, virtually no protein left the particles during the

hold period (no protein was indeed found in solution based on A280 measurements). However, it is apparent that the protein was redistributed within the Fractogel beads attaining local adsorbed intraparticle concentrations much lower than the saturation capacity q_m. These results indicate that while the protein is essentially immobile after adsorption in the UNOsphere resin, it retains some degree of diffusional mobility in the Fractogel resin, which allows the protein to be redistributed across the particle volume over sufficiently long times.

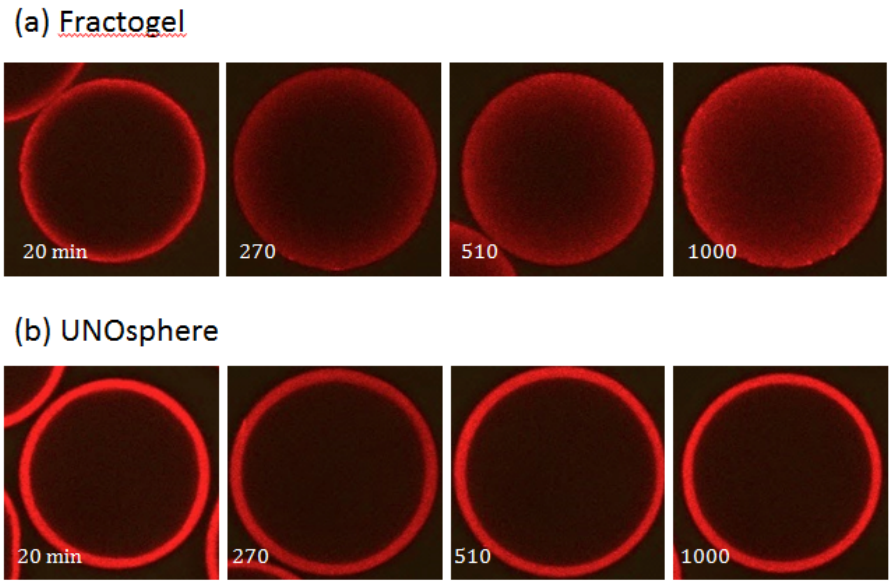

Figure 2.9. CLSM images of Fractogel (a, top) and UNOsphere (b, bottom) particles at hold times of 20, 270, 510, and 1000 min following adsorption of 2 mg/mL mAb for 1 min. All data in 40 mM $NaCH_3COO$ at pH 5. Actual particle diameters were, from left to right, 74, 82, 78, and 82 μm for Fractogel and 81, 88, 90, and 84 μm for UNOsphere.

Figures 2.10a and b shows representative CLSM images of Fractogel particles initially loaded for 1 and 20 min, respectively, from a 2 mg/mL mAb solution in 40 mM $NaCH_3COO$ at pH 5, held in the protein-free buffer for 1000 min, and then subjected to a two-step desorption process, first in 0.33 M NaCl and then in 1 M NaCl, both in the same 40 mM buffer. Images are shown at the end of each step. As discussed previously, at the end of the 1000 min hold step the

protein appears to be redistributed somewhat uniformly over the particle volume even though both 1 and 20 min load times are sufficient to saturate only a relatively thin layer of the particle near its external surface (cf. Fig. 2.8). As seen in both Fig. 2.10a and 2.10b, the protein left over in the particle at the end of the 0.33 M NaCl desorption step is uniformly distributed over the particle volume and its concentration, based on the fluorescence intensity, was apparently the same whether the partciels were initially loaded with protein for 1 min or for 20 min. Finally, the last image in each row shows that little if any protein was left in the particles at the end of the 1 M NaCl desorption step. These results are qualitatively consistent with both the two-peak chromatographic elution behavior and with the batch two-step desorption behavior. Striking, however, the residual protein found at the end of the first desorption step is uniformly distributed across the particle.

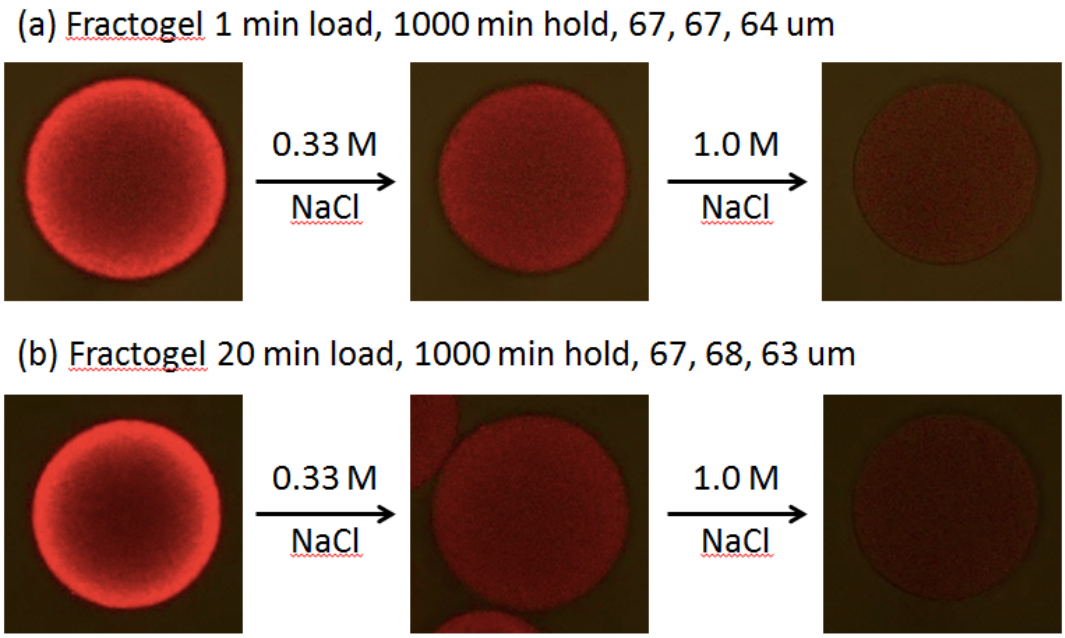

Figure 2.10. CLSM images of Fractogel particles after a 1000 min hold following (a) adsorption of 2 mg/mL mAb for 1 min and (b) adsorption of 2 mg/mL mAb for 20 min. Images are shown at the end of the hold period (left), after desorption in 0.33 M NaCl (middle), and after desorption in 1 M NaCl. All data is in 40 mM $NaCH_3COO$ at pH 5. Actual particle diameters were, from top left to bottom right, 67, 67, 64, 67, 68, and 63 μm.

2.4. Discussion

The chromatographic behavior observed in our work for our glycosylated IgG2 is in many ways consistent with the observations of Gillespie et al. [17] for an aglygosylated IgG1. Although the effects are, in general, less pronounced at comparable times for the glycosylated IgG2, likely because of its inherently greater stability, both systems exhibit a two-peak elution behavior in the Fractogel column the magnitude of which is strongly correlated with pH (increasing as the pH decreases), hold-time before elution (increasing as the hold time increases), and load buffer concentration (increasing as the load buffer concentration decreases). The effect is similar whether elution is carried out with a linear NaCl gradient or with a two-step process.

The effect of protein mass load on the two-peak elution behavior also has trends similar to those observed by Gillespie et al., being relatively insensitive in both cases in column experiments at low protein loads. Newly observed in this work is the effect of flow rate (or residence time) during the load step. We found that loading the column with the same amount of protein but at lower flow rates dramatically reduced the two-peak elution behavior. Since protein mass transfer within the particles has been shown in our work to be highly limiting, it is likely that these load flow rate effects are caused by the different distribution along the column length of the initially loaded protein.

Unlike prior work, we have also explored the batch adsorption behavior both macroscopically, through adsorption-desorption experiments, and microscopically, using CLSM to determine the distribution of adsorbed protein within the particle at the end of loading, hold, and desorption steps. The results of these studies clearly show that the two-peak elution behavior is dramatically reduced at protein loads that approach the resin's saturation binding capacity. For these conditions we observed that virtually all the protein is desorbed at relatively low salt concentrations. However, increasingly greater amounts of protein can be desorbed from the resin as the protein load is reduced. This behavior is confirmed by the CLSM results. Additionally, these results showed that the bound protein retained diffusional mobility over long time scales in Fractogel particles, likely provided by the polymer-grafted architecture of this resin. By comparison, a macroporous cation exchanger showed no movement of the mAb within the particles after binding and no evidence of the formation of multiple bound protein forms that can only be desorbed at high salt concentration. Thus, it appears that the two-peak elution behavior and the resin architecture are interdependent.

What then is the mechanism that explains the two peak elution behavior? We hypothesize that the two-peak elution behavior is caused by the formation of a strongly bound unfolded intermediate caused by strong interactions with the resin's tentacles. We next hypothesize that its formation is "catalytic" in the sense that it is facilitated by the polymer grafts and occurs as a function of time. Further, we hypothesize that its formation is dependent on the local bound protein concentration, increasing as the local bound protein concentration decreases. Finally, we hypothesize that upon desorption, the destabilized unfolded intermediate in part refolds to the native monomer and in part forms aggregates. Figure 2.11 shows the behavior expected based on these hypotheses for low and high average protein loads. In both cases, since as seen experimentally, the isotherm is highly favorable and the adsorption front in the particle is sharp, the protein is initially adsorbed at a bound concentration equal to the binding capacity but over different depths of penetration into the particle dependent on the protein load level. During the hold period the protein migrates from the saturated layer and is redistributed across the particle. At low initial protein loads, low levels of local saturation are attained which lead to the formation of the unfolded intermediate as a result of strong interactions with the grafted polymers. At high initial protein loads, the average adsorbed concentration at the end of the hold period is higher causing a smaller fraction of the bound protein to unfold. In 0.33 M NaCl, only the native mAb is desorbed, while the unfolded intermediate is retained. In 1 M salt, the destabilized, desorbed unfolded intermediate in part refolds to the native mAb and in part aggregates resulting in a late eluting peak, which as seen experimentally is a mixture of monomer and aggregates.

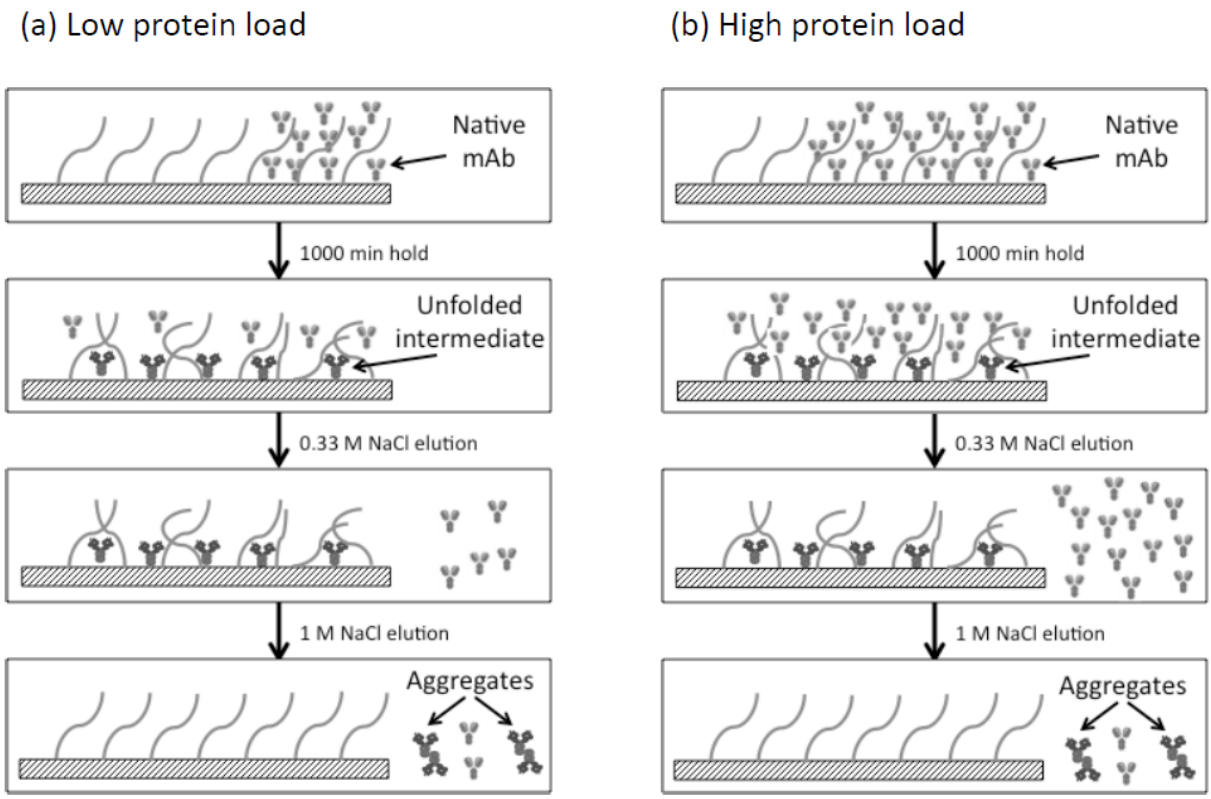

Figure 2.11. Schematic illustrating the hypothesized path leading to the two-peak elution behavior at low (a) and high (b) protein loads. In both cases, the protein is initially bound at an adsorbed concentration equal to the binding capacity but over layers with different depths of penetration into the particle. The protein migrates during the hold period and is redistributed across the particle. At low initial protein loads, low levels of local saturation are attained which lead to the formation of an unfolded intermediate as a result of strong interactions with the grafted polymers. At high initial protein loads, the average adsorbed concentration at the end of the hold period is higher causing a smaller fraction of the bound protein to unfold. In 0.33 M NaCl, only the native mAb is desorbed, while the unfolded intermediate is retained. In 1 M salt, the destabilized, desorbed unfolded intermediate in part refolds to the native mAb and in part aggregates resulting in a late eluting peak, which is a mixture of folded monomer and aggregates. The percentage of aggregates in the combined elution pool decreases with protein load since,

according to this conceptual model, the amount of protein that unfolds remains the same while the total protein bound increases.

Based on the conceptual model described above, if unfolding only occurs for protein molecules that are bound at adsorbed protein concentrations below a threshold value for which interactions with the grafted polymers are sufficiently strong to destabilize the protein structure, the amount of protein unfolded would be expected to be relatively independent of protein load provide the hold time sufficiently long to allow the protein to diffuse through particle. In this case, the percentage of protein unfolded and, thus, the percentage of the bound protein in the late eluting peak should decrease (as seen experimentally in the batch experiments) as the total protein load increases. Since, as seen experimentally, adsorption of the mAb on the Fractogel resin occurs by a shrinking core mechanism (cf. Fig. 2.8), we conjecture that the amount of protein that unfolds is proportional, for a given hold time, to the volume of the free core, based on the assumption that as protein molecule diffuse in this area during the hold step are rapidly unfolded. Accordingly, the fraction of adsorbed protein that is unfolded and, thus, elutes at high salt is given by:

$$f_{unfolded} = \frac{k\rho_s^3}{1-\rho_s^3} = \frac{k\,\bar{q}/q_m}{1-\bar{q}/q_m} \tag{2.2}$$

where k is a dimensionless rate constant dependent on the hold time and the ability of the Fractogel surface to catalyze the formation of the unfolded intermediate and $\bar{q}$ is the average bound protein concentration. Figure 2.7 shows a comparison of this equation with the batch experimental data at 1000 min hold times. As seen in this figure, the equation provide a reasonable description of the data with $k = 0.023$.

A final consideration is whether the conceptual model described above can also explain the dependence of the percentage of protein eluting in the second peak on the flow rate during

the protein load step in the chromatographic experiments with the Fractogel column. In order to establish the reasons for this relationship, one must consider the distribution of the protein at the end of the load step. As seen in Fig. 2.6b, the binding kinetics is slow, requiring over 200 min to achieve saturation in a batch experiment with 2 mg/mL mAb concentration. However, the column experiments were done at flow rates between 1 and 0.005 mL/min, which, for the 0.5 mL feed volume used correspond top load times between 0.5 and 100 min, all shorter than needed to saturate the resin beads. Thus, it is apparent that the protein loaded was distributed along the column length to a different degree, dependent on the load flow rate. As a result, different initial particle-average protein loads existed along the column length during the hold step and, thus, different degrees of formation of the unfolded intermediate could be expected as a function of load flow rate. In order to quantify these effects, we used the solution of Weber and Chakraborty [46] to describe the position of the adsorption front at the end of the load step within the particles at different distances from the column entrance. The model assumes pore diffusion with a rectangular isotherm and is consistent with the models used in this work to describe the batch and CLSM adsorption behavior of the mAb on the Fractogel resin. Calculations were carried out using the average D_e = 1.8x10^{-8} cm^2/s of the values of obtained in this work from batch and CLSM experiment, respectively, and with the experimental extraparticle column porosity $\varepsilon = 0.38$ determine from the retention of blue dextran. The results are shown in Fig. 2.12 for the highest and lowest flow rates used in our column experiments. At the highest flow rate, the residence time in the column is very short (~1 min) which causes the protein loaded to be initially distributed over a relatively large section of the column. As a result, for all the particles in this section, at the end of the load step the protein is concentrated in a very thin layer near the particle surface. Migration of the protein in the initially extensive empty core occurs during the

hold step, resulting in a high fraction of the protein loaded converted to the unfolded intermediate. On the other hand, at the lowest flow rate used, the residence time in the column is sufficiently long (~100 min) to result in a relatively sharp breakthrough front and thus, a relatively high protein load for the particles in the top section of the column. The high protein load results in a small protein-free core for most particles, which, in turn results in a small fraction of protein unfolded.

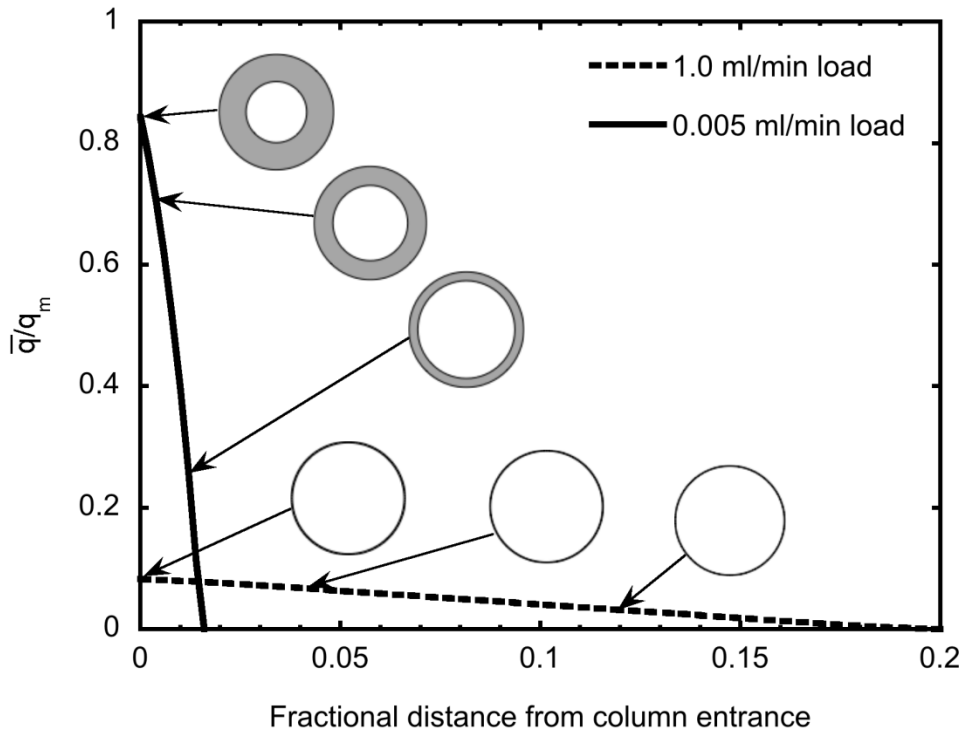

Figure 2.12. Predicted adsorbed protein concentration profiles in the Fractogel column as a function of distance from the entrance at the end of the protein load step based on the pore diffusion model at highest and lowest load flow rates used experimentally in Fig. 2.2d. The position of the adsorption front inside the particles for the two cases is shown at representative distances from the column entrance.

2.5. Conclusions

A two-peak elution behavior is observed for a glycosylated IgG2 on a Fractogel CEX column. This behavior is accompanied by the formation of mAb aggregates with various sizes, which elute only at high salt concentrations (e.g. 1 M NaCl) in a mixture with monomeric mAb. Aggregate formation in this column increases as the binding strength increases (lower pH and lower load buffer concentration), and as the load flow rate increases. Batch experiments at higher protein loads show that aggregate formation decreases rapidly as protein mass load increases and

is nearly completely suppressed if the Fractogel particle are initially completely saturated with protein. CLSM experiments have shown that the two-peak elution behavior is correlated with the unique protein binding kinetics in the Fractogel resin. Studies with a macroporous CEX resin without “tentacles” or grafted polymers showed no evidence of two-peak elution behavior or aggregate formation and no evidence of movement of the protein within the beads during the hold step. This suggests that either the tentacle structure or differences in binding strength during loading for the two resins is responsible for the two-peak behavior. In either case, a conceptual model is advanced according to which unfolding occurs when protein molecules slowly migrate to regions of the particle that are initially protein free. For these conditions, interactions of the protein with the resin’s tentacles are expected to be strongest leading to conformational changes that lead to unfolding and, eventually, aggregate formation when the destabilized unfolded intermediate, which is more strongly bound than the native monomer, is eluted at high salt. While the model is semi-quantitatively consistent with the experimental observations, its molecular basis is tenuous. Thus, Chapter 3 uses hydrogen-deuterium exchange mass spectrometry (HDX-MS) to probe the conformational changes hypothesized in this work and to obtain a molecular scale explanation of the catalytic effect of the Fractogel surface on destabilizing the bound protein. From the practical viewpoint, it is apparent that conditions where protein binding is weaker (higher salt or higher pH) tend to reduce aggregate formation and the ensuing two-peak elution behavior. However, this needs to be balanced against reduced binding capacity and, perhaps, selectivity.

Chapter 3

Protein structure effects by hydrogen deuterium exchange mass spectrometry

---

3.1. Introduction

In Chapter 2, we have examined the binding and elution behavior of a glycosylated IgG2 mAb on a "tentacle" type Fractogel CEX column. The mAb exhibited a two-peak elution behavior when loaded at low pH and eluted with a salt gradient. The early eluting peak was shown to consist exclusively of monomeric species whose retention was the same as that of the native mAb. The later eluting peak, on the other hand, was shown to consist of a mixture of monomeric species and mAb aggregates. The percentage of protein eluting in the second peak was found to increase when conditions favored stronger initial binding of the antibody, when the hold time prior to elution was longer, when the initial protein mass load was lower, and when the load flow rate was higher. Confocal laser scanning microscopy (CLSM) was used to examine the kinetics of protein adsorption on the resin and the intraparticle distribution of bound protein at the end of the load, hold, and elution steps. We showed that, for typical conditions, the protein loaded to the column is initially distributed entirely within a thin layer near the resin particle surface, where it attains a locally high bound protein concentration. However, over time the initially loaded protein becomes redistributed throughout the particle volume eventually attaining a locally low bound protein concentration. An inverse relationship was thus established between the local bound protein concentration and the percentage of protein in the aggregate-containing, late eluting peak. A conceptual model was developed to describe the mechanisms leading to aggregate formation in the Fractogel resin. According to this model, the bound protein is destabilized, to an extent that depends on the hold time and mobile phase conditions, when

present below a threshold value of the bound-protein concentration forming a strongly-bound, unfolded intermediate. Following load and hold steps, as the salt concentration is increased either in a gradient or in a two-salt step elution scheme, the more weakly retained native protein elutes first, while the unfolded intermediate remains bound. Upon further increasing the salt concentration the destabilized intermediate eventually elutes in part by refolding to the native conformation and in part forming aggregates. While this conceptual model was qualitatively consistent with the observed experimental trends, molecular-level insight is needed to ascertain its validity.

The goal of this chapter is thus to establish a molecular basis to determine what protein conformational changes, if any, are involved in these processes and how they lead to the formation of aggregates. The approach used is based on hydrogen-deuterium exchange mass spectrometry (HX-MS). The method depends on the fact that amide hydrogens on the protein backbone are exchangeable for deuterium to an extent that depends on their exposure to the solvent. Amide hydrogens associated with residues that are completely exposed to the solvent exchange quickly, while others associated with buried residues exchange very slowly or not at all. The method can be used either to differentiate between native and unfolded species based on the total deuterium content, or to determine local unfolding by performing MS following digestion of the protein and establishing which peptides along the protein backbone had greater deuterium content and, thus, became more solvent exposed. As recently reviewed by Brock [47] and Iacob and Engen [48], the method has been used extensively to study protein stability in solution in response to various factors including glycosylation [22], oxidative stresses [49], freeze-thaw stresses [50], and salt type and concentration of additives commonly used in formulation [51][52].

HX-MS has also been proposed as a tool for screening protein stability in chromatography and a general protocol has been presented by Fogle and Fernandez [53] for this purpose. Applications of this approach to chromatography have thus far focused primarily on hydrophobic stationary phases. Jones and Fernandez [54], for example, used HX-MS to elucidate the two-peak elution behavior exhibited by α-lactalbumin on a SOURCE Phenyl HIC column. Whole protein HX-MS was used to differentiate between native and unfolded forms in the two peaks and MS following proteolytic fragmentation of the eluted protein was used determine the stability of different domains in the protein tertiary structure. Fogle et al. [39] and Xiao et al. [55] extended this work to different HIC resins with varying hydrophobicity using whole protein HX-MS to determine the effects of protein load and kosmotrope concentration of the stability of bound apo-α-lactalbumin. Stability of this protein, as measured by differences in solvent accessibility, was found to increase dramatically with protein load and was nearly undetectable when the stationary phase was nearly completely saturated. The results were used to develop a thermodynamic framework to describe surface and kosmotrope effects on protein conformation. Stability of other proteins, including α-chymotrypsinogen A, α-lactoglobulin B, holo-α-lactalbumin, bovine β-lactoglobulin, and human serum albumin was also studied using HX-MS on a variety of HIC stationary phases by Deitcher et al. [56] and Gospodarek et al. [57].

Despite the many HX-MS studies on protein stability in HIC, only recently has HX-MS been used to elucidate protein stability in stationary phases for ion exchange chromatography. Gillespie et al. [17] used whole-protein on-column HX-MS to differentiate between native and unfolded forms of their aglycosylated IgG1 antibody eluting from a Fractogel EMD SO3- CEX column. Their HX-MS results confirmed that species present in the late eluting peak, which comprised a mixture of monomeric and aggregated mAb, experienced more solvent exposure

while bound to the column than the species the early eluting peak, suggesting that conformational changes were induced by interactions with the CEX resin. However, since only the global deuterium content was determined, detailed information about local unfolding with peptide-level structural resolution could not be obtained.

In this chapter, we apply HX-MS coupled with proteolytic fragmentation to understand the mechanisms leading to the two-peak elution behavior of a pure glycosylated antibody on the CEX resin Fractogel EMD SO3- described in Chapter 2. Our first objective is to determine the conformation of the species eluted from the CEX column relative to the native protein. For this purpose, size exclusion chromatography is used to separate aggregates and monomers from fractions collected from the two CEX peaks. The separated species are then labeled with D_2O, proteolytically digested, and then subjected to MS analysis to determine changes in solvent exposure relative to the native protein. Our second objective is to determine the conformation of the mAb bound to the resin by performing on-column hydrogen-deuterium exchange, followed by elution, proteolytic digestion, and MS.

3.2. Materials and Methods

3.2.1. Materials

The cation exchange resin, Fractogel EMD SO3- (M), used in this work was from EMD Millipore (Darmstad, Germany). The monoclonal antibody used was provided by Amgen (Seattle, WA, USA). Both the resin and the mAb are the same as those used in Chapter 2. The Fractogel resin is “tentacle” type, containing charged polymeric surface extenders designed to facilitate interactions with the protein. The mAb is a glycosylated IgG2 antibody with molecular mass ~150 KDa and a pI of 8.7 theoretically calculated based on its amino acid sequence.

Porcine pepsin, Sodium acetate, sodium sulfate, ethanolamine were purchased from Sigma-Aldrich (St. Louis, MO, USA). Acetic acid, sodium chloride, potassium phosphate, ammonium sulfate, sodium citrate, sodium cyanoborohydride, ethylenediaminetetraacetic acid (EDTA), citric acid, formic acid, and trifluoroacetic acid (TFA) were purchased from Fisher Scientific (Houston, TX, USA). Guanidine hydrochloride (GdnHCl) was purchased from MP Biomedicals (Solon, OH, USA). Tris(2-carboxyethyl)phosphine hydrochloride (TCEP) was purchased from Thermo Scientific (Rockford, IL, USA). Deuterium oxide was purchased from Cambridge Isotope Laboratories, Inc. (Andover, MA, USA). All experiments were conducted at room temperature (22±2 ℃) unless otherwise indicated.

3.2.2. Methods

3.2.2.1. Chromatographic experiments

All chromatography runs were conducted using an AKTA Explorer 10 unit from GE Healthcare (Piscatawy, NJ, USA). The resin was packed in a 0.5 cm × 5 cm Tricorn column from GE Healthcare (Piscataway, NJ, USA) with an actual packed bed volume of 0.982 mL as described in Chapter 2. The column was first equilibrated with 5 column volumes (CVs) of loading buffer (40 mM $NaCH_3COO$ adjusted to pH 5.0 with acetic acid) and then loaded with 0.5 mL of 6 mg/mL mAb. After loading, the flow was stopped and the column was held idle for 1000 min. Two CVs of loading buffer were then supplied followed by a two-step elution protocol comprising first a step from 0 to 0.33 M NaCl, also in 40 mM $NaCH_3COO$, followed by a second step to 1 M NaCl. UV absorbance at 280 nm and conductivity were monitored and 1-mL effluent samples collected for offline analyses using a model Frac-900 fraction collector from GE Healthcare (Piscataway, NJ, USA).

3.2.2.2. Collection of mAb samples for HXMS analysis in solution

Figure 3.1 shows the procedure used to generate samples for HX-MS analysis obtained from a single CEX two-step elution run. Two 1-mL fractions were collected at 4.1 and 13.7 CV, respectively, as shown in the top panel of Fig. 3.1 and each was concentrated to about 1 mg/mL with 10 kDa microcentrifuge filter tubes from Millipore Corporation (Billerica, MA, USA). Each CEX fraction was then separated by size exclusion chromatography (SEC) using a 30 cm × 0.78 cm Yarra 3u 3000 SEC obtained from Phenomenex (Torrance, CA, USA) with an AKTA Explorer 10 unit from GE Healthcare (Piscataway, NJ, USA). For this purpose 500 μL samples of the CEX fractions were injected into the SEC column and eluted at 1 mL/min in 40 mM $NaCH_3COO$ at pH 5.0. Fractions were collected from the SEC runs at 6.7 and 8.7 mL as indicated in Fig. 3.1, corresponding, respectively, to the elution of aggregated and monomeric species, and concentrated to about 1 mg/mL by ultrafiltration with 10 kDa micrcentrifuge tubes. Batch dynamic light scattering (DLS) analyses conducted according to the procedure described in Chapter 2 gave hydrodynamic radii of 5.2 ± 0.1 and 8.6 ± 0.3 nm, respectively, for the late and early SEC peaks. Virtually identical radii were obtained before and after ultrafiltration. In total, four mAb samples were thus obtained:

(A) A sample containing the monomer present in CEX fraction 1 eluting in 0.33 M from the Fractogel column, referred to as the “early eluting monomer”;

(B) A sample containing the monomer present in CEX fraction 2 eluting in 1 M NaCl from the Fractogel column, referred to as the “late eluting monomer”;

(C) A sample containing the aggregates present in CEX fraction 2 eluting in 1 M NaCl from the Fractogel column, referred to as the “late eluting aggregates”; and

(D) A sample obtained by dissolving 1 mg/mL of the mAb without contact with the Fractogel resin in 40 mM $NaCH_3COO$ at pH 5.0, referred to as the “native monomer”.

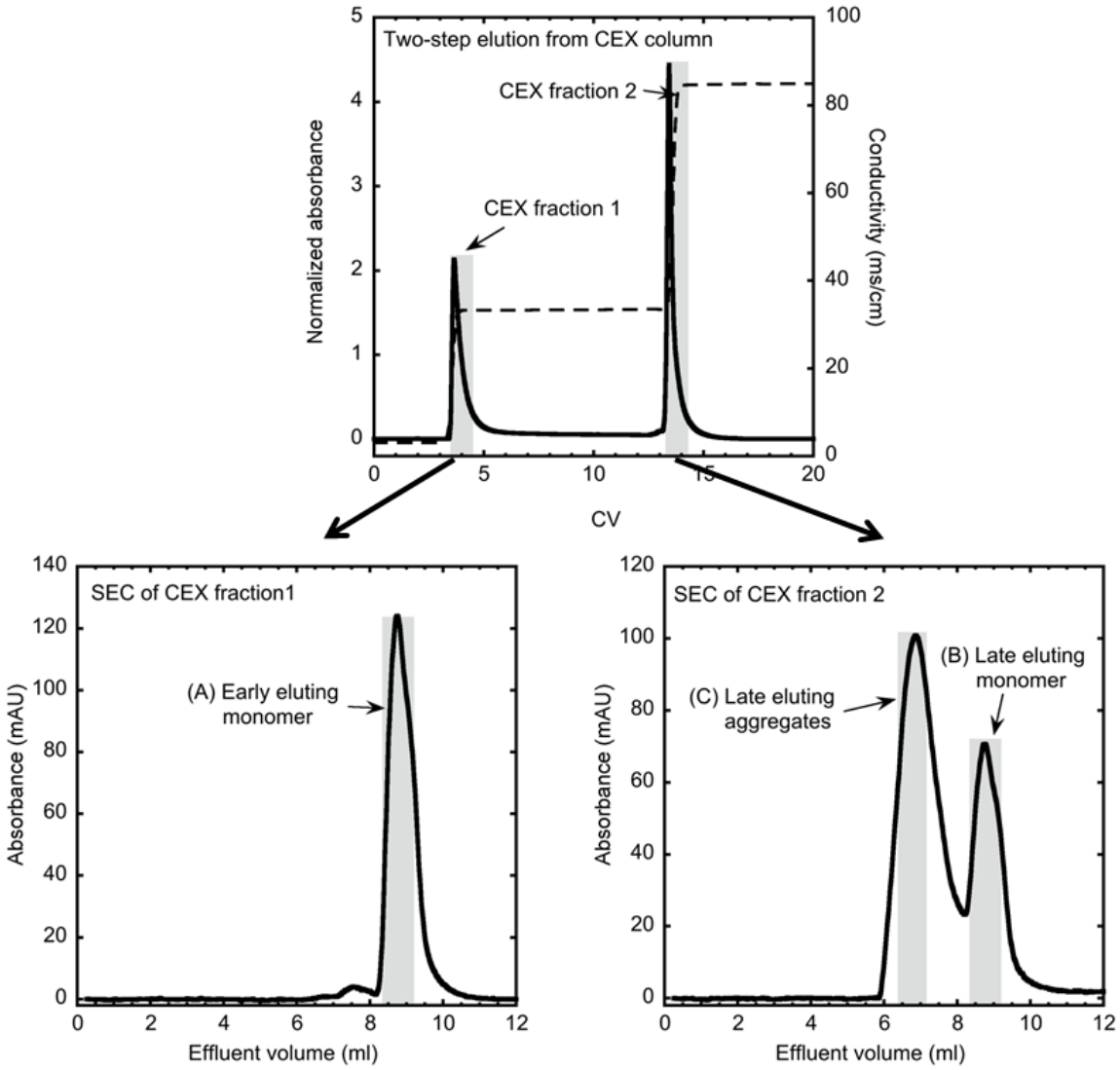

Figure 3.1. Two-step elution of the mAb loaded on the Fractogel column (top panel) and SEC analyses of the eluted fractions (bottom panels). Load was 0.5 mL of 6 mg/mL mAb in 40 mM $NaCH_3COO$ at pH 5.0. After loading, the flow was stopped and the column was held idle for 1000 min. Elution was first with 0.33 M NaCl and then with 1 M NaCl in 40 mM $NaCH_3COO$ at pH 5.0. The percentages of the loaded protein eluted in 0.33 and 1 M NaCl were 40 and 60%, respectively. See text for SEC conditions. Shaded areas show the fractions collected.

3.2.2.3. HXMS analysis of eluted samples

The four mAb samples outlined in Section 3.2.2.2 were prepared for HX-MS analysis according to the following protocol adapted from Gospodarek et al. [57]. For this purpose, a 20-μL volume of each mAb sample was mixed with 180 μL of D_2O containing 40 mM $NaCH_3COO$ at pH 5.0 (the pH value for D_2O buffer was directly from pH meter reading without correction for the deuterium isotope effect). After a predetermined labeling time, the solution was chilled in an ice batch and mixed with 50 μL of ice-chilled 150 mM potassium phosphate at pH 1.5 to bring the pH down to 2.6 and quench the hydrogen-deuterium exchange [58]. 100 μL of 8 M GdnHCl containing 100 mM TCEP and 25 mM EDTA at pH 2.6 were then added in order to aid the subsequent pepsin digestion step. Finally, after 2 min in the ice bath, 200 μL of a solution containing 95% water, 5% ACN, 0.1% formic acid, and 0.01% TFA at pH 2.6 was added bringing the GdnHCl concentration down to approximately 1.5 M.

A 500 μl volume of each mAb sample prepared as described above was loaded into a sample loop and pumped into an immobilized pepsin column at 0.1 mL/min with a Series I pump from Lab Alliance (Syracuse, NY, USA). The pepsin column was prepared according to the method of Wang et al. [59], by first immobilizing pepsin on an Applied Biosystems POROS-20AL resin (obtained from Life Technologies, Grand Island, NY, USA). For this purpose, 25 mg of pepsin were dissolved in 4 mL of 50 mM sodium citrate at pH 4.4. 0.66 mL of 1 M sodium cyanoborohydride were then added, followed by the slow addition of 2.3 mL of 1.5 M sodium sulfate. A 1.4 g sample of the POROS-20AL resin was added, followed by the addition of 4.6 mL of 1.5 M sodium sulfate with a syringe pump at a rate of 2.3 mL/hr. The resin suspension was then incubated at 4 ℃ for 17 h with gentle agitation. 1 mL of 0.1 M ethanolamine was then added to quench the reaction. After incubating the solution for another 5 h, the residual free

pepsin was removed by first washing with 50 mL of 50 mM sodium citrate at pH 4.4, then with 20 mL of 1 M NaCl in 50 mM sodium citrate at pH 4.4, followed by adding 50 mL of 50 mM sodium citrate at pH 4.4. The POROS resin containing the immobilized pepsin was packed in two 0.21 cm x 3.0 cm HPLC columns by suspending the resin in 50 mL of 50 mM sodium citrate at pH 4.4 to form a 50:50 slurry and pumping the slurry into the column at flow rates increasing gradually over about 20 min from 0.5 mL/min until the pressure reached 48 bar. The two columns prepared in this manner were connected in series to improve digestion efficiency.

The effluent from the pepsin columns flowed directly into a 0.1 cm x 0.8 cm C8 reversed phase chromatography column from Michrom BioResources (Auburn, CA, USA) in order to capture and desalt the peptides. After 9 min, the bound peptides were eluted with an acetonitrile gradient delivered by a Surveyor MS pump from Thermo Finnigan (San Jose, CA, USA) at 0.1 mL/min into a 0.21 cm x 10 cm Kinetex C18 column from Phenomenex (Torrance, CA, USA), connected in series with the C8 capture/desalting column, in order to separate the peptides formed by pepsin digestion. Two different gradients were used for elution. A long gradient from 5 to 40% ACN in 31 min followed by a 5 min gradient to 90% ACN was used for peptide identification in blank runs without hydrogen exchange. A shorter gradient from 30% ACN to 60% ACN in 17 min followed by a 2 min gradient to 90% ACN was used to determine the extent of hydrogen-deuterium exchange for the peptides identified. The shorter time was used to minimize deuterium-hydrogen back exchange.

The peptides eluted from the C18 columns were sent directly to an LTQ linear ion trap mass spectrometer from Thermo Finnigan (San Jose, CA, USA). Data were collected in a positive ion, profile mode with an ESI voltage of 4.3 kV, a capillary temperature of 250°C, and sheath gas flow rate of 15 units. Peptide matching was done using Proteome Discoverer software

from Thermo Scientific (Rockford, IL, USA) based on the amino acid sequence of the mAb provided by Amgen (Seattle, WA, USA). 240 peptides providing 78% coverage of the known sequence, were identified by the Proteome Discoverer software as candidate reporter peptides. HDExaminer software from Sierra Analytics (Modesto, CA, USA) was then used to select peptides with high signal-to-noise from the short gradient run as the final reporter peptides. Ultimately, 29 peptides providing 49% coverage of the mAb sequence were selected as the final reporter peptides.

A statistical analysis of the MS results was done following the method outlined in Houde et al. [22] in order to determine the confidence limits of the determination of differences in peptide mass between a sample and the corresponding reference. For this purpose, three replicate experiments were done with a 10 min labeling time giving a 99% confidence limit of ±0.43 Da.

3.2.2.4. HXMS analysis of bound protein

Batch adsorption experiments were used to determine whether conformational changes resulting in altered solvent exposure occur while the protein is bound to the Fractogel resin. For this purpose, a 10-mg sample of resin was incubated for 1000 min with 200 μL of a 40 mM $NaCH_3COO$ solution at pH 5.0 with initial mAb concentration of 0.5 mg/mL (corresponding to 10 mg of protein per g of resin) in a 2 mL microcentrifuge filter tube agitated at 300 rpm for on a Model Lab Companion SI-300 orbital shaker (Gasan-Dong, Geumcheon-Gu, Seoul, Korea) and then centrifuged at 5000 rpm for 1 min to remove the extraparticle liquid. Since, as shown in Chapter 2, protein binding is extremely favorable for these conditions, most of the mAb initially in solution (> 98%) was bound to the resin as indicated by mass balance using the initial and final UV absorbance of the supernatant. The bound protein was then desorbed batch-wise in two steps by first adding 0.33 M NaCl in 40 mM $NaCH_3COO$ at pH 5 and equilibrating for 45 min

and then adding 1 M NaCl in the same buffer also for 45 min. As shown in Chapter 2, for these conditions approximately 70% of the total protein bound is desorbed in the first step while the remaining 30% is desorbed in the second. These percentages were shown to be consistent with the column gradient and two-step elution results for comparable hold times and local protein loads. In order to generate a control sample, the same procedure was repeated by incubating resin and protein for 30 min instead of 1000 min, which would result in essentially all of the protein eluting in 0.33 M NaCl.

HX-MS analyses were conducted for these two resin-bound protein samples as follows. After the incubation period, 10 μL of 40 mM $NaCH_3COO$ at pH 5 in H_2O and 90 μL 40 mM $NaCH_3COO$ at pH 5 in D_2O were added to the resin in the microcentrifuge filter tube and mixed for different periods of time. 25 μL of ice-cold quench buffer (150 mM potassium phosphate at pH 1.5) was then mixed with the resin, which was then centrifuged at 8900 rpm for 30 s to remove the liquid. 100 μL of the dissociation buffer (8 M GndHCl, 100 mM TCEP, 25 mM EDTA, at pH 2.6) was then added to the resin and mixed under ice for 2 min during which most of the protein (>90%) was desorbed. Finally, the desorbed protein was collected by centrifuging at 8900 rpm for 30 s in a new microcentrifuge tube, mixed with 450 μL of a solution containing 95% water, 5% ACN, 0.1% formic acid, and 0.01% TFA at pH 2.6, fragmented by pepsin digestion, separated by HPLC, and analyzed by MS as described in Section 3.2.2.3.

3.3. Results

Table 3.1 provides a listing of the 29 reporter peptides identified in this work, which cover 49% of the actual mAb sequence. Greater coverage could be obtained by using a longer gradient capable of greater resolution. However, a longer gradient also results in greater hydrogen-deuterium back exchange, which would compromise the determination of unfolded

regions. In order to obtain an estimate of the location of these peptides in the protein structure, we followed the homology modeling approach of Majumdar et al. [51] using human IgG1 (Protein Data Bank entry 1HZH) as a template. Because of the high degree of primary amino sequence homology of human IgG subclasses [60], nearly all of the reporter peptides could be aligned with this structure. A coverage map showing the reporter peptides relative to the mAb template visualized using PyMOL software (Schrodinger LLC, Portland, OR, USA) is shown in Fig. 3.2. Although the structure shown is only an approximation, 24 of the 29 reporter peptides could be aligned. As seen in Fig. 3.2, all three mAb domains are represented by the reporter peptides so that meaningful structural information can be obtained despite the modest degree of coverage.

Table 3.1. Reporter peptides identified in short gradient HPLC-MS. Residues from 1 to 215 are from the light chain of the antibody, and those from 216 to 659 are from the heavy chain. The peptides cover 49% of the sequence.

Peptide	Start	End	Sequence
1	34	47	LAWHQQKPGQAPRL
2	76	84	ISRLEPEDF
3	117	126	FIFPPSDEQL
4	137	144	LNNFYPRE
5	145	162	AKVQWKVDNALQSGNSQE
6	163	179	SVTEQDSKDSTYSLSST
7	220	232	LESGGGLVQPGGS
8	247	251	YVMSW
9	251	261	WVRQAPGKGLE
10	262	274	WVSSISGSGLGSY
11	275	283	YADSVKGRF
12	284	294	TISRDNSKNTL
13	299	308	RSLRAEDTAV
14	362	371	VKDYFPEPVT
15	372	390	VSWNSGALTSGVHTFPAVL
16	401	413	VVTVPSSNFGTQT
17	454	464	LFPPKPKDTLM
18	478	489	VSHEDPEVQFNW
19	519	530	TVLHQDWLNGKE
20	531	545	YKCKVSNKGLPAPIE
21	561	577	YTLPPSREEMTKNQVSL
22	569	577	EMTKNQVSL
23	581	588	VKGFYPSD
24	593	610	WESNGQPENN
25	603	610	YKTTPPML
26	611	616	DSDGSF
27	617	622	FLYSKL
28	623	635	TVDKSRWQQGNVF
29	643	658	ALHNHYTQKSLSLSPG

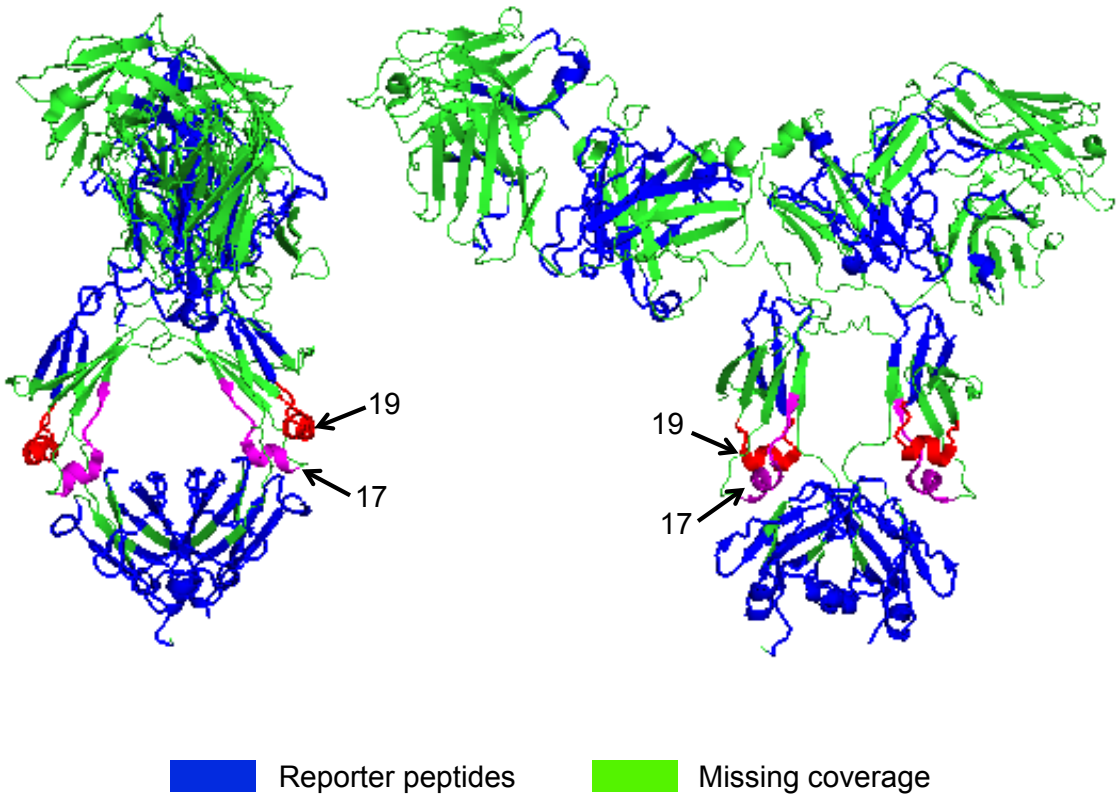

Figure 3.2. Three-dimensional coverage map of reporting peptides identified in short gradient HPLC-MS runs. The mAb structure is obtained by homology modeling using human IgG 1 (1HZH in the Protein Data Bank) as a template. The blue regions in both views show the location of the 24 of the 29 reporter peptides covering 49% of the sequence, which were found in the 1 HZH structure. Green regions represent the missing coverage. Peptides 17 and 19, shown in magenta and red, respectively, exhibited the greatest differences in hydrogen-deuterium exchange between late eluting aggregate and an unfolded intermediate relative to the native protein.

Figure 3.3 shows a mass difference plot for the 29 reporter peptides based on solution HX-MS with a 10 min labeling time comparing the early eluting monomer (sample A) to the native mAb (sample D). The dashed lines represent the 99% confidence limits on the mass difference values. A seen from these data, none of the reporter peptides exhibit a significant

difference in mass suggesting that the early eluting monomer and the native mAb have the same conformation. This result is, of course, expected since, as shown in Chapter 2, the elution behavior of the early eluting monomer was the same regardless of the hold time and of the percentage of protein that eluted at high salt. Figure 3.4 compares the mass differences of the reporter peptides for the late eluting monomer (sample B) with those of the native monomer (sample D). Although some slight differences are seen, none of these differences are significant at 99% confidence level with either 2 or 10 min labeling time. This result suggests that the late eluting monomer has the same conformation as the early eluting and native monomer species.

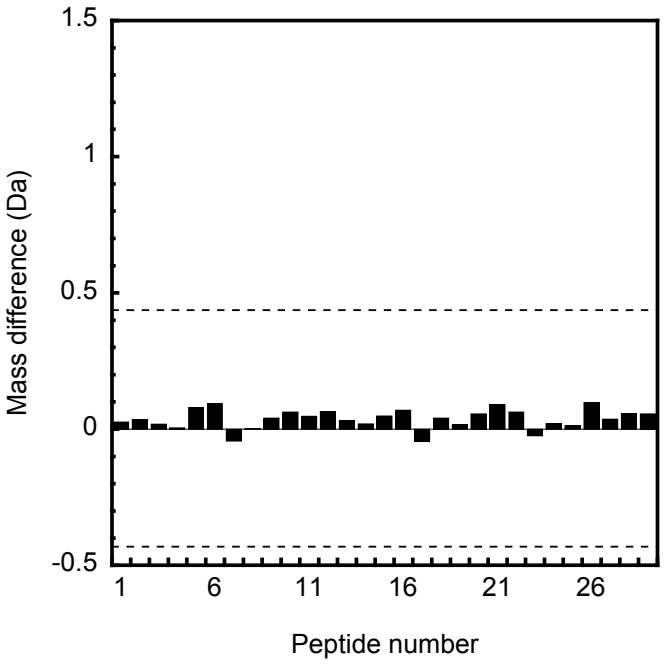

Figure 3.3. Difference between the masses of the 29 reporter peptides in the early eluting monomer (sample A) and those in the native monomer (sample D) with a 10 min labeling time. The dashed lines represent the 99% confidence limit for the mass difference values. The horizontal axis represents the peptides numbers, which are sorted in ascending number based on the midpoint of their sequences. Positive vertical bars suggest increased solvent exposure in early-eluted monomer compared with native monomer, and negative vertical bars suggest decreased solvent exposure.

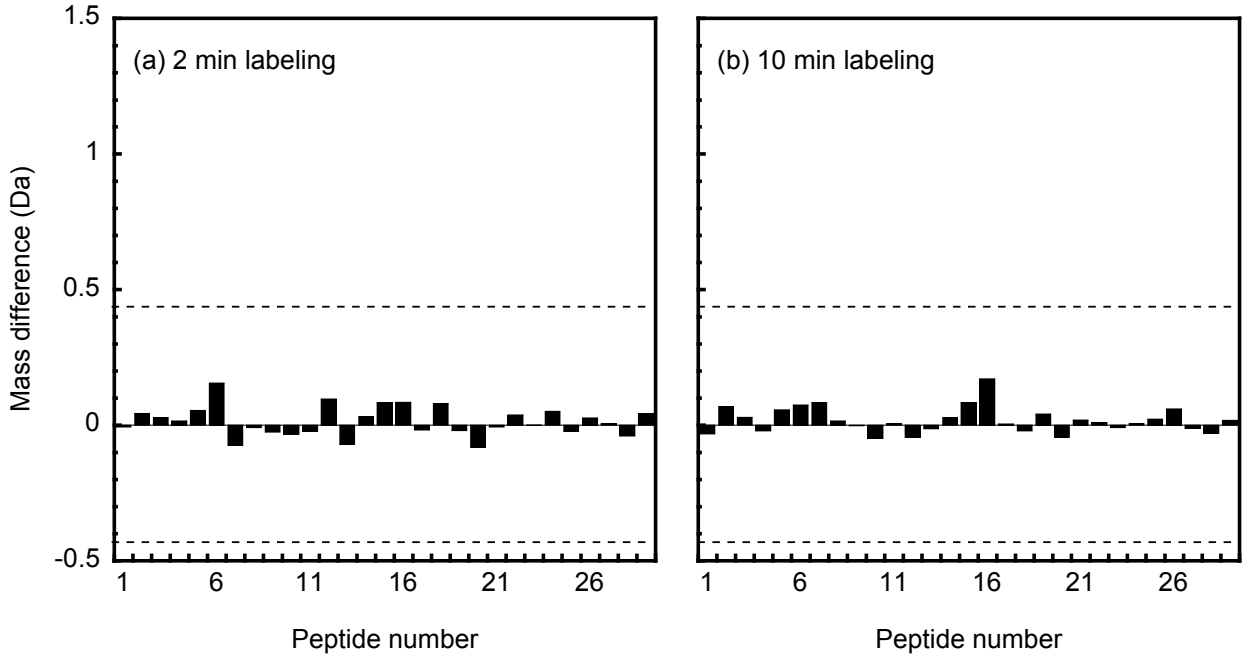

Figure 3.4. Difference between the masses of the 29 reporter peptides in the late eluting monomer (sample B) and those in the native monomer (sample D) with (a) 2 min labeling time, and (b) 10 min labeling time. The dashed lines represent the 99% confidence limit for the mass difference values. The horizontal axis represents the peptides numbers, which are sorted in ascending number based on the midpoint of their sequences.

Figure 3.5 compares the mass differences of the reporter peptides for the late eluting aggregates (sample C) with those of the native monomer (sample D). Although many of the peptides appear to exhibit a mass increase, which would indicate increased solvent exposure and, thus, localized unfolding, two, in particular, peptides 17 and 19, exhibit differences that are clearly significant at the 99% confidence level. The increased mass suggests that the aggregates are comprised of locally unfolded protein. Interestingly, none of the peptides exhibit statistically significant solvent protection (which would be characterized by a negative mass difference larger than the 99% confidence limit) indicating that the aggregates are likely to be relative loose

structures. As seen in Fig. 3.2, peptides 17 and 19 happen to be in the Fc region of the mAb. We do not know the specific reasons why this is the case, but other authors [3][61][62][63] have also found that the Fc fragment of different IgGs is, for example, more sensitive to low pH denaturation, indicating that this region may be intrinsically less stable and, therefore, more susceptible to conformational changes caused by binding to the CEX resin.

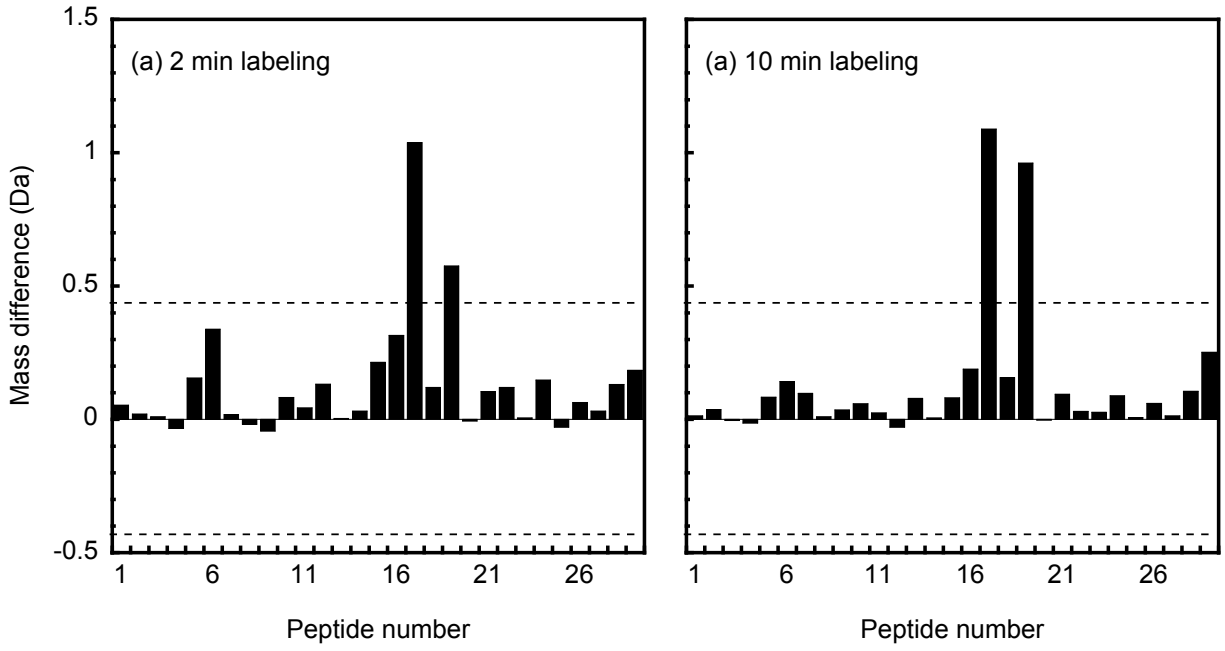

Figure 3.5. Difference between the masses of the 29 reporter peptides in the late eluting aggregates (sample C) and those in the native monomer (sample D) with (a) 2 min labeling time, and (b) 10 min labeling time. The dashed lines represent the 99% confidence limit for the mass difference values. The horizontal axis represents the peptides numbers, which are sorted in ascending number based on the midpoint of their sequences.

Some additional insight about the unfolding behavior affecting peptides 17 and 19 can be obtained from the data in Figs. 3.6 and 3.7. Figure 3.6 shows the mass gain due to deuterium uptake by the two peptides as a function of labeling time for the native monomer (sample D) and

for the late eluting aggregates (sample C). It can be seen that it takes only about 2 to 10 min of labeling time for either peptide to exchange two hydrogens for deuterium when they in aggregate form, while it takes between 50 and 120 min when they are in monomer form, suggesting that these two peptides are highly solvent exposed in the aggregates compared to native monomer. Figure 3.7 shows the mass gain due to deuterium exchange of peptides 17 and 19 in the late eluting aggregates as a function of the time elapsed since collection of the fractions from the CEX column, compared to the values for the same peptides in the native monomer. In Fig. 2.4b of Chapter 2, using DLS, we showed that the late eluting aggregates are relatively unstable, partially reversing to monomer, with a concomitant decrease in average hydrodynamic radius, over long time scales (order of 100's of seconds). The change in deuterium uptake as a function of collection time follows the same qualitative trend as the change in hydrodynamic radius and over the same time scale suggesting that the aggregates slowly refold to the native monomer conformation as they reverse to monomer. By comparison, the monomer was virtually indefinitely stable once place in solution.

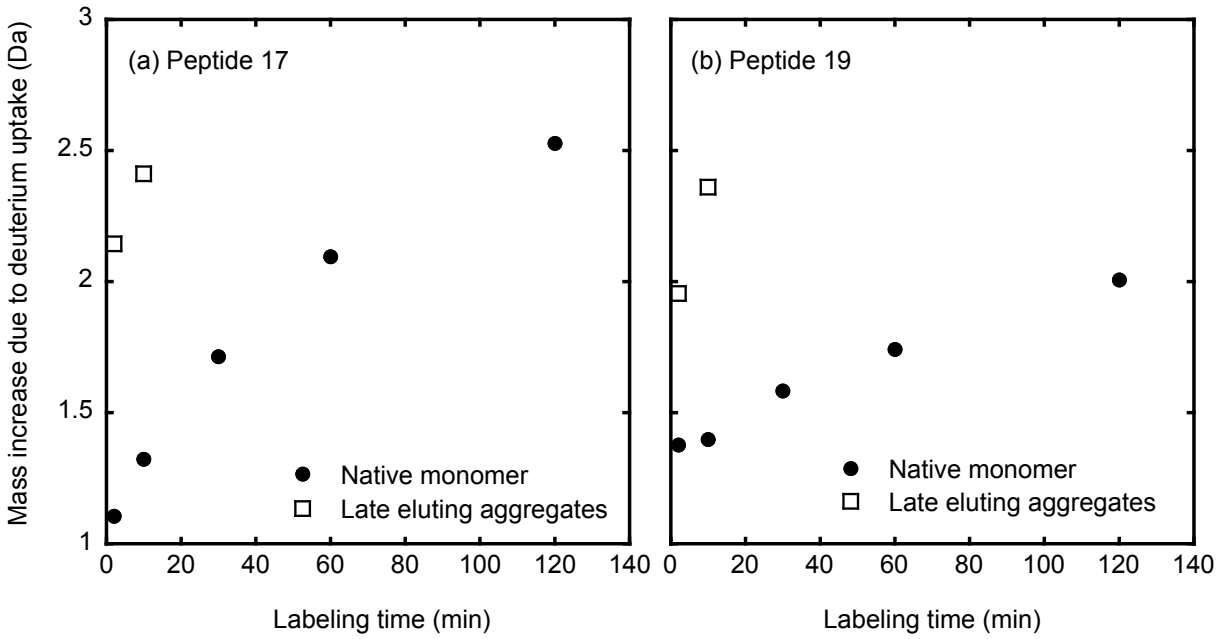

Figure 3.6. Mass increase of peptides 17 (a) and 19 (b) as a function of labeling time for native monomer (sample D) and late eluting aggregates (sample C).

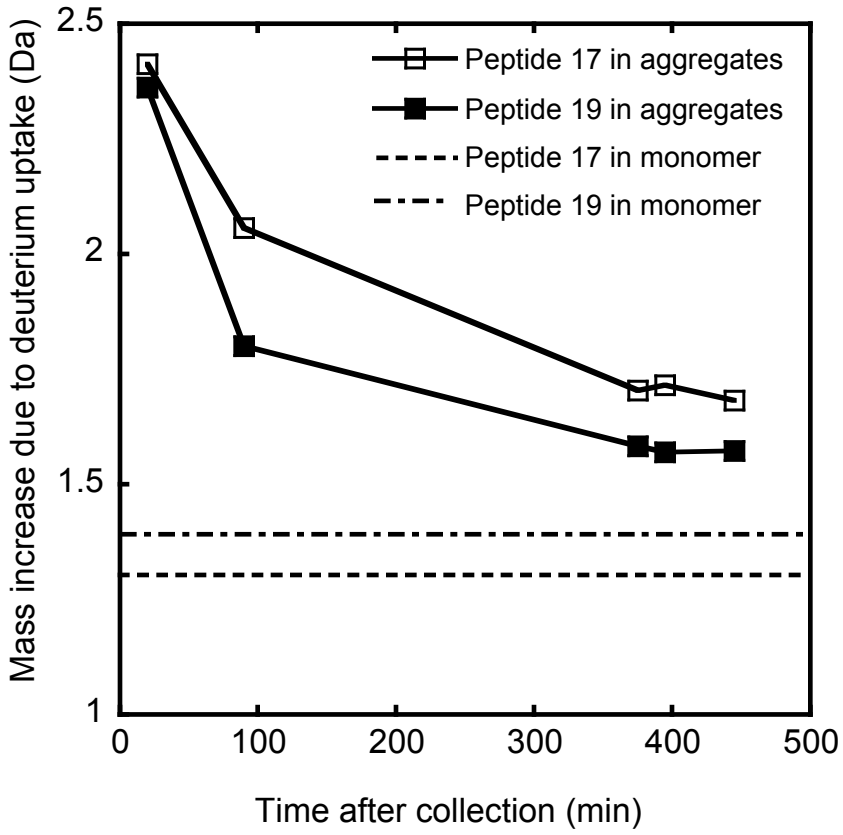

Figure 3.7. Mass increase of peptides 17 and 19 as a function of time after collection from the CEX column for late eluting aggregates using a 10 min labeling time.

Figure 3.8 shows the results for HX-MS for the protein labeled while in the bound state according to the procedure in Section 3.2.2.4. The figure compares the results obtained for the protein that remained bound following 0.33 M NaCl desorption with a 1000 min hold time and those obtained when the protein was adsorbed for just 30 min. As shown in Chapter 2, 30 min is not sufficient to generate a significant percentage of late eluting protein. Thus, it seems reasonable to assume that the 30 min-hold sample is representative of protein bound in its native conformation. The comparison shows that several peptides had increased solvent accessibility indicating that local unfolding occurred. Peptide 19, in particular, has a relatively large mass increase which is significant at the 99% confidence level. This peptide is also among those that

showed the greatest mass difference for the late eluting aggregates subject to hydrogen-deuterium exchange in the solution phase. This similarity suggests that the late eluting aggregates are related to the unfolded species that exists in the bound state after 1000 min of incubation. Interestingly, none of the peptides in the bound protein exhibited a statistically significant negative mass difference indicating that any unfolding that occurred when the protein was held for a long time in the bound state did not result in increased solvent protection, which one might have expected since the unfolded species is much more tightly bound than the native monomer.

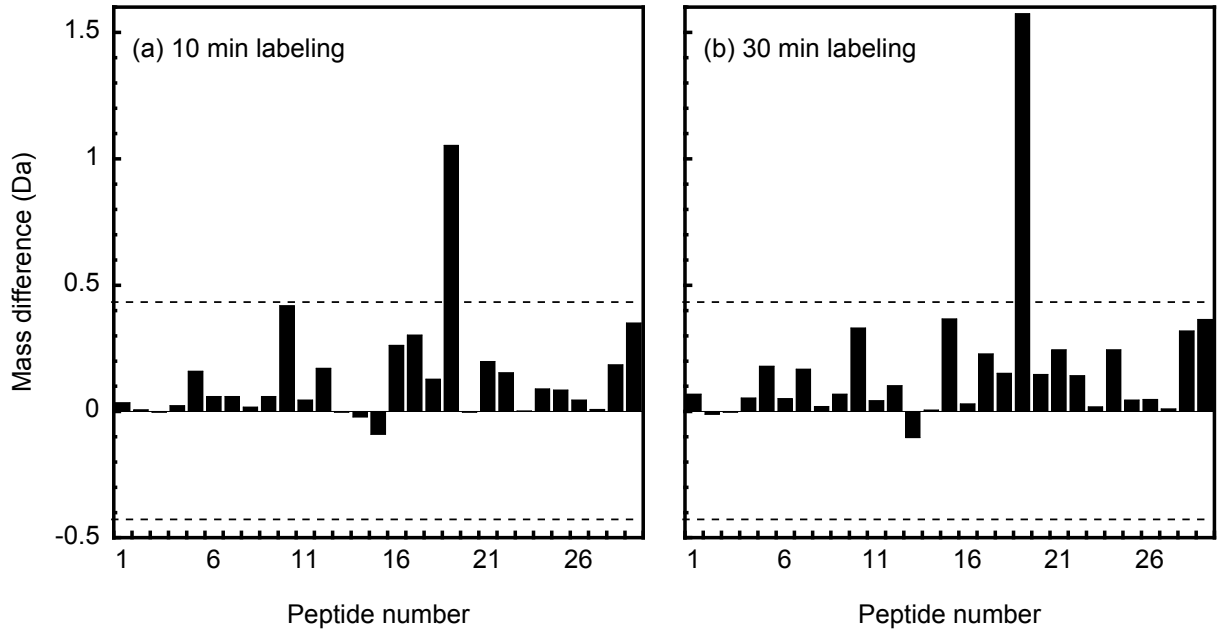

Figure 3.8. Difference between the masses of the 29 reporter peptides for the bound protein held on the resin for 1000 min and those for the bound protein held on the resin for 30 min with 10 min (a) and 30 min (b) labeling time. The dashed lines represent the 99% confidence limit for the mass difference values. The horizontal axis represents the peptides numbers, which are sorted in ascending number based on the midpoint of their sequences. Positive vertical bars suggest increased solvent exposure in 1000 min hold time protein sample compared with 30 min hold time protein sample, and negative vertical bars suggest decreased solvent exposure. The 30 min hold time did not result in a significant percentage of late eluting protein.

3.4. Discussion

In Chapter 2, it was hypothesized that the two-peak elution behavior exhibited by a glycosylated IgG1 monoclonal antibody on a tentacle-type Fractogel CEX column was caused by the resin-catalyzed formation of a strongly-bound unfolded intermediate. Upon elution with a linear salt gradient to 1 M NaCl or with two salt steps, the first to 0.33 M and the second to 1 M

NaCl, the protein was to shown to elute in two different forms – an early eluting monomer and a late eluting mixture of monomeric and aggregated forms. HX-MS with peptide level resolution was performed in this work in order to identify the nature of the eluted species with regards to varied solvent exposure and, thus, local unfolding, caused by binding, hold, and elution steps. The HX-MS results show that the early eluting monomeric species are consistent with the native monomer structure. Their elution behavior is the same regardless of the hold time, even though the proportion of early eluting species decreases as the hold time (i.e. the time the protein spends bound to the resin) increases. The monomeric species co-eluting with aggregates in the late eluting fraction are also consistent with the native protein in terms of solvent exposure. On the contrary, the aggregate species in this fraction exhibit substantially greater localized solvent exposure. The key question is now why do we find native-like monomeric species in the late eluting fraction? Comparing HX-MS results for the bound protein following elution of the more weakly retained native-like fraction provides the answer. It appears that an unfolded intermediate is indeed formed on the resin over relatively long times. As shown in Chapter 2, this unfolding appears to occur as the protein migrates during the hold step from regions of the particle where the initial bound protein concentration is close to saturation to regions where the bound protein concentration is zero. As this occurs a fraction of the protein unfolds, likely because of interactions with the resin's tentacles, which are strongest at the lowest extent of surface coverage, forming a strongly-bound unfolded intermediate. Upon further increasing the salt concentration the unfolded intermediate is rapidly desorbed either refolding to a native-like structure or forming aggregates. Since the peptides that were identified to have the greatest of solvent exposure, as measured by HX-MS, are the same for the fraction of protein that strongly bound to the resin as for the aggregates, we can conclude that the aggregates are directly related

to the unfolded intermediate. Interestingly, we found no evidence that a monomeric species with the same pattern of unfolding as the unfolded intermediate is present in any of the eluted fraction, indicating that, upon desorption, the unfolded intermediate follows two rapid parallel paths – refolding to the native structure and aggregate formation. Figure 3.9 shows the mechanism that is consistent with our comprehensive observations for the load conditions used in this work. It should be noted, however, that, as shown in Chapter 2, increasing the salt concentration or increasing the pH during load, will decrease the strength of protein binding and, thus, likely reduce the extent of unfolding during the hold step.

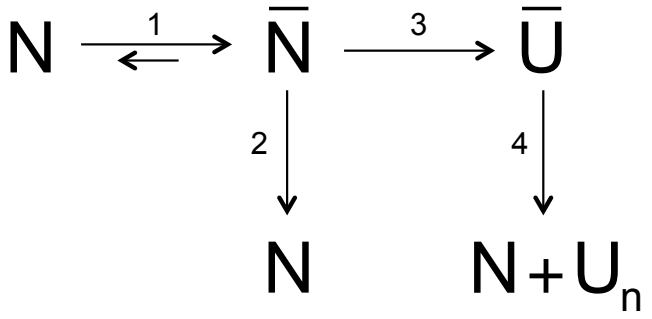

Figure 3.9. Mechanism leading to two-peak elution behavior. N, U, and U_n represent native, unfolded, and aggregated forms of the mAb. Overbars denote resin bound species. Step 1 is the diffusion-controlled adsorption of the native mAb. Step 2 is desorption of the native mAb at intermediate salt concentrations. Step 3 is the slow, surface-catalyzed unfolding of the mAb leading to an unfolded intermediate. Step 4 is desorption in high salt leading to elution of a mixture of refolded and aggregated species.

3.5. Conclusions

HX-MS studies with peptide level resolution confirm that an unfolded intermediate that is strongly held by the Fractogel resin is responsible for the two-peak elution behavior and for the formation of on-column generated aggregates when a glycosylated mAb is bound at low salt concentrations and eluted with either a slat gradient or with two salt steps at increasing salt concentrations. The strongly bound intermediate has a pattern of unfolding consistent with that of the aggregates, but no monomeric species in the eluted fraction are found to have the same pattern indicating that upon desorption from the resin the intermediate either refolds or forms aggregates leading to a late-eluting peak that is a mixture of the two. Two peptides of the mAb were identified as being more solvent exposed than the native protein in both the bound unfolded intermediate and in the aggregates. Based on homology modeling using the known structure of a model human antibody as a template, both peptides were found to be in the Fc region of the mAb, seemingly corresponding to α-helical elements. One issue that chapter 2 and 3 do not allow to resolve is whether the tentacles cause unfolding through specific interactions or whether they just increase the strength of protein binding. We are going to explore a broader range resins and load conditions in Chapter 4 to answer this question.

Chapter 4

Effects of resin type, load buffer, and protein stability

4.1. Introduction

In Chapter 2 and Chapter 3, we reported a two-peak elution behavior of a glycosylated IgG2 on a Fractogel SO3 (M) column. In our study, we found that the percentage of the protein that eluted late was higher when the initial protein binding strength was greater, which occurred either at a lower pH or at a lower salt concentration, when the hold time between load and elution steps was longer, when the protein load was smaller, and when the load flow rate was higher. The late eluting peak was found to be a mixture of monomers and higher molecular mass species that appeared to be fairly stable over long periods of time. The CEX resin structure was also found to affect this behavior. For example, while the "tentacle type" Fractogel SO3 resin gave a strong two-peak elution behavior, only one peak eluted from a macroporous CEX resin without tentacles (UNOsphere Rapid S) for otherwise identical conditions. Confocal laser scanning microscopy (CLSM) observations of protein binding in individual resin particles revealed that protein binding in the Fractogel and UNOsphere resins occurred by different mechanisms. While the bound protein remained immobilized in an area near the outer edge of the UNOsphere particles during the hold step after partial loading of the resin, the protein appeared to retain diffusional mobility after binding on the Fractogel resin, which resulted in a redistribution of the protein throughout particle prior to elution. This redistribution resulted in a low local bound protein concentration, which, in turn, was shown to facilitate protein conformational changes. Hydrogen-deuterium exchange mass spectrometry (HX-MS) coupled with proteolytic fragmentation was used to determine the conformation changes involved in this

process. The results showed that a strongly-bound unfolded intermediate, characterized by greater solvent exposure of residues in the Fc region of the mAb, was formed gradually as a function of time following binding to the Fractogel resin. During elution, the native protein, which was shown to bind more weakly, eluted at low salt concentration while the destabilized unfolded intermediate eluted only at high salt concentrations, in part refolding to the native protein conformation and in part forming aggregates with unfolding pattern similar to that of the bound intermediate.

This chapter has four primary objectives. The first is to extend our studies to a broader range of resin structures including CEX resins that contain different types of surface extenders and different pores sizes and pore size distributions. The second objective is to determine how load and elution conditions affect conformational changes of the bound protein and the ensuing two-peak elution behavior. While our previous data were limited to a few different load salt concentrations, which affected the protein binding strength, the type of counterion used in the load buffer can also have significant effects in this regard. Perez-Almodovar et al. [34], for example, showed that different protein binding strengths resulted when using acetate buffers prepared with tetra-n-butylammonium (TBAH), arginine, or calcium instead of sodium. By studying the counterion effect we can separate the effects of ionic strength from those that result from specific ion exchange interactions. Moreover, arginine has been suggested as a mean of suppressing protein aggregation and improving recovery in different types of chromatography, including affinity chromatography [64], HIC [65], and multimodal chromatography [66]. Gillespie et al. [17] also reported that arginine reduced the percentage of protein eluting late and hypothesized that arginine prevented protein unfolding by decreasing protein binding strength in the load/wash step and by facilitating refolding and inhibiting aggregation during the elution step.

Luo et al. [18] also observed that arginine reduced the percentage of the late eluting peak, but, unlike Gillespie et al., they hypothesized that arginine worked only by inhibiting reversible self-association (RSA) induced by high NaCl concentrations. Arakawa [67] and Das [68] provide mechanistic explanations of the arginine effects on preventing aggregate formation in concentrated mAb solutions, but it is unclear whether these mechanisms are at play in the resin-induced aggregation. Thus, establishing the effects of arginine on the structure of the bound protein and chromatographic behavior can help establish the dominant mechanism.

The third objective is to determine the effects of resin type and load conditions on conformational changes using, as shown in our prior work, HX-MS coupled with proteolytic fragmentation. As previously discussed, this method is based on the dependence of the exchange of deuterium for amide hydrogen on the degree of their solvent exposure. Since buried amides exchange very slowly or not at all while solvent exposed amides exchange quickly, determining the degree of deuterium exchange provides a measure of unfolding. When coupled with proteolytic fragmentation and HPLC separation of the ensuing peptides, the method also provides information about which regions of the protein structure are affected [49][50][51][52][53][54][56][57][69].

The fourth and final objective is to extend our previous work to other mAbs and to determine whether a correlation exists between the intrinsic stability of the protein and the surface-induced conformational changes that lead to the two-peak elution behavior and on-column aggregate formation. For this purpose, CEX gradient elution experiments are conducted with two additional mAbs. Circular dichroism (CD) is used to determine their stability both by measuring their melting temperature and by analyzing the patterns of change of the CD spectra as a function of temperature [35][63][70][71][72].

4.2. Materials and Methods

4.2.1. Materials

The resins used in this work were obtained as follows. Fractogel EMD SO3- (M) and Eshmuno S were obtained from EMD Millipore (Darmstad, Germany). According to the manufacturer, both of these two resins have a polyacrylate backbone grafted with charged polymers or "tentacles" to facilitate binding with proteins. Nuvia S and UNOsphere Rapid S were obtained from Bio-Rad Laboratories (Hercules, CA). Both these resins are based on an acrylamide polymeric backbone but while Nuvia S is grafted with polymeric surface extenders, UNOsphere Rapid S does not contain grafted polymers. POROS HS 50 and Source 30 S were obtained from Applied Biosystems (Life Technologies Corporation, Grand Island, NY) and GE Healthcare (Piscataway, NJ, USA), respectively. Both resins are based on a poly(styrene-divinyl benzene) backbone and are macroporous. POROS HS 50 has a bi-modal pore size distribution, with large pores as well as small pores [73]. The relevant physical properties of the above six resins are summarized in Table 4.1.

Three monoclonal antibodies were used in this work. mAb A is a glycosylated IgG2 antibody with molecular mass of 150 kDa and a pI of 8.7 theoretically calculated based on its amino acid sequence and is the same mAb used in our prior work [74][75]. The other two mAbs (mAb B and mAb C) have similar molecular mass and pI, as determined by SEC and isoelectric focusing, but, as shown in this work, exhibit different thermal stability. L-arginine, sodium acetate, acetic acid, sodium chloride, sodium phosphate, potassium phosphate, tetra-n-butylammonium hydroxide (TBAH), ethylenediaminetetraacetic acid (EDTA), formic acid, trifluoroacetic acid (TFA), guanidine hydrochloride (GdnHCl) were obtained from Fisher Scientific (Houston, TX, USA). Tris(2-carboxyethyl)phosphine hydrochloride (TCEP) was

purchased from Thermo Scientific (Rockford, IL, USA). Deuterium oxide was obtained from Cambridge Isotope Laboratories, Inc. (Andover, MA, USA). All experiments were conducted at room temperature (22±2 ℃) except otherwise noted.

Table 4.1. Mean particle diameter and charge density of resin samples.

	Fractogel SO3 (M)	Eshmuno S	Nuvia S	UNOsphere rapid S	POROS HS 50	Source 30 S
Mean particle diameter (μm)	74[a]	85[b]	85[c]	90[d]	52[d]	30[d]
Charge density[d] (μeq/mL)	70-110	50-100	90-150	140	135	N/A

a. Ref. [74]
b. Ref. [76]
c. Ref. [26]
d. Manufacturer values

4.2.2. Methods

4.2.2.1. Chromatographic experiments

All chromatography runs were conducted on an AKTA Explorer unit from GE Healthcare (Piscataway, NJ, USA). The resins were packed into 0.5 cm diameter × 5 cm long Tricorn columns from GE Healthcare (Piscataway, NJ, USA) with an actual packed bed volume of 1.00±0.04 mL. Each column was first equilibrated with 5 column volumes (CV) of load buffer prepared by titrating 40 mM $NaCH_3COOH$ with acetic acid and then loaded with 0.5 mL of 2 mg/mL mAb. After loading, the flow was stopped and the column was held idle for different time periods. Two column volumes of load buffer were then supplied followed by a 20 CV gradient to 1 M sodium chloride also in 40 mM $NaCH_3COOH$ titrated to the same pH with acetic acid. Arginine acetate and TBAH acetate were also used as load buffers instead of sodium

acetate. These buffers were prepared starting with 40 mM arginine or 40 mM TBAH in free base form and titrating to pH 5.0 with acetic acid. UV absorbance at 280 nm and conductivity were monitored. All chromatograms, except those obtained for mAb C after 1000 min hold on the Fractogel resin, were normalized to a total peak area proportional to the amount of protein injected per unit of column volume in order to account for small differences in actual protein feed concentration and column volumes and thus facilitate comparisons between runs.

4.2.2.2. HXMS analysis of bound protein

Batch adsorption experiments were conducted to determine conformational changes for the bound protein as described in our previous work [75]. Briefly, a 10-mg sample of the resin was first mixed with a 200 μL sample of 0.5 mg/mL mAb in the load buffer and allowed to equilibrate for 1000 min. The resin sample was then mixed with 500 μL of either 250 or 330 mM NaCl in the load buffer and mixed for 45 min to desorb any native mAb species that corresponds to the early elution peak. The resin sample was then placed in a mixture containing 10 μL of the load buffer in H_2O and 90 μL of the same buffer in D_2O for different periods of time, after which the hydrogen-deuterium exchange process was quenched by adding 25 μL of ice-cold buffer containing 150 mM potassium phosphate at pH 1.5 to the resin. 100 μL of the dissociation buffer (8 M GdnHCl, 100 mM TCEP, 25 mM EDTA, at pH 2.6) was then added to the resin under ice for 2 min that resulted in desorption of essentially all of the residual bound protein. The supernatant was then mixed with 450 μL of an aqueous solution containing solution 5% ACN, 0.1% formic acid, and 0.01% TFA at pH 2.6 to bring the GdnHCl concentration down to approximately 1.5 M. All of the steps described above were conducted in a 2 mL microcentrifuge filter tube slowly rotated end-over-end which allowed washing the resin and removing the supernatant by centrifugation at 8600 rpm in a few minutes.

Table 4.2 summarizes the conditions for the four experiments conducted in this manner. Note that for UNOsphere with the sodium acetate load buffer and for Fractogel with the arginine acetate the first desorption step was omitted since, for these two cases, all of the protein bound would have eluted. In all four cases, following the on-resin deuterium labeling process described above, 500 μL of the mAb sample was loaded into a sample loop and pumped into an immobilized pepsin column at 0.1 mL/min with a Series I Pump from Lab Alliance (Syracuse, NY, USA). The pepsin column was prepared as in our previous work [75], based on the protocol of Wang et al. [59]. After pepsin digestion, the peptides were pumped into a 0.1 cm diameter × 0.8 cm long C8 reversed phase column from Michrom BioResources (Auburn, CA, USA) for trapping and desalting. After 9 min, the adsorbed peptides were eluted with an acetonitrile gradient delivered by a Surveyor MS pump from Thermo Finnigan (San Jose, CA, USA) at 0.1 mL/min into a 0.21 diameter × 10 cm long Kinetex C18 column from Phenomenex (Torrance, CA, USA) to separate the peptides. Two different gradients were used to elute those peptides. A long gradient from 5 to 40% ACN in 31 min followed by a 5 min gradient to 90% ACN was used to identify peptides in blank runs without hydrogen exchange. A short gradient from 30 to 60% ACN in 17 min followed by a 2 min gradient to 90% ACN was used for the hydrogen exchange studies. The shorter time was used to minimize the back exchange from deuterium to hydrogen during acetonitrile gradient elution. An LTQ linear ion trap mass spectrometer from Thermo Finnigan (San Jose, CA, USA) was used to determine the mass of the eluted peptides. Data were collected in a positive ion, profile mode with an ESI voltage of 4.3 kV, a capillary temperature of 250 ℃, and sheath gas flow rate of 15 units. Proteome Discover software from Thermo Scientific (Rockford, IL, USA) was used to identify the peptides and HDExaminer software from Sierra Analytics (Modesto, CA, USA) was used to select the identified peptides with high signal-to-

noise ratio. Finally, 29 peptides with 49% coverage of the mAb A sequence were selected as the reporter peptides.

The difference between the mass of each deuterated peptides obtained from a particular mAb sample and the mass of the corresponding peptide obtained for the same mAb under a reference condition was used to assess conformational changes. A statistical analysis based on the method described in Houde et al. [22] was done to determine the confidence limits of the differences in peptide mass. Accordingly, the 99% confidence limit was calculated to be ± 0.43 Da based on replicate experiments with a 10 min labeling time.

Table 4.2. Experimental conditions used for adsorbed HXMS experiments with mAb A.

Experiment	Resin	Load buffer	First desorption buffer after 1000 min hold	Labeling buffer
1	Fractogel SO3 (M)	40 mM $NaCH_3COO$, pH 5.0 in H_2O	330 mM NaCl in 40 mM $NaCH_3COO$, pH 5.0	40 mM $NaCH_3COO$, pH 5.0 in D_2O
2	Nuvia S	20 mM $NaCH_3COO$, pH 4.8 in H_2O	250 mM NaCl in 20 mM $NaCH_3COO$, pH 4.8	20 mM $NaCH_3COO$, pH 4.8 in D_2O
3	UNOsphere rapid S	40 mM $NaCH_3COO$, pH 5.0 in H_2O	N/A	40 mM $NaCH_3COO$, pH 5.0 in D_2O
4	Fractogel SO3 (M)	40 mM Arginine acetate, pH 5.0 in H_2O	N/A	40 mM Arginine acetate, pH 5.0 in D_2O

4.2.2.3. Circular dichroism

Circular dichroism measurements were performed with a Model 410 circular dichroism spectropolarimeter from Aviv Biomedical (Lakewood, NJ, USA) operated in the far-UV range. For this purpose, each mAb was dissolved at a 0.3 g/L concentration in 50 mM sodium phosphate at pH 7. Full CD spectra were collected with 0.2 cm path-length cuvettes at room temperature while the CD ellipticity, θ, at 215 nm was recorded as a function of temperature from 25 ^{o}C to 95 ^{o}C at 2 ^{o}C increments. The equilibration time at each temperature was 2 min. The CD signal was averaged with 1 s and the bandwidth was 1 nm. The buffer signal was subtracted to obtain the final value. In order to compare the behavior of the different mAbs, the

CD ellipticities as a function of temperature were normalized for each mAb with the following equation:

$$f = \frac{\theta - \theta_0}{\theta_f - \theta_0} \times 100\% \tag{4.1}$$

where f is the normalized CD signal, θ_0 and θ_f are the initial and final 215 nm ellipticities, corresponding to the folded and melted states, respectively.

4.3. Results

4.3.1. Chromatographic behavior

Figure 4.1 shows the chromatograms for mAb A with a 20 CV gradient from 0 to 1 M NaCl for the six resins considered in this work. The load buffer used in these runs was 40 mM $NaCH_3COOH$ at pH 5.0 for Fractogel and 20 mM $NaCH_3COOH$ at pH 4.8 for the other resins. The reason for this difference is that all of the mAb eluted in the second peak when the Fractogel column was operated at pH 4.8 as a result of the strong tendency of this resin to induce conformational changes. The elution flow rate was also different. We used 0.3 mL/min for Eshmuno and Nuvia in order to increase the resolution of the two peaks and 1 mL/min for the other resins. As seen in Fig. 4.1, for the conditions chosen, all of the protein elutes in a single peak when elution starts immediately after loading and washing the column (0 min hold time). On the other hand, different patterns of elution are seen for the different resins with a 1000 min hold before wash and elution. In this case, a pronounced two-peak elution behavior is seen for Fractogel, Eshmuno, Nuvia, and POROS, each with a different percentage of protein eluting in the second peak. In each case, the first peak has the same retention as the protein eluted with a zero hold time. Source and UNOsphere obviously behave differently from the other resins with a

1000 min hold time. For Source, most of the protein elutes early in a narrow peak followed by a small, but rather broad late eluting portion. For UNOsphere, all of the protein elutes early in the same manner as the zero-hold time result.

The two-peak elution behavior seen above appears to be related to the resin structure as certain common traits can be noted. Fractogel, Eshmuno, and Nuvia contain grafted polymers that are designed to enhance binding capacity. In these materials, binding is not restricted to monolayer coverage, but is believed to occur throughout the grafted polymer layer [26][77]. All of these resins gave a distinct two-peak elution behavior with a relatively large fraction of the protein eluting late. Source and UNOsphere, on the other hand, have an open pore structure, reportedly without grafted polymeric extenders, but different particle sizes. UNOsphere showed no evidence of two-peak elution while Source, which gave a sharper peak as a result of its smaller particle size, gave only a small, broad second peak. The behavior of POROS, which has a bi-modal pore size distribution and, reportedly no grafted polymeric extenders, also gave a distinct two-peak elution behavior. It is possible that this occurs because most of the protein binds in the small pores present in this material in a manner analogous to binding on a grafted polymer layer.

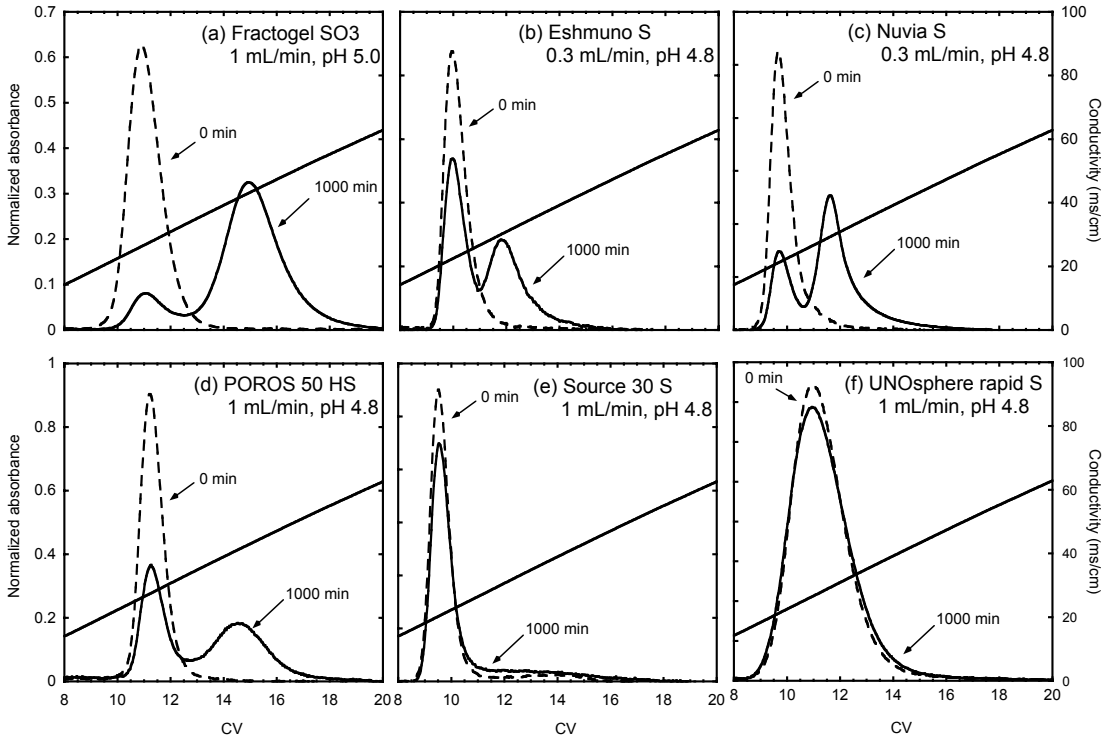

Figure 4.1. Chromatographic behavior of mAb A on columns packed with (a) Fractogel, (b) Eshmuno, (c) Nuvia, (d) POROS, (e) Source, and (f) UNOsphere resins. For Fractogel (a), the load buffer was 40 mM $NaCH_3COOH$ at pH 5.0 while for the other five resins, the load buffer was 20 mM $NaCH_3COOH$ at pH 4.8. The elution flow rate was 0.3 mL/min for (b) and (c) and 1 mL/min for (a), (d), (e), and (f). Other conditions are described in Section 4.2.2.1. The percentage of protein eluting in the second peak with 1000 min hold time was 87%, 44%, 73%, 51%, 14%, and 0% for (a), (b), (c), (d), (e), and (f), respectively.

Figure 4.2 shows the chromatograms obtained for mAb A for different salt concentrations and pH in the load buffer for columns packed with (a) Fractogel SO3 (M), (b) Eshmuno S, (c) Nuvia S, and (d) UNOsphere rapid S, all with a 1000 min hold time prior to elution. As in the previous case, the elution flow rate was 0.3 mL/min for Eshmuno and Nuvia and 1 mL/min for Fractogel and UNOsphere. As seen in this figure, only one peak is observed for UNOsphere

regardless of load conditions. On the other hand, for the other three resins, the two-peak elution behavior appears to be correlated with the expected trends of protein binding strength, becoming more pronounced at lower sodium ion concentrations or lower pH. Table 4.3 summarizes this trend quantitatively. Of these three resins, the effect is most pronounced for Fractogel and least pronounced for Eshmuno.

Table 4.3 summarizes the percentage of protein eluting in the second peak for these runs along with the Na^+ concentration at which the peaks elute, $C^E_{Na^+}$, in the gradient elution runs. As seen from this table, despite the fact that under the same load condition (e.g. 20 mM $NaCH_3COOH$, pH 4.8), the value of $C^E_{Na^+}$ of the first peak is higher for UNOsphere (300 mM) than for Eshmuno (240 mM) and Nuvia (240 mM), which, in turn, suggests a greater binding strength for UNOsphere, there was no evidence of a two-peak elution behavior for this resin while the effect was significant for both Eshmuno and Nuvia. This result suggests that the resin structure, in addition to the protein binding strength during load, has an effect on the resin-induced two-peak elution behavior.

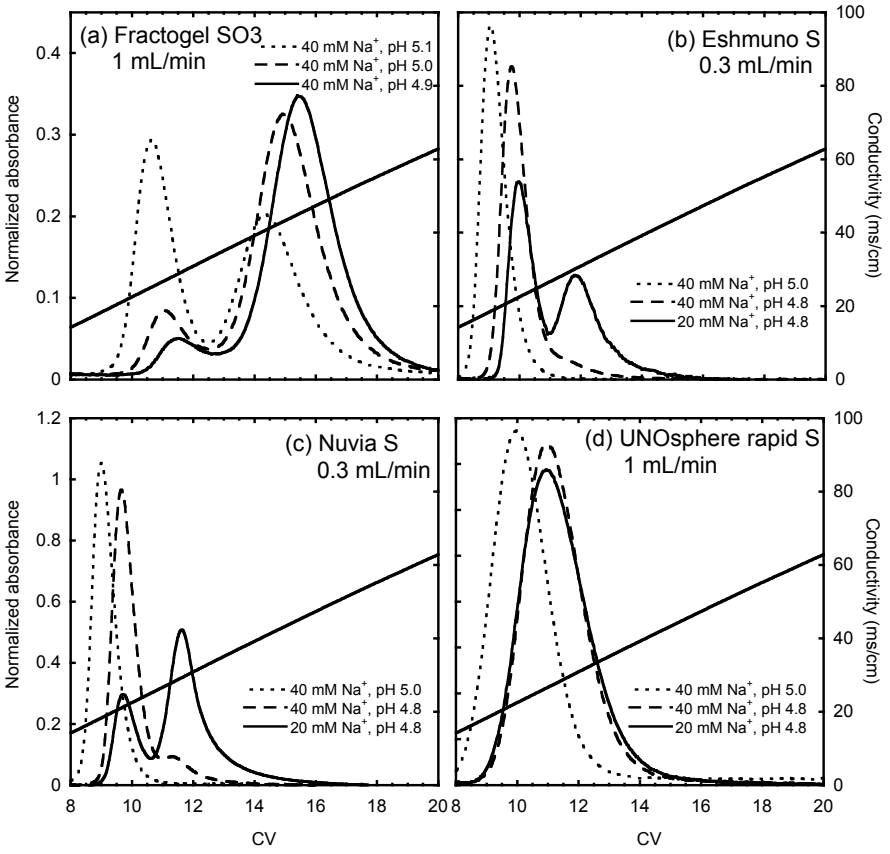

Figure 4.2. Effects of load buffer pH and sodium ion concentration on the elution profile of mAb A on columns packed with (a) Fractogel, (b) Eshmuno, (c) Nuvia, (d) UNOsphere. The hold time was 1000 min. The elution flow rate was 0.3 mL/min in (b) and (c), and 1 mL/min in (a) and (d). Other conditions are described in Section 4.2.2.1. The percentage of protein eluting in the second peak is given in Table 4.3 for each case.

Table 4.3. Effects of pH and Na^+ concentration in the load buffer on the two-peak elution behavior of mAb A with a 1000 min hold.

Resin	Load buffer	$C^E_{Na^+}$ for early eluting peak* (mM)	$C^E_{Na^+}$ for late eluting peak* (mM)	% of second peak
Fractogel SO3 (M)	40 mM Na^+, pH 5.1	280	460	53
	40 mM Na^+, pH 5.0	300	480	87
	40 mM Na^+, pH 4.9	320	500	92
Eshmuno S	40 mM Na^+, pH 5.0	210	N/A	0
	40 mM Na^+, pH 4.8	240	320	8
	20 mM Na^+, pH 4.8	240	320	44
Nuvia S	40 mM Na^+, pH 5.0	210	N/A	0
	40 mM Na^+, pH 4.8	240	310	13
	20 mM Na^+, pH 4.8	240	330	73
UNOsphere rapid S	40 mM Na^+, pH 5.0	250	N/A	0
	40 mM Na^+, pH 4.8	300	N/A	0
	20 mM Na^+, pH 4.8	300	N/A	0
POROS HS 50	20 mM Na^+, pH 4.8	310	460	51
Source 30 S	20 mM Na^+, pH 4.8	230	330	14

* $C^E_{Na^+}$ is the Na^+ concentration at peak maximum

Figure 4.3 compares the chromatograms obtained for mAb A on Fractogel using TBAH and arginine as counterions in the acetate load buffer at pH 5 with those obtained using sodium as the counterion for otherwise identical conditions. Hold times in these runs were 1000 min for arginine and 270 min for TBAH. The shorter time was chosen for TBAH to highlight the two-

peak elution behavior since, in this case, with a 1000 min hold all of the protein eluted in the second peak. In all cases, elution was in 40 mM $NaCH_3COOH$ pH 5 buffer with NaCl concentration increasing from 0 to 1 M in 20 CV. As seen in this figure, substituting arginine for sodium in the load buffer dramatically reduced the percentage of protein eluting late from the 87% value obtained with sodium to a value of 0%. TBAH, on the other hand, dramatically increased this percentage form the value of 48% obtained with sodium as the load counterion at 270 hold time to a value of 84%. Based on frontal analysis experiments, cycling the column between sodium acetate and arginine or TBAH acetate at the same pH and counterion concentration, Perez-Almodovar et al. [34] found that for Nuvia S the preference of these counterions for the resin's charged sulfonic acid ligands varies in the order of TBAH < Na < Arg. On the contrary, the relative binding strength of a mAb was shown to decrease in the same order, which is expected based on the stoichiometric displacement or mass action law of ion exchange. These experiments were repeated for Fractogel in this work. The results (not shown for brevity) showed the same trends for this resin indicating that strongest protein binding is obtained with TBAH and the weakest with arginine, further supporting the hypothesis that the protein binding strength determines the magnitude of the resin-induced two-peak elution behavior.

A further experiment was done to determine whether addition of relatively low concentrations of arginine to the elution buffer could result in a significant reduction of the two-peak elution behavior. For this purpose the Fractogel column was loaded in 40 mM $NaCH_3COO$ at pH 5.0 and eluted with the same buffer containing 100 mM arginine acetate with a 0-1 M NaCl gradient in 20 CV following a 1000 min hold. These conditions reduced the percentage of protein eluting in the second peak from 87 to 78% (results not shown for brevity), suggesting

that low levels of arginine are insufficient to prevent the formation of aggregates induced by the destabilization of the protein during the hold step.

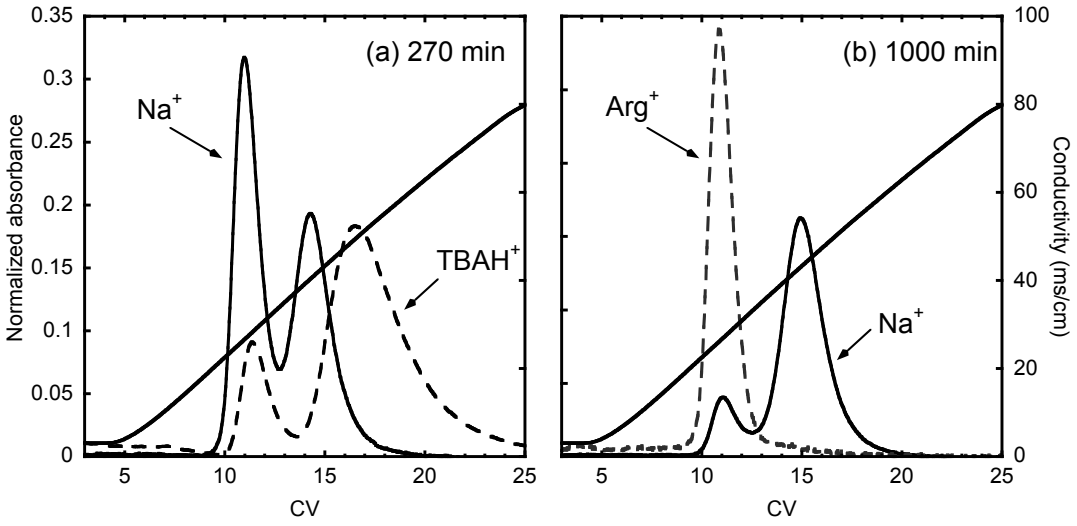

Figure 4.3. Effects of load buffer counterion on elution profile of mAb A on the Fractogel column for hold times of 270 min (a) and 1000 min (b). Conditions are described in Section 4.2.2.1. The percentage of protein eluting in the second peak was 48% and 84% for Na^+ and $TBAH^+$, respectively, in (a), and 87% and 0% for Na^+ and Arg^+, respectively, in (b).

Figure 4.4 compares the chromatograms obtained for mAb B and C with those obtained for mAb A on the Fractogel column for otherwise identical conditions. A single peak is obtained for all three mAbs if elution is started immediately after the load/wash steps; i.e. with a zero hold time. However, the elution behavior with 1000 min hold time is dramatically different for the three mAbs. As shown previously, mAb A shows a pronounced two-peak elution behavior with 87% of the protein eluting late. mAb B shows only a second peak accounting for only about 16% of the total mAb C, on the other hand, shows that only about 15% of the protein is eluted in the first peak, with the balance remaining irreversibly bound to the resin. Cleaning the column with

500 mM NaOH was, however, able to remove most of the residual protein suggesting that this mAb is either mostly denatured while held on the resin in the load buffer or forms large aggregates during the elution step that remain trapped within the resin and that cannot be removed without harsh cleaning conditions. Interestingly, among the three mAbs, the salt concentration at which the first peak elutes was also greatest for mAb C (320 mM) and smallest for mAb B (250 mM), indicating a trend where the mAb least strongly bound is also the one that leads to the smallest two-peak elution behavior.

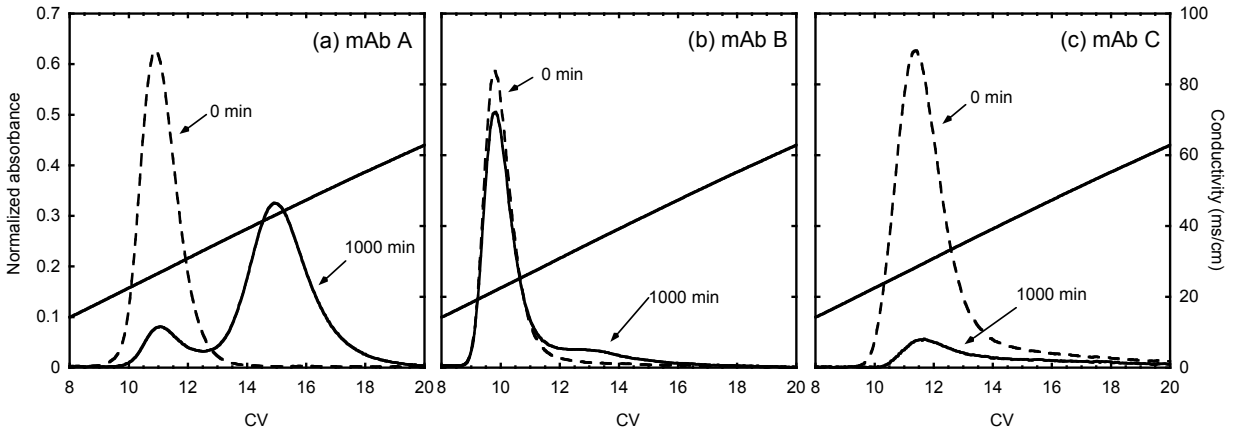

Figure 4.4. Chromatographic behavior of (a) mAb A, (b) mAb B and (c) mAb C on the Fractogel column with 0 and 1000 min hold times. Conditions are described in Section 4.2.2.1. The percentage of protein eluting in the second peak was 87% in (a) and 16% in (b). The yield of protein for 1000 min hold time in (c) was 15%.

4.3.2. HX-MS analysis of bound protein

Figure 4.5 shows the difference between the mass of each of the 29 reporter peptides obtained for the bound mAb A held on the resin for 1000 min and the mass of the corresponding peptide obtained for the bound protein held on the resin for only 30 min. As shown in our previous work [74], 30 min is not sufficient to generate a significant percentage of the second

peak for these conditions on Fractogel suggesting that the protein is likely still in its native conformation after 30 min hold time. As discussed in Section 4.2.2.2., for Fractogel and Nuvia, deuterium labeling was done after desorbing the more weakly bound protein species (presumably corresponding to the first elution peak in the LGE experiments) using either 250 or 330 mM NaCl. This step was omitted for UNOsphere since all of the protein eluted at this salt concentration. As seen in Fig. 4.5, many peptides derived from the protein bound on either Fractogel or Nuvia exhibit an appreciable mass increase indicating increased solvent exposure. Peptides 17 and 19, found in the Fc region of the mAb (as seen in Fig. 3.2), in particular, exhibit large mass differences, which are statistically significant at the 99% confidence level. This result suggests that localized unfolding occurs in the bound state after 1000 min incubation on both Fractogel and Nuvia. Interestingly, the same peptides and, hence, region of the molecule appear to be involved in the conformational change that occurs for both resins. As reported by other authors for different mAbs ([61][62][63]), the Fc region is often the most sensitive region to various stresses (e.g. low pH denaturation). Our results suggest that the same region may also be most affected by stresses caused by strong binding on the CEX resin surface. By comparison, few of the 29 reporter peptides showed an appreciable mass change when the protein was bound on UNOsphere resin and none of the peptides, including peptides 17 and 19, showed a difference significant at the 99% confidence level.

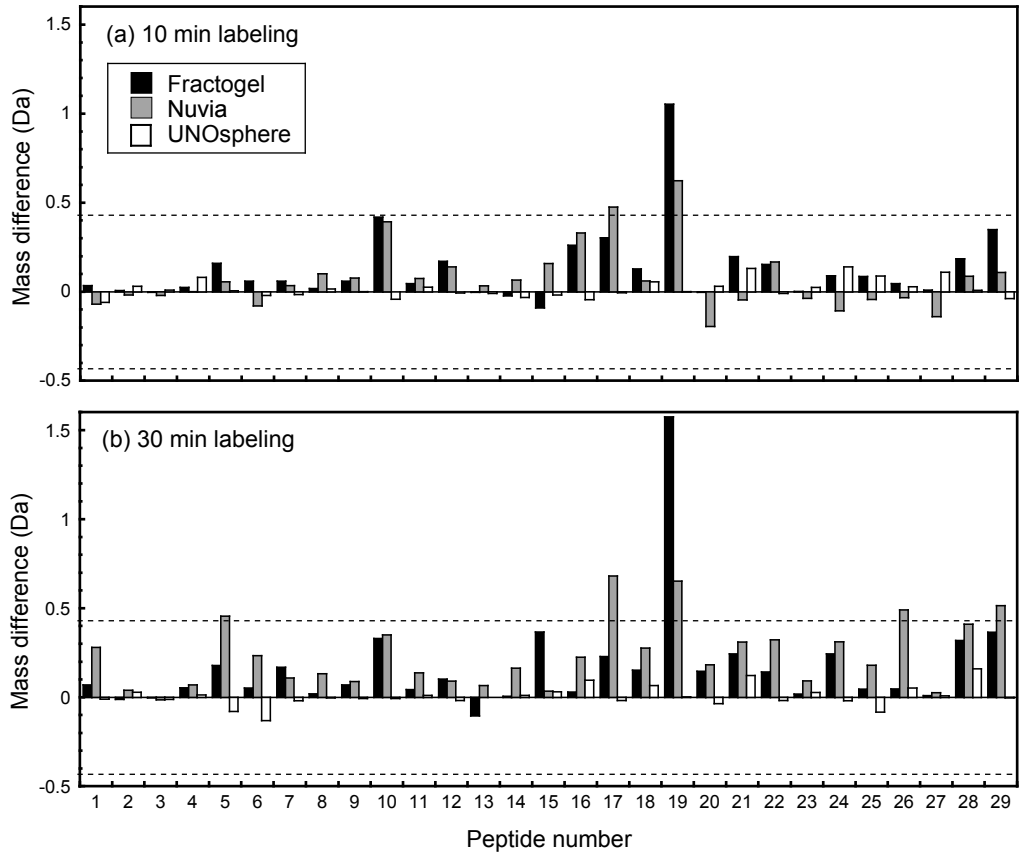

Figure 4.5. Difference between the mass of each of the reporter peptides obtained for the bound protein held on the resin for 1000 min and that of the corresponding peptides obtained for the bound protein held on the resin for 30 min. Results are shown for Fractogel, Nuvia, and UNOsphere and with labeling times of 10 min (a) and 30 min (b). The dashed lines represent the 99% confidence limits for the mass difference values. The peptides are sorted in ascending number along the protein sequence. Positive vertical bars suggest increased solvent exposure in bound protein held on the resin for 1000 min compared with bound protein held on the resin for 30 min. The conditions are given in Table 4.2. The 30 min hold time did not result in a significant percentage of late eluting protein.

Figure 4.6 compares the mass difference results for the 29 reporter peptides obtained for Fractogel resin with the 40 mM $NaCH_3COO$ pH 5.0 load buffer with those obtained substituting arginine for sodium in the load buffer for otherwise identical conditions. In both cases, the peptide masses obtained for the protein held in the bound state for only 30 min are subtracted from the masses obtained with a 1000 min hold. As seen from this figure, when arginine is the counterion in the load buffer, only a few peptides show appreciable mass differences and none shows differences significant at the 99% confidence level, including peptides 17 and 19. This result clearly points to the stabilizing effect of arginine as a counterion in the load buffer. This effect appears to be related primarily to the weakened binding of the mAb, which, in turn, prevented the conformational changes that led to the formation of a destabilized bound intermediate that, ultimately, led to the two-peak elution behavior with sodium as a counterion.

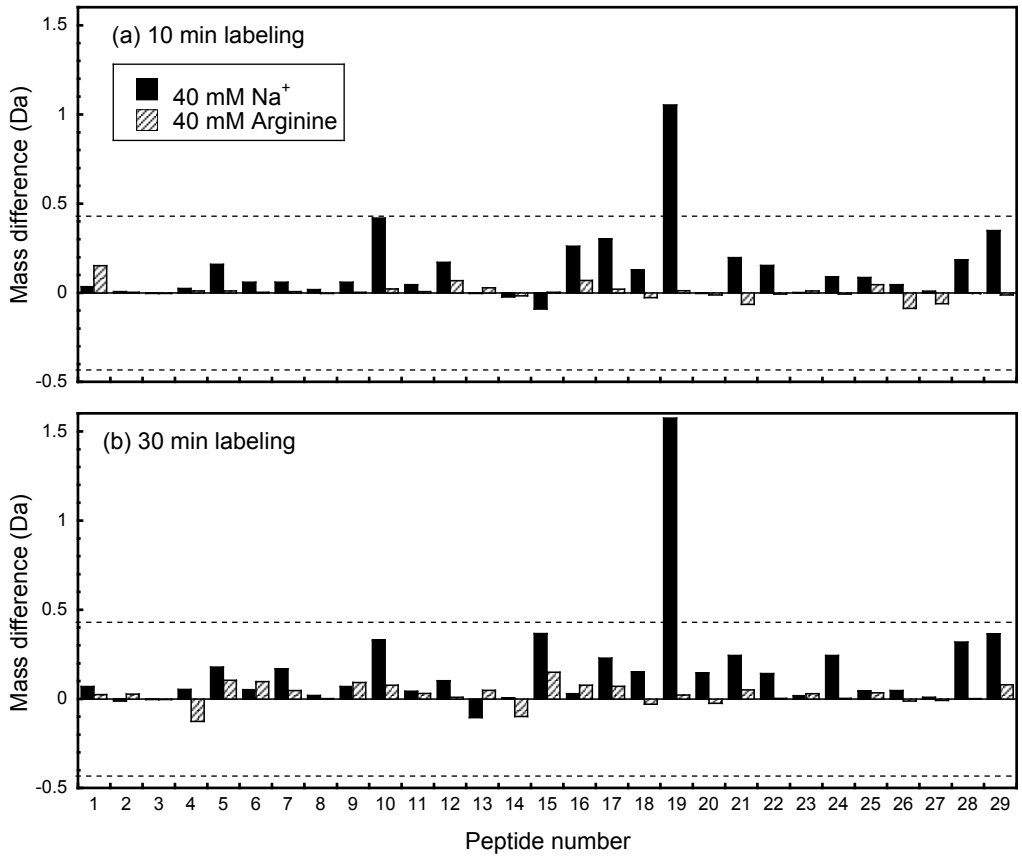

Figure 4.6. Difference between the mass of each of the reporter peptides obtained for the bound protein held on the resin for 1000 min and that of the corresponding peptides obtained for the bound protein held on the resin for 30 min. Results are shown for acetate load buffers preparaed with 40 mM Na^+ and 40 mM arginine and with labeling times of 10 min (a) and 30 min (b). The dashed lines represent the 99% confidence limit for the mass difference values. The peptides are sorted in ascending number along the protein sequence. Positive vertical bars suggest increased solvent exposure in bound protein held on the resin for 1000 min compared with bound protein held on the resin for 30 min. The conditions are given in Table 4.2. The 30 min hold time did not result in a significant percentage of late eluting protein.

4.3.3. Circular dichroism analysis

As discussed in Section 4.2.2.3, circular dichroism measurements were made to assess the inherent stability of the three mAbs used in this work and determine if a correlation can be established between these CD measurements and two-peak elution tendency. For this purpose, CD spectra were obtained at 2 ^{o}C intervals between 25 and 95 ^{o}C. Figure 4.7 shows the results. While large differences were seen between the three different mAbs considered in this work with regards to the effect of temperature over the entire range of wavelengths studied (205 to 260 nm), for simplicity, Fig. 4.7 only shows the results at 215 nm. All three mAbs show a strong ellipticity at this wavelength at 25 ^{o}C, suggesting that all three mAbs are rich in β-sheets, which normally give the strongest signal in this part of the CD spectrum. As Fig. 4.7 shows, for all three mAbs, the normalized ellipticity remains essentially constant up to about 65 ^{o}C. Above this temperature, mAb C shows a sharp rise indicating a melting temperature of about 69 ^{o}C. mAb A, on the other hand, shows a large dip in the normalized CD signal with a strong minimum at 75 ^{o}C, followed by a sharp rise indicating a melting temperature of about 78 ^{o}C. The behavior of mAb B appears to be intermediate, exhibiting only a modest minimum also around 75 ^{o}C, but also a sharp rise at 78 ^{o}C.

Results analogous to those shown in Fig. 4.7 have been observed previously for different antibodies [35][63][71][72]. It has been suggested that a strong dip in the 215 nm CD signal is caused by the formation of inter-molecular β-sheets to stabilize the protein before precipitation at the melting temperature.

A quantitative relationship between the CD results and the chromatographic behavior of the three mAbs cannot be expected since the conditions are obviously different in the two types of experiments. However, a qualitative relationship between CD measurements and trends

observed in the chromatography appears to exist. Based on this work and our previous results [74][75], it is evident that mAb A had tendency not only to undergo a significant resin-induced conformational change, but also a tendency to form stable aggregates that are seen in the late eluting peak. On the other hand, mAb C, which has the lowest melting temperature and no evidence of stabilizing inter-molecular β-sheets, could not be eluted to a large extent after a 1000 min hold. Finally, mAb B, which had a relatively high melting temperature and only a small tendency to form stabilizing inter-molecular β-sheets, as determined by the lack of a strong dip prior to melting, showed only a small two-peak elution behavior. While the molecular basis is still uncertain, we advance the hypothesis that a combination of native protein stability and tendency to form stabilizing inter-molecular β-sheets is responsible for the observed chromatographic behavior. Since CD provides a qualitative measure of native protein stability and unfolding behavior as a function of temperature, our experimental observations suggest that the molecular basis for the tendency to unfold and aggregate as a function of temperature may be the same as the tendency observed as a function of protein binding and elution on a CEX surface.

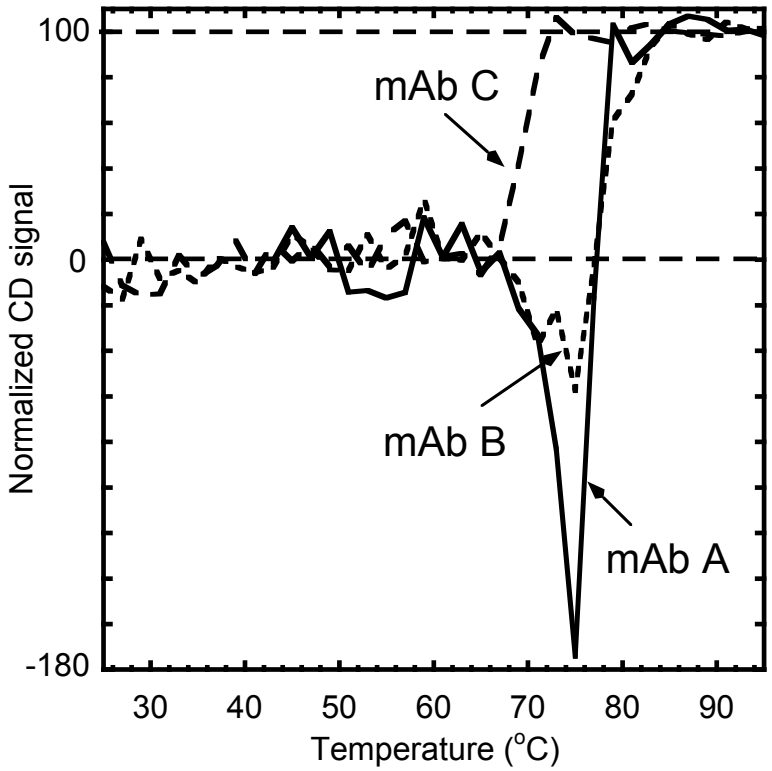

Figure 4.7. Normalized 215 nm CD signal as a function of temperature for mAb A, B, and C at a 0.3 g/L concentration in 50 mM phosphate buffer at pH 7.0.

4.4. Discussion and Conclusions

A two-peak elution behavior has been shown to occur for a mAb on different CEX resins. The two-peak behavior is more pronounced for polymer-grafted resins including Fractogel, Eshmuno, and Nuvia and for POROS, which has bimodal pore size distribution including small pores where most of the protein binding takes place. This behavior is greatly diminished or even absent in macroporous resins without polymeric extenders such as Source and UNOsphere. Besides resin structure, the strength of protein binding to the resin during the load and hold steps, also affects the two-peak behavior with the percentage of protein eluting in the second peak increases as the initial binding strength increases. Qualitatively, this occurs when the pH and salt

concentration of the load buffer are higher or when arginine, which weakens protein binding, replaces sodium as the counterion in the load buffer. Replacing sodium with TBAH, which increases the protein binding strength, conversely, enhances the two-peak elution behavior. A quantitative determination of the protein binding strength was not made for the mAbs used in this work. A suitable approach would be to determine the protein effective charge (or number of binding sites) and binding equilibrium constant from linear gradient elution experiments, as shown, for example, Perez-Almodovar et al. [34]. These authors found that for a different mAb on Nuvia S at pH 5, the counterion type did not affect the effective charge significantly affecting instead the equilibrium binding constant. Unfortunately, these results cannot be easily extended to other mAbs, such as the one principally used in this work or to different resin types. For example, Pabst et al. [78] observed very different effective charge values for two different mAbs at pH 5 on the same CEX resin. Moreover, the two mAbs exhibited very different trends of the effective charge with resin type. For instance, one of the mAbs showed much higher effective charge on Fractogel SO3 and POROS HS 50 compared to UNOsphere rapid S, while the other showed very similar (but all substantially lower) value on all three resins. Neither of these two references indicated multiple peak elution behavior. Thus, it is not possible, without further study to predict, a quantitative relationship between unfolding of our mAb and either the effective charge or the value of the equilibrium binding constant.

As shown by HX-MS with proteolytic fragmentation, the root of the two-peak elution behavior is a resin-induced protein conformational change that occurs gradually in time and affects principally the Fc region of the mAb. Fractogel and Nuvia were shown to cause increased solvent exposure, which are characteristic of localized unfolding, in this region of the mAb,

while no such changes occur when the same mAb is bound on UNOsphere for the same conditions or on Fractogel when arginine replaces sodium as the counterion in the load buffer.

CD measurements appear to provide some clues regarding the chromatographic behavior of different mAbs. Although probably insufficient to establish a definitive molecular basis for the underlying phenomena, the chromatographic behaviors observed appear consistent with inherent stability of the native mAb structure and with the tendency of different mAbs to either precipitate directly or form stabilizing intermolecular structures before precipitation. Further work is needed to expand the measurements to a larger number of mAbs in order to be able to conclusively establish the general validity of these observations.

Chapter 5

Three-peak elution behavior of a monoclonal antibody during cation exchange chromatography

---

5.1. Introduction

In Chapter 2, Chapter 3 and Chapter 4, we reported a two-peak elution behavior for a glycosylated IgG2 mAb on various CEX resins including Fractogel SO3. In this case, the two-peak elution behavior was accompanied by the on-column formation of more-strongly bound high molecular species. Based on solution-phase and on-column hydrogen deuterium exchange mass spectrometry coupled with proteolytic fragmentation (HXMS) it was found that a portion of the bound mAb became partially unfolded while bound to the resin resulting in specific areas of the Fc region that became more solvent exposed compared to the native protein. During elution, the native mAb eluted early in the gradient while the destabilized, unfolded bound species eluted late in the gradient, in part refolded to native monomer and in part in the form of aggregates. Further studies indicated that the two-peak elution behavior is dependent on the resin type, composition of the load buffer, and on the inherent stability of the mAb [79]. Aggregate formation was shown to be facilitated by CEX resins containing grafted polymers, such as Fractogel SO3, Eshmuno S, and Nuvia S, and on resins having a bimodal pore size distribution, such as POROS HS, while it was nearly absent for CEX resins with an open-pore structure and no grafted polymers, such as UNOsphere S and Source 30S. In general, weaker binding conditions, including higher pH, higher salt concentration, and replacing sodium with arginine, reduced or eliminate aggregate formation, while different elution conditions did not seem to have a significant effect. Different mAbs also had distinct elution behavior on the same resin under the

same operating conditions, and it was shown by circular dichroism (CD) that this effect appears to be correlated with the protein melting process when exposing the protein to increasing temperatures. In all cases, however, the two-peak elution behavior was directly correlated with the length of time that the protein remained bound on the resin indicating that the ensuing two-peak elution behavior was surface catalyzed.

In this chapter, we explore the behavior of a mAb that exhibits a two-peak elution behavior for short hold times and a three-peak elution behavior for longer hold times on the CEX resin POROS XS. To our knowledge such behavior has not been previously reported. A number of biophysical measurements are used to characterize this system, including off-line and in-line dynamic light scattering (DLS), circular dichroism (CD), in-line fluorescence spectroscopy, and HXMS. These measurements indicate that the two-peak behavior is associated with heterogeneous binding on the POROS XS resin likely due to existence of weak and strong binding sites. Three elution peaks are observed when the protein held on the stronger binding sites increasingly undergoes conformational changes, which ultimately results in the formation of late eluting aggregated species. The effects of flow rate and arginine replacing sodium as a counter-ion in the buffer are also studied along with the behavior of the same mAb on the open-pore resin Nuvia HR-S. This resin reportedly contains neither grafted polymers nor a significant bimodal pore size distribution [80].

5.2. Materials and Methods

5.2.1. Materials

POROS XS was obtained from Applied Biosystems (Life Technologies Corporation, Grand Island, NY). According to the manufacturer [81], this resin is based on a crossed-linked poly(styrene-divinylbenzene) backbone with a polyhydroxyl surface coating functionalized with sulfopropyl groups. As shown in previous work, POROS resins have a bimodal pore size distribution, which includes large "throughpores", about 500 nm in diameter, as well as small pores, about 22 nm in diameter [73][82]. The average particle size of the POROS XS resin used in this work is about 50 μm. Nuvia HR-S was obtained from Bio-Rad Laboratories (Hercules, CA, USA) and used for comparison. According to its manufacturer, this resin is based on a hydrophilic polyacrylamide backbone also functionalized with sulfopropyl groups. This resin also has an average particle size of about 50 μm. Basic properties of this resin can be found in ref. [80].

The monoclonal antibody used in this work was provided from Bristol-Myers Squibb (Hopewell, NJ, USA). The pI of the mAb, calculated based on the amino acid sequence, is 7 and the molecular mass is around 150 kDa. Size exclusion chromatography with in-line dynamic light scattering analysis showed that the mAb sample is essentially only monomer with a hydrodynamic radius of 5.3±0.2 nm (see Fig. 5.S1 in the Supplementary Material). L-arginine, sodium acetate, acetic acid, sodium chloride, tetra-n-butylammonium hydroxide (TBAH), ethylenediaminetetraacetic acid (EDTA), formic acid, trifluoroacetic acid (TFA), guanidine hydrochloride (GdnHCl) were obtained from Fisher Scientific (Houston, TX, USA). Tris(2-carboxyethyl)phosphine hydrochloride (TCEP) was purchased from Thermo Scientific (Rockford, IL, USA). Deuterium oxide was obtained from Cambridge Isotope Laboratories, Inc.

(Andover, MA, USA). All experiments were conducted at room temperature (22±2 ℃) except otherwise noted.

5.2.2. Methods

5.2.2.1. Chromatographic experiments

Chromatographic experiments were conducted primarily with a Waters e2695 Alliance HPLC unit (Milford, MA, USA) interfaced with an in-line dynamic light scattering (DLS) instrument, DynaPro NanoStar with a fiber optics connections to a miniDAWN TREOS, obtained from Wyatt Technologies (Santa Barbara, CA, USA). Each resin was packed into 0.5 cm diameter × 5 cm long Tricorn columns from GE Healthcare (Piscataway, NJ, USA) with actual packed bed volumes of 1.0 and 1.1 ml for POROS XS and Nuvia HR-S, respectively. Each column was first equilibrated with 5 column volumes (CV) of load buffer prepared by titrating 40 mM sodium acetate with acetic acid to pH 5. After that the column was loaded with 100 μL of 5 g/L protein and washed with the load buffer for different periods of time from 0 to 240 min at the same flow rate. This time period is referred to as the hold time. For 1000 min hold time, the flow was stopped after loading and restarted after 1000 min. In all cases, after the hold step, the protein was eluted with a 20 CV linear salt gradient from 0 to 1 M NaCl with each buffer in 40 mM sodium acetate at pH 5. The default load and elution flow rate was 0.5 ml/min but load and elution flow rates of 0.25 and 1 ml/min were also used. UV absorbance was monitored and the hydrodynamic radius of the eluted species was determined by fitting the correlation function of the DLS signal assuming a single exponential decay. A Shimadzu 20AB HPLC (Kyoto, Japan) fluorescence detector was used to obtain the in-line fluorescence signal of the eluted species. The excitation wavelength of the fluorescence detector was set at 295 nm and the emission signal at 335 nm.

Some of the chromatography experiments were also conducted on an AKTA Explorer 10 unit from GE Healthcare (Piscataway, NJ, USA) to test the chromatographic behavior of protein

samples obtained from fractions eluted from the POROS XS column. For these experiments 1 to 2 ml effluent samples were collected using a model Frac-900 fraction collector from GE Healthcare (Piscataway, NJ, USA) and re-injected into the POROS XS or Nuvia HR-S column after buffer exchange to the load buffer using a 30 kDa cut-off centrifugal filter units from EMD Millipore (Darmstad, Germany).

Off-line DLS measurements of the eluted species were also made with the DynaPro Nanostar instrument in batch mode at 20 °C. Before analysis, the eluted fractions were filtered through a 0.22 μm syringe filter into the instrument cell. As for the in-line DLS measurements, the signal of the correlational function were processed with a cumulant fit corresponding to a single exponential decay [29].

Far-UV CD spectra were collected for fractions eluted from the POROS XS column with a JASCO J-710 spectropolarimeter from JASCO (Easton, MD, USA). The path length of the cuvettes used was 0.1 cm. Full spectra were obtained from 200 to 260 nm with a step wavelengof 1 nm. The signal from a buffer sample was deducted for each run and the final signal was an average of the results from three replicate measurements. To compare CD results for each individual eluted species with different concentration, the CD ellipticities for each mAb were normalized by dividing the observed ellipticities by the mAb concentration.

5.2.2.2. HXMS analysis

HXMS was conducted both on fractions eluted from the chromatographic column for conditions where either two or three peaks were obtained as well as with the bound protein with a protocol aimed at elucidating conformational changes of the protein in the adsorbed state. For the first set of measurements, fractions corresponding to the first and second peak eluted after a 0

min hold-time and a fraction corresponding to the third peak obtained after a 1000 min hold time were collected. Solutions were also prepared with protein concentrations matching that of the fractions using the fresh mAb sample without prior contact with the POROS XS. The method used to perform HXMS on these samples is the same as that described in prior publications [75][79]. Briefly, a 20 μL volume of each sample was mixed with 180 μL of D_2O for 10 min, followed by quenching of the hydrogen-deuterium exchange with 50 μL of cold 150 mM potassium phosphate at pH 1.5 [58], and adding 100 μL of 8 M GdnHCl containing 100 mM TCEP and 25 mM EDTA at pH 2.6 to facilitate the subsequent pepsin digestion step. After dilution with 95% water, 5% ACN, 0.1% formic acid, and 0.01% TFA at pH 2.6 to bring down the GdnHCl concentration to 1.5 M, the sample was pumped into an immobilized pepsin column. The ensuing peptide mixture was first desalted with a C8 reversed phase column and then separated with a C18 UPLC column 5 to 40% ACN gradient. The effluent from the C18 column was finally analyzed with an LTQ linear ion trap mass spectrometer from Thermo Finnigan (San Jose, CA, USA). Data were collected in a positive ion, profile mode with an ESI voltage of 4.3 kV, a capillary temperature of 250 °C, and sheath gas flow rate of 15 units. Proteome Discover software from Thermo Scientific (Rockford, IL, USA) was used to identify the peptides and only the peptides with high signal-to-noise ratio were selected for following analysis. HDExaminer software from Sierra Analytics (Modesto, CA, USA) was used to calculate the mass increase of each peptide due to hydrogen deuterium exchange. 23 peptides providing 50% coverage of the mAb were selected for further analysis.

The difference between the mass of each deuterated peptide obtained from a particular mAb sample and the mass of the corresponding peptide obtained for the same mAb under a reference condition was used to assess conformational changes. A statistical analysis based on

the method described in Houde et al. [22] was done to determine the confidence limits of the differences in peptide mass. Accordingly, the 99% confidence limit was calculated to be ± 0.43 Da based on replicate experiments with a 10 min deuterion labeling time.

Batch adsorption experiments were conducted to determine conformational changes for the bound protein by HXMS. For this purpose, a 10-mg sample of the resin was first mixed with a 200 μL sample of 0.5 mg/ml mAb in the load buffer and allowed to equilibrate for 1000 min. The resin sample was then mixed with 500 μL of 240 mM NaCl in the load buffer and mixed for 30 min to desorb the mAb species corresponding to the two early elution peaks. The resin sample was then placed in a mixture containing 10 μL of the load buffer in H_2O and 90 μL of the same buffer in D_2O for 10 min, after which the hydrogen-deuterium exchange process was quenched by adding 25 μL of ice-cold buffer containing 150 mM potassium phosphate at pH 1.5 to the resin. 100 μL of the dissociation buffer (8 M GdnHCl, 100 mM TCEP, 25 mM EDTA, at pH 2.6) was then added to the resin under ice for 2 min that resulted in desorption of essentially all of the residual bound protein. 450 μL of an aqueous solution containing solution 5% ACN, 0.1% formic acid, and 0.01% TFA at pH 2.6 was then added to the supernatant to bring the GdnHCl concentration down to approximately 1.5 M. All of the steps described above were conducted in a 2 ml microcentrifuge filter tube slowly rotated end-over-end which allowed washing the resin and removing the supernatant by centrifugation at 8600 rpm in a few minutes. Finally, the desorbed protein was fragmented by pepsin digestion, separated by UPLC, and analyzed by MS as described above.

5.3. Results and Discussion

5.3.1. Three-peak elution behavior

We report first on the chromatographic conditions that lead to a three-peak elution behavior and on the effects of various parameters including hold time in the bound state, resin type, and load buffer composition. Figure 5.1 shows the gradient elution behavior on the POROS XS column as a function of hold time. Essentially only two peaks are obtained with a zero-hold time (Fig. 5.1a). A third peak with peak maximum around 8 CV is barely visible for these conditions. Increasing the hold time to 10 min (Fig. 5.1b) already shows three peaks with maxima at about 5, 6, and 8 CV, respectively. As the hold time is increased further (Figs. 5.1c-f), the area of each of the three peaks as a fraction of the total area changes. The first peak decreases as the hold time increases and the third peak increases while the second peak first increases from 0 to 10 min hold time, and then decreases as the hold time changes from 10 to 1000 min hold time. The position and breadth of the early two peaks remain exactly the same as the hold time is increased. However, the third peak becomes increasingly broader with the peak maximum shifting to somewhat higher CVs as the hold time increases. The right-hand scale of each graph in Fig. 5.1 shows the hydrodynamic radius obtained by in-line DLS. The hydrodynamic radius of the species in the two early eluting peaks is around 5.3 nm and is the same as that of the original monomeric species. The hydrodynamic radius starts to increase from the left to the right for the last peak, from about 5.3 nm in Fig. 5.1c to approximately 10 nm in Fig. 5.1f suggesting that the third peak contains increasing amounts of aggregates species that are eluted at higher salt concentrations.

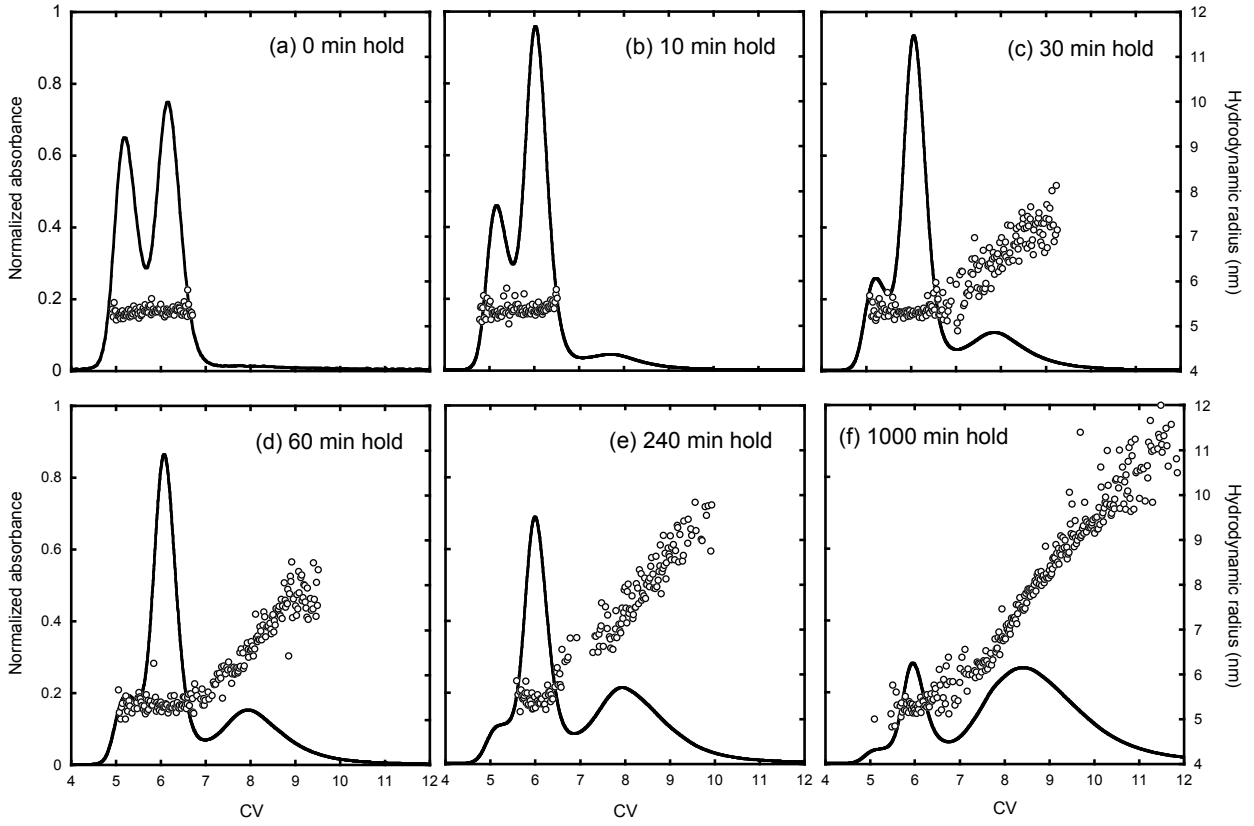

Figure 5.1. Elution behavior for the POROS XS column with (a) 0 min, (b) 10 min, (c) 30 min, (d) 60 min, (e) 240 min, and (f) 1000 min hold time followed by a 20 CV 0-1 M NaCl gradient in 40 mM sodium acetate at pH 5. For simplicity the gradient is not shown. Dots show the hydrodynamic radii obtained by in-line DLS.

Figure 5.2 shows the batch DLS results and CD spectra for fractions collected from the experiment in Fig. 5.1d with a 60 min hold time at 5.2, 6, 8, and 9 CV. The first three of these fractions correspond to the maxima of the three elution peaks, while the last is beyond the third peak maximum. The batch DLS results in Fig. 5.2a show that the first two fractions remain relatively stable as a function of time after collection with a hydrodynamic radius of 5.5±0.5 nm even after 25 h at room temperature. On the other hand, both the third peak fraction and the 9 CV fraction slowly return to monomer over many hours from the time of collection (5 h and > 25 h,

respectively) indicating that there is significant reversibility of this resin-catalyzed aggregation process. CD spectra of the fractions at the three peak maxima obtained immediately after elution (Fig. 5.2b), show only minor changes indicating that only relatively small conformational changes, if any, occurred insufficient to be revealed by this global secondary structure measurement. In-line fluorescence measurements obtained with a 1000 min hold time for the conditions of Fig. 5.1f showed no difference between normalized UV and fluorescence signal for the first two peaks and only slight differences for the third peak suggesting minor conformational changes for the late eluting species, but no difference between the species in the first and second peaks (see Fig. 5.S2 of the Supplementary Material).

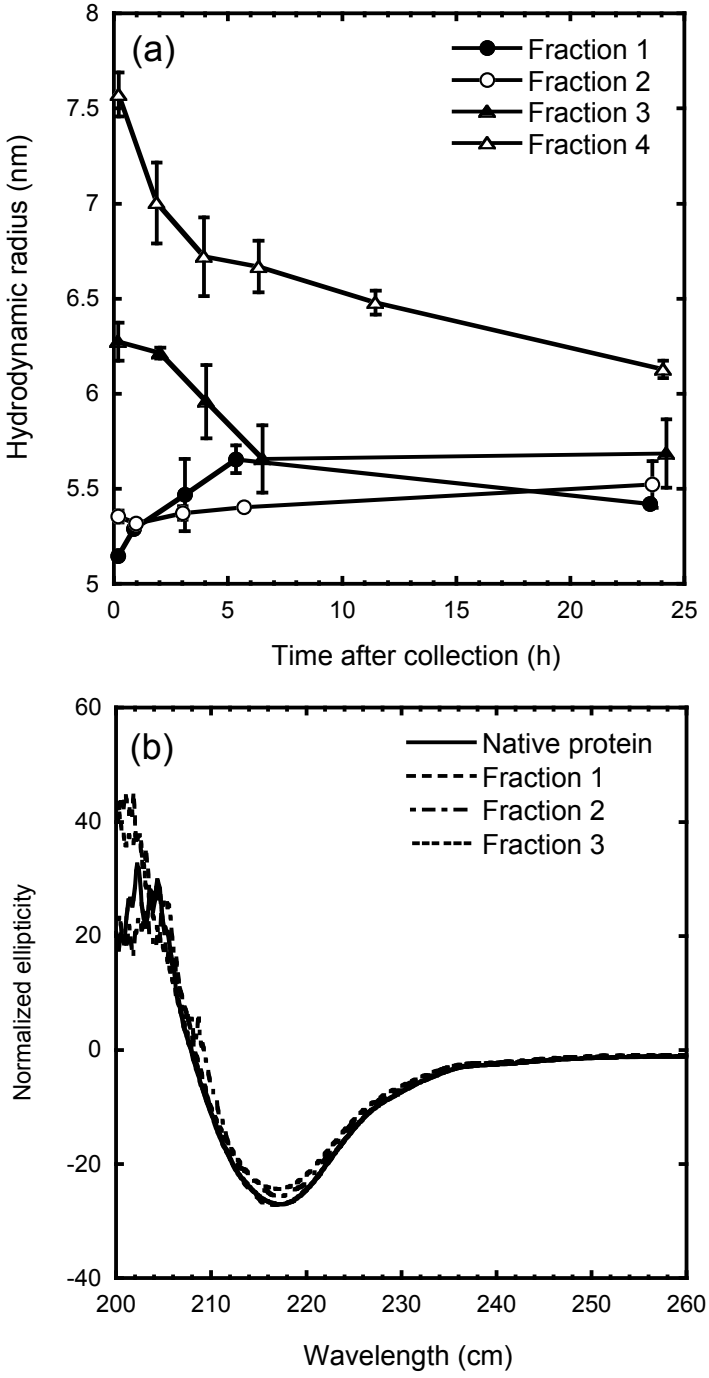

Figure 5.2. Characterization of fractions collected from the POROS XS column with a 60 min hold time followed by a 20 CV 0-1 M NaCl gradient in 40 mM sodium acetate at pH 5

(chromatogram in Fig. 5.1d) by (a) DLS and (b) CD. Fractions 1, 2, and 3 correspond to the maxima of the first, second, and third elution peak, respectively. Fraction 4 is collected at 9 CV.

Figure 5.3 shows the solution HXMS results for the fractions of the first two peaks obtained with zero hold time and of the third peak obtained with a 1000 min hold time (Fig. 5.3a) as well as the bound-state HXMS for a 1000 min hold time (Fig. 5.3b). In our work we were able to reliably identify 23 peptides covering about 50% of the mAb sequence. The location of these reporter peptides is shown in Fig. 5.4, which was obtained by homology modeling using human IgG1 (Protein Data Bank Entry 1HZH) as a template and PyMOL as a visualization tool. For each of these reporter peptides, Fig. 5.3a and Fig. 5.3b show the difference between the mass after deuterium exchange and the mass of the same deuterated peptide derive from the protein in a reference state. The dashed lines show the 99% confidence limits for the mass differences based on replicate measurements. Positive values of the mass difference indicate greater solvent exposure while negative values indicate protection relative to the reference state. For the solution measurements in Fig. 5.3a, the reference state is the native mAb without any contact with the POROS XS resin while for the bound state measurement in Fig. 5.3b, the reference is the mAb held on the resin for 30 min during which only minor amounts of aggregates were seen in the elution (cf. Fig. 5.1c). As seen in Fig. 5.3a, none of the peptides derived from the first and second peak fraction show significant mass difference relative to the native monomer, suggesting that the species in the first and second peak have the same conformation as the native mAb, which is consistent with the CD and fluorescence measurements. On the other hand, peptides 15 and 16 in the third peak fraction show statistically significant mass increase relative to the native monomer, indicating partial unfolding of the species eluted in the third peak. As seen in Fig. 5.4, these two peptides are located in the Fc region of the mAb. The partial unfolding behavior in the

Fc region of another mAb on strong cation exchange resins has been reported by our group [75][79]. Additionally, the Fc fragment of different IgGs has been reported to be less stable when exposed to other stresses such as low pH denaturation [61][62][63] suggesting that this characteristic may be a general phenomenon.

As seen in Fig. 5.3b, the bound state HXMS results show that many of the peptides exhibit significant mass differences including peptides 3, 8, 12, 15, 16, 20, 21, 22, suggesting that in this state, after 1000 min hold on the resin, the mAb exhibits greater conformational changes resulting in more substantial solvent exposure. Since many of the peptides do not show such differences for the protein eluted in the third peak, we surmise that a majority of the unfolded regions refold quickly upon desorption from the resin. Peptides 15 and 16 still remain more solvent exposed when eluted suggesting that the refolding kinetics in this region of the mAb is slow.

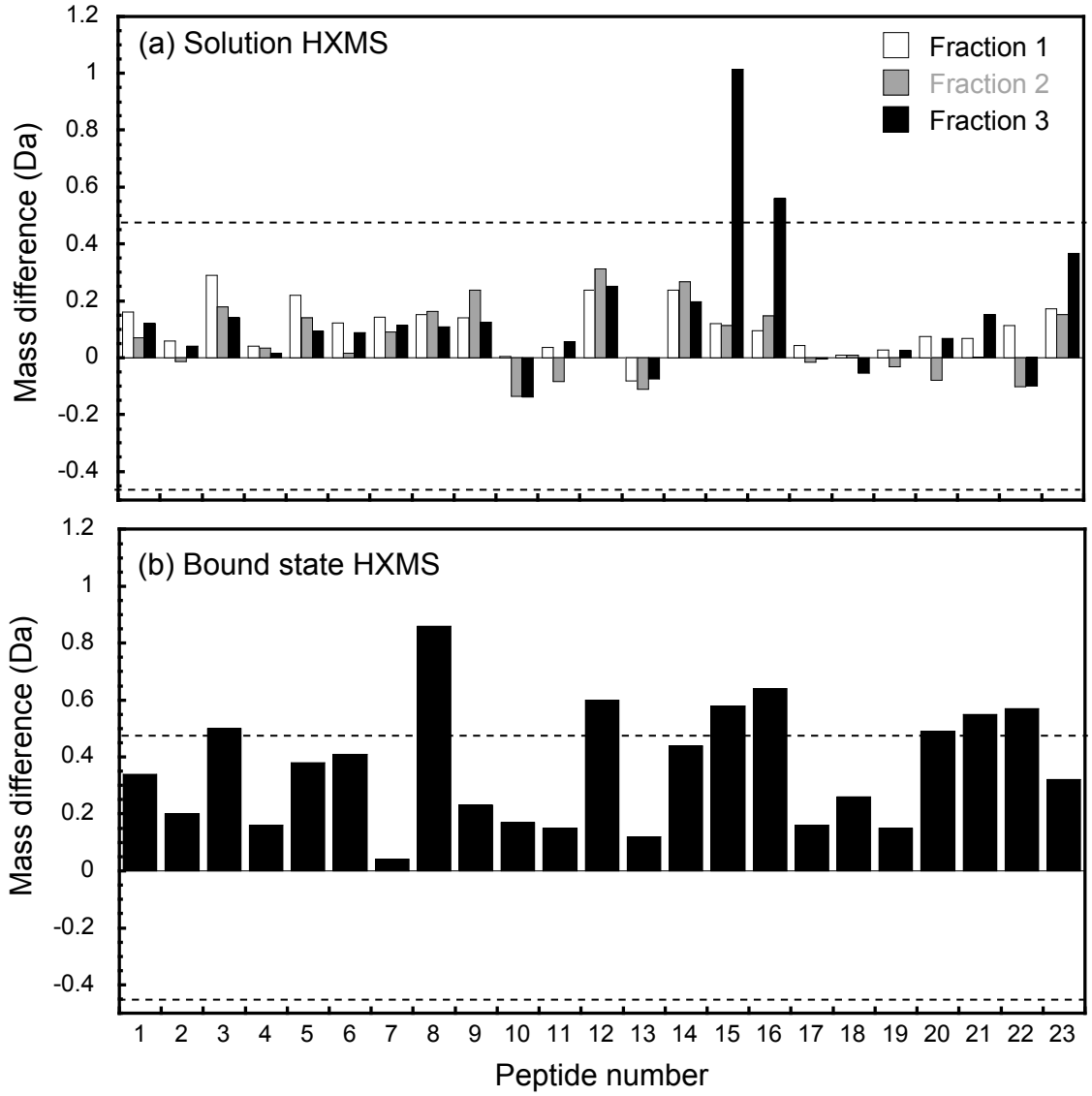

Figure 5.3. Results for (a) solution and (b) bound state HXMS. (a) Shows the difference between the mass of each of the 23 reporter peptides obtained from fractions collected from the POROS XS column after 0 or 1000 min hold time followed by a 20 CV 0-1 M NaCl gradient (Fig. 5.1a and Fig. 5.1f) and the mass of the corresponding peptide obtained from the native mAb. Fractions 1, 2, and 3 correspond to the maxima of the first, second, and third eluted peak. (b) Shows the difference between the mass of each of the 23 reporter peptides obtained from the mAb held on the resin for 1000 min in batch mode and that of the corresponding peptide for the

mAb held on the resin for 30 min. In both cases, the dashed lines represent the 99% confidence limits for the mass difference values. The peptides are sorted in ascending number along the protein sequence. Positive vertical bars suggest increased solvent exposure in each eluted peak fraction, respectively, compared with the protein in the reference state.

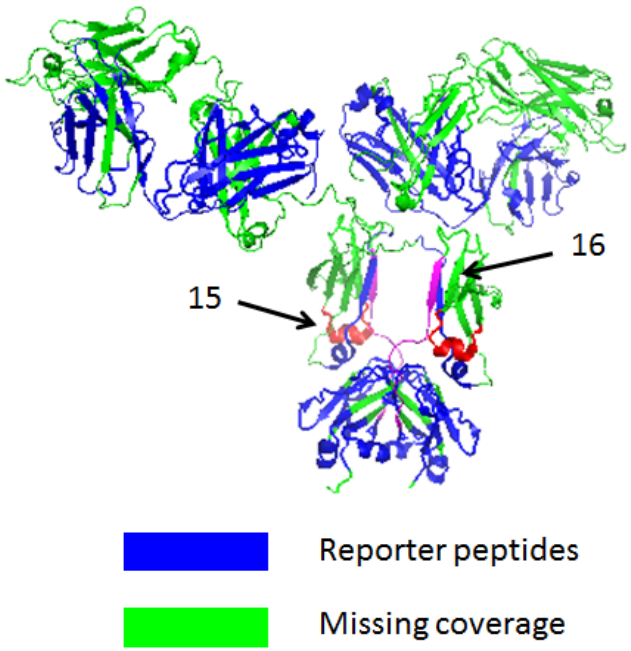

Figure 5.4. Map of reporter peptides identified for the mAb. The mAb structure is obtained by homology modeling with human IgG1 (1HZH in the Protein Data Bank) as a template. Blue regions show the location of the 23 reporter peptides. Green regions represent the missing coverage. Peptides 15 and 16, shown in red and magenta, respectively, exhibited the greatest solvent exposure in the aggregates of the third eluting peak.

Figure 5.5 compares the mAb elution behavior obtained with POROS XS with that obtained for Nuvia HR-S with a 30 min hold time for identical conditions. While two- or three-peak elution is observed for the mAb on POROS XS dependent on hold time, a single peak is

obtained for NUVIA HR-S regardless of hold time. The in-line hydrodynamic radius measurements confirm that the single elution peak obtained for Nuvia HR-S consists exclusively of monomeric species. Since the Nuvia HR-S has the same particle size as POROS XS and similar peak widths are obtained, the single peak elution behavior is not a result of different resolving power of the two resins. Rather, the distinct elution behaviors of the mAb on columns packed with the two resins indicate that the elution behavior is dependent on the resin properties. Based on this comparison it is evident that two distinct phenomena occurring over very different time scales determine how the mAb elutes from POROS XS. The first of these phenomena, occurring over a short time scale, results in the elution of two peaks both containing monomeric species, while the second, occurring over a relatively long time scale, result in the formation of aggregated species that elute late in the gradient. To further elucidate the second of these effects we conducted experiments in an arginine acetate load buffer since previous work with a different mAb has shown that replacing sodium with arginine as a counterion reduced or nearly completely eliminated on-column aggregate formation [79]. Arginine as a counterion has been shown to reduce the protein binding strength on CEX resins [34] and, in general, is thought to be a useful additive to control protein aggregation both in solution and during chromatographic separations [64][65][66][67][68]. Figure 5.6 shows results obtained by loading and holding the protein on POROS XS in a buffer containing 40 mM arginine acetate at the same pH. As seen in this figure, while the two-peak elution behavior persists, there is no evidence of a third peak indicating that replacing sodium with arginine in the load/hold buffer effectively prevents the formation of aggregates. Adding arginine to the NaCl elution buffer after having loaded the mAb in the sodium acetate buffer had no effect on aggregate formation. This result suggests that arginine's modulating effect on the mAb binding strength [34] is likely responsible for

eliminating the conformational changes that ultimately cause aggregate formation upon elution [79].

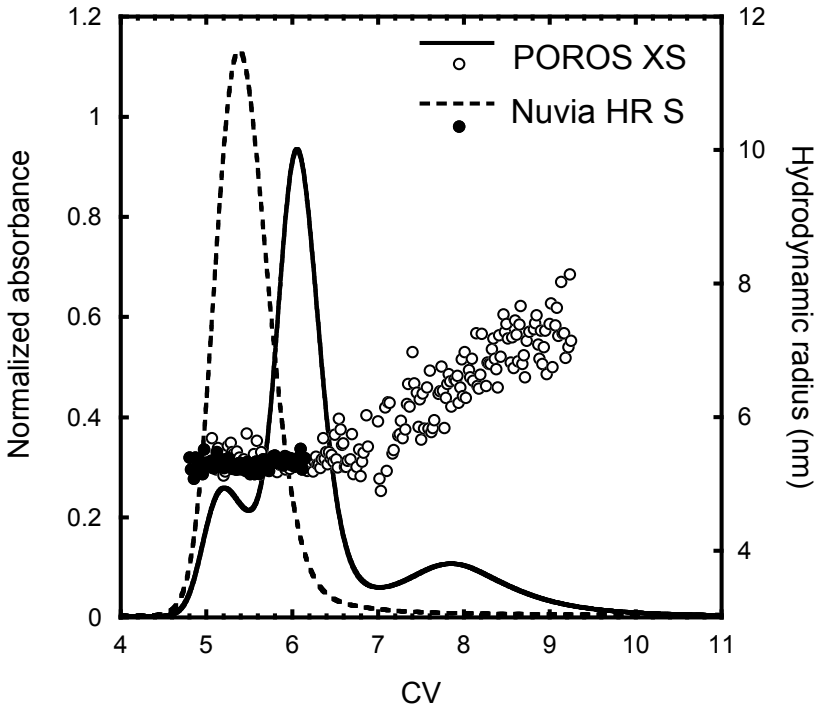

Figure 5.5. Comparison of elution behavior of the mAb on columns packed with POROS XS and Nuvia HR S resins with a 30 min hold time followed by a 20 CV 0-1 M NaCl gradient in 40 mM sodium acetate at pH 5. Dots show the hydrodynamic radii obtained by in-line DLS.

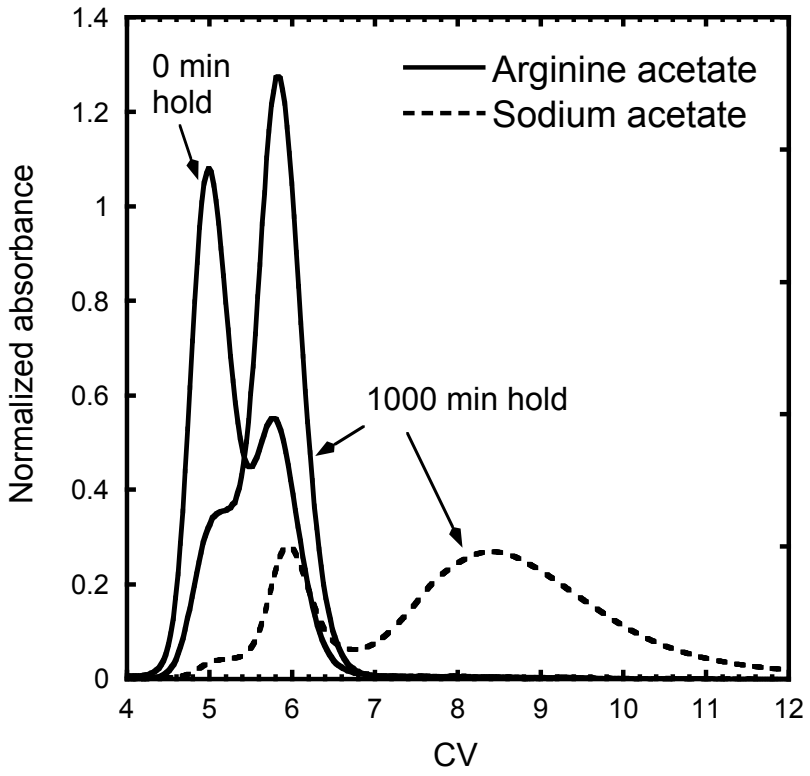

Figure 5.6. Comparison of POROS XS elution behavior obtained using a 40 mM sodium acetate load buffer with a 1000 min hold with the elution behavior obtained using a 40 mM arginine acetate buffer with 0 and 1000 min hold times. For both load buffers elution was with a 20 CV 0-1 M NaCl gradient.

5.3.2. Two-peak elution behavior

The remainder of this work focuses on the two-peak elution behavior obtained for POROS XS when the protein is eluted immediately after loading, i.e. with zero hold time.

Figure 5.7 shows the results obtained when fractions of the first and second peak obtained with the POROS XS column with zero hold time are dialyzed against the original load buffer (40 mM sodium acetate) and then individually re-injected to either the POROS XS column (Fig. 5.7a) or the Nuvia HR-S column (Fig. 5.7b). As seen in Fig. 5.7a, for POROS XS

re-injecting either the first or the second peak fraction gives exactly the same two-peak elution behavior as the fresh mAb sample suggesting that the underlying phenomenon that leads to elution of the mAb in two peaks is reversible. In principle, this behavior is consistent with either the elution of two different protein conformations (one more strongly retained than the other by the resin), with the altered conformation reverting back to the original one after elution, or with the presence of two different binding sites in the resin that bind the mAb with different strengths and at different rates. Based on the CD, in-line fluorescence, and HXMS results, which showed no difference between the first and second peak fractions, it appears that the last of these two possible mechanisms is more likely. For Nuvia HR-S (Fig. 5.7b) the same single peak is eluted regardless of which POROS XS produced fraction was re-injected, further indicating that both of the peaks eluted from the POROS XS column contain the same species.

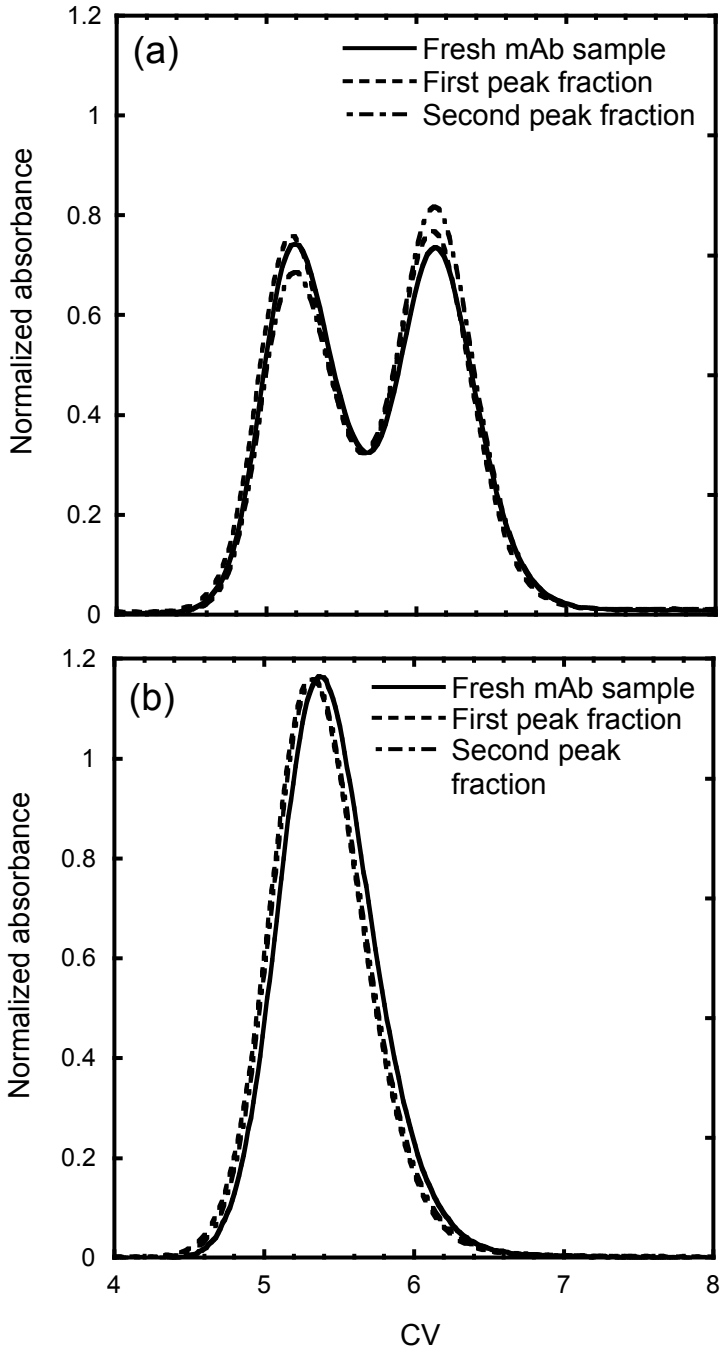

Figure 5.7. Comparison of elution of fresh mAb sample with results obtained by re-injecting fractions from the POROS XS column with 0 min hold time followed by a 20 CV 0-1 M NaCl gradient in 40 mM sodium acetate at pH 5. (a) Results for samples injected into the POROS XS

column. (b) Results for samples injected into the Nuvia HR S column. Conditions are identical for all runs.

Figure 5.8 provides additional information on the two-peak elution behavior of POROS XS by illustrating the effects of load and elution flow rates (Fig. 5.8a and 5.8b, respectively). As shown in this figure, the load flow rate had no effect (contrary to what we observed for another mAb on the resin Fractogel SO3 [74]), while the elution flow rate significantly affected the relative magnitude of the two peaks. In the latter case, while the breadth of the peaks decreased as the elution flow rate was decreased, as expected because of the increased residence time and, thus, increased plate number, a much greater portion of the protein eluted in the second peak. This result suggests that the distribution of the protein between the two peaks is kinetically controlled over time scales that are comparable to the elution times.

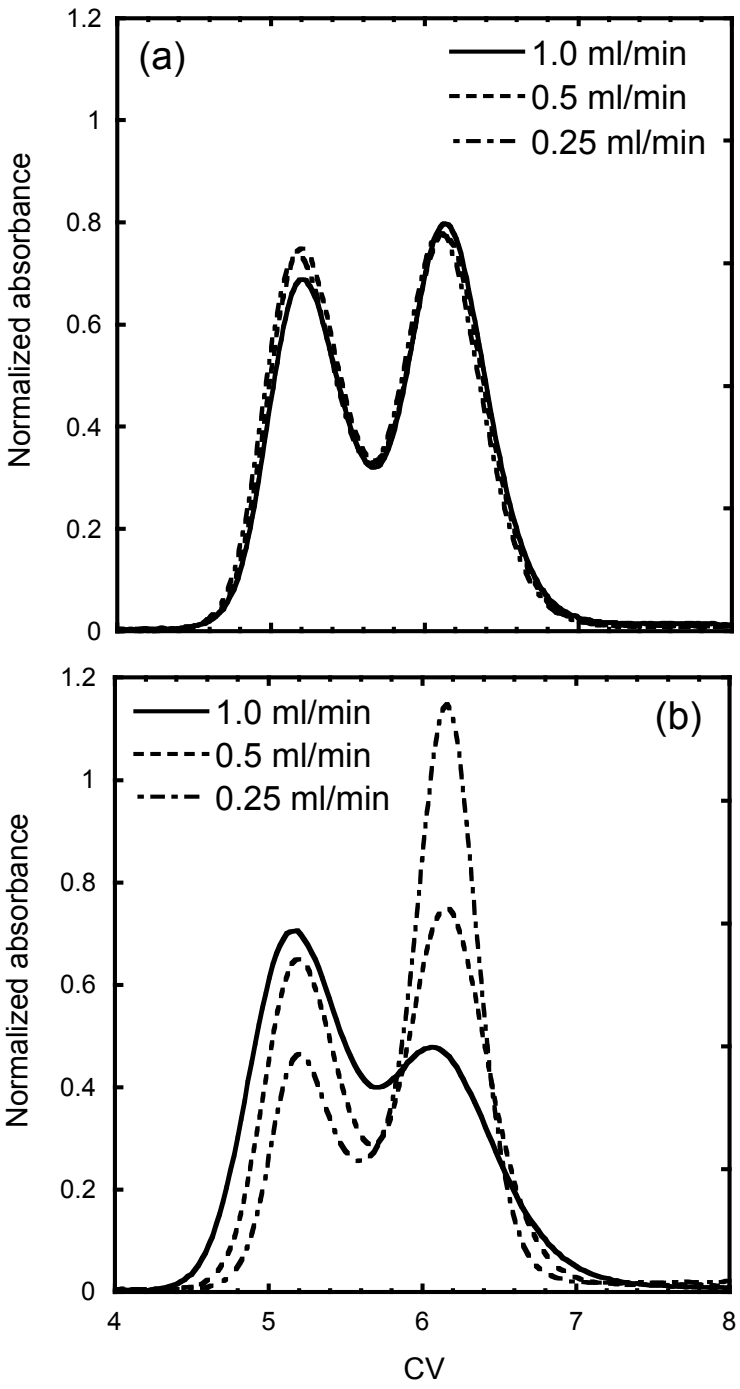

Figure 5.8. Effects of (a) load flow rate and (b) elution flow rate on elution behavior of the POROS XS column with 0 min hold time followed by a 20 CV 0-1 M NaCl gradient in 40 mM sodium acetate at pH 5.

5.3.3. Modeling of the two-peak elution behavior

While developing a model to describe the unfolding/aggregation behavior is beyond the scope of this work, a mechanistic model was developed for the two-peak behavior with the intent of helping to elucidate the underlying causes. The model assumes that POROS XS contains two independent binding sites: weak binding sites (1) assumed to have fast on/off kinetics and strong binding sites (2) assumed to have slow on/off kinetics. The physical nature of the two assumed binding sites is not certain, but POROS resins are designed with a bi-modal pore size distribution [73][82] including very large pores, where protein molecules can presumably bind quickly but more weakly, and small pores where presumably protein molecules can bind more strongly but also more slowly. Accordingly, for each of the two types of binding sites i=1 and i=2, protein binding equilibrium is described by the mass action law model, which can be written as follows [83][84]:

$$q_i = A_i \left(C_{Na^+} \right)^{-z_i} c \tag{5.1}$$

where q_i is the bound protein concentration, A_i is an equilibrium constant, z_i is the effective protein binding charge, C_{Na^+} is the Na^+ concentration, and c is the protein concentration in the particle pores. The corresponding binding kinetics is described for each site type by the following equation:

$$\frac{\partial q_i}{\partial t} = k_i \left(c - \frac{\left[Na^+ \right]^{z_i}}{A_i} q_i \right) \tag{5.2}$$

where k_i is a binding rate constant.

Equations (5.1) and (5.2) are coupled with the following equations and boundary conditions:

$$\begin{cases} \varepsilon_p \dfrac{\partial c}{\partial t} + \left(1-\varepsilon_p\right)\sum_i \dfrac{\partial q_i}{\partial t} = \dfrac{D_e}{r^2}\dfrac{\partial}{\partial r}\left(r^2 \dfrac{\partial c}{\partial r}\right) \\ t = 0, c = 0, q_i = 0 \\ r = 0, \dfrac{\partial c}{\partial r} = 0 \\ r = r_p, c = C \end{cases} \tag{5.3}$$

$$\begin{cases} \varepsilon \dfrac{\partial C}{\partial t} - \dfrac{3\left(1-\varepsilon\right)D_e}{r_p}\left(\dfrac{\partial c}{\partial r}\right)_{r=r_p} + u\dfrac{\partial C}{\partial x} = 0 \\ t = 0, C = 0 \\ x = 0, C = C_{\text{feed}} \end{cases} \tag{5.4}$$

which describe, respectively, mass transfer in the particles and convective transport along the column length, x. In these equations, C is the protein concentration in the mobile phase outside the particles, ε_p is the intraparticle porosity, D_e is the effective pore diffusivity, and r_p is the particle radius. The Na^+ concentration as a function of time and position in the column during the gradient was simulated neglecting any dispersion effects. The resulting set of partial differential equations was solved numerically by finite differences using 30 and 100 discretization points in the radial and axial direction, respectively, which were sufficient to eliminate any numerical dispersion effects. The resulting system of ordinary differential equation was integrated using MATLAB's variable order solver routine *ode15s*.

The parameters appearing in these equations were estimated as follows. ε = 0.35 was obtained using the Carman-Kozeny equation from the column pressure drop. ε_p = 0.58 and D_e = 7.0×10^{-8} cm^2/s where obtained from pulse injections of the mAb under non-binding conditions (1

M NaCl) at different flow rates of the mobile phase as described in ref. [30]. Next we assumed that the weak binding sites have fast kinetics and used k_1 = 100 s^{-1}, which is sufficiently large to ensure that the simulated binding kinetics does not influence retention of the first peak. In this case, A_1 = 5.37x10^{28} $(mM)^{12.3}$ and z_1 =12.3 for the weak binding sites could be determined with the method outlined in ref. [30] from the retention of the first peak as a function of gradient slope obtained in separate experimental linear gradient elution runs (see Fig. 5.S3 in the Supplementary Material). The remaining parameters k_2 = 0.013 sec^{-1}, A_2 = 2.56x10^{49} $(mM)^{20.6}$, and z_2 = 20.6 for the strong binding sites were estimated by regressing the data at varying salt gradients using MATLAB's nonlinear least squares function, *lsqnonlin*. Figure 5.9 shows the modeling results illustrating the predicted dependence of the elution peaks for different values of the rate constant for adsorption on the strong binding sites (Fig. 5.9a) and the predicted dependence on the flow rate, using k_2=0.013 s^{-1} (Fig. 5.9b) for the experimental conditions of Fig. 5.8b. As seen in Fig. 5.9a, a value of k_2 = 0 obviously leads to a single early-eluting peak and a value of k_2 = 0.1 s^{-1} leads to a single late-eluting peak. Intermediate values around 0.01 s^{-1} obviously yield two peaks. As seen in Fig. 5.9b using the regressed values of k_2 = 0.013 s^{-1}, the model predicts a two-peak elution profiles that vary with flow rate in a manner consistent with the experimental results shown in Fig. 5.8b. In this case, as shown by the model at 1 ml/min, a majority of the protein elutes early as the elution time is too short to permit the protein's full interaction with the strong, but slow binding sites. At 0.25 ml/min, more time is available for interaction with the strong binding sites, which end up dominating the elution process.

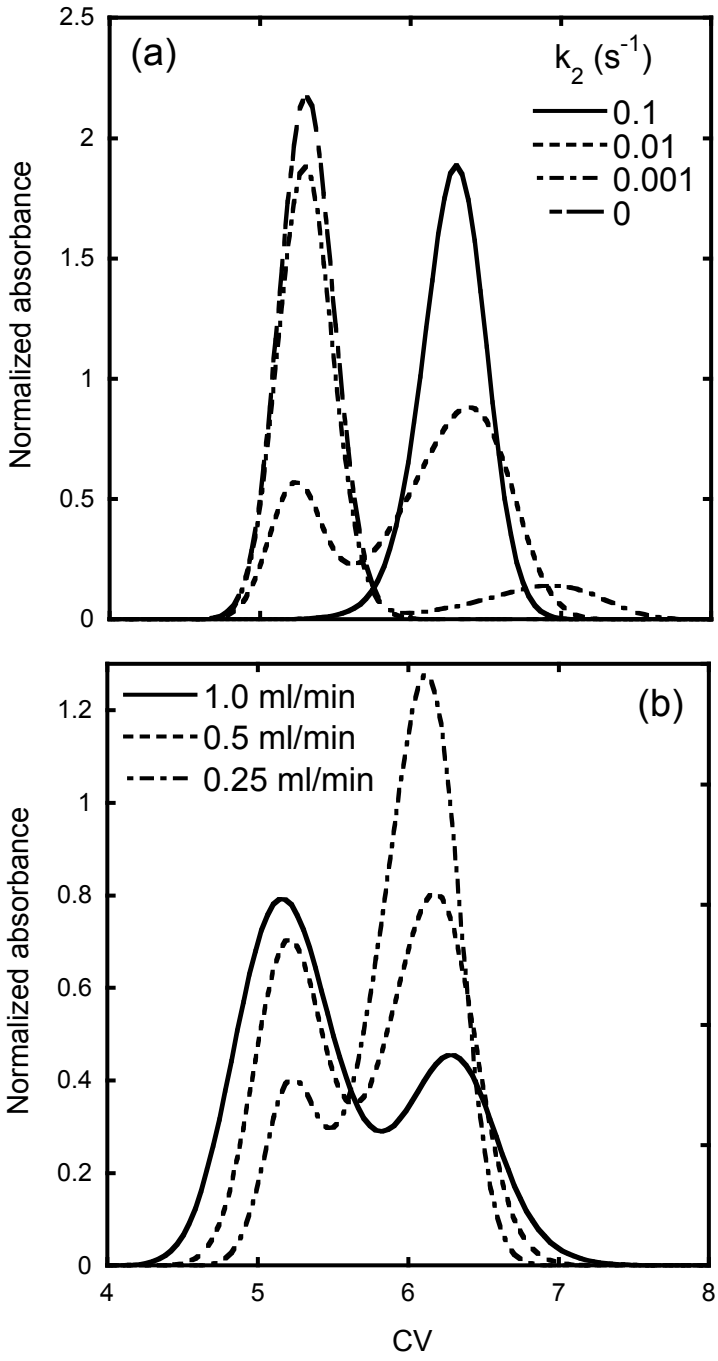

Figure 5.9. Elution profiles predicted by the model described in Section 5.3.3 for POROS XS with a 20 CV 0-1 M NaCl gradient. (a) Effect of varying k_2 while keeping k_1 = 100 s^{-1} at 0.25

ml/min. (b) Effect of elution flow rate for the conditions of Fig. 5.8b predicted with k_1 = 100 s^{-1} and k_2 = 0.013 s^{-1}. Other model parameters are given in the text.

5.3.4. Overall mechanism

Figure 5.10 illustrates schematically the proposed overall mechanism leading to the mAb's three-peak elution behavior on POROS XS. The first step in the process is binding to the resin on two different binding sites – one weak but with fast kinetics (step 1) and one strong but with slow kinetics (step 2). As noted earlier, the two binding sites may be associated with the bi-modal pore size distribution of POROS XS, with weaker binding occurring in the larger pores and stronger binding in the small pores. The protein bound to the weak sites remains stable while the protein bound to the strong sites undergoes kinetically limited conformational changes that result in a destabilized surface species (step 3). If the salt gradient (step 4) begins immediately after loading, before the strongly bound protein has undergone significant conformational changes, two elution peaks are obtained. In this case, during gradient elution, the mAb molecules continue to interact with both binding sites. At high flow rates, when the time is short, elution is dominated by interaction with the weak and fast binding sites. At low flow rates, on the other hand, when the time is long, elution is dominated by interactions with the strong and slow binding sites. In either case, however, the same monomeric species is eluted in both peaks as confirmed by CD, in-line fluorescence, and HXMS. Re-injection of fractions collected from the POROS XS column results in exactly the same two peaks when the gradient elution conditions are the same since molecular properties are the same and interactions with the binding sites are reversible. Starting the gradient after a substantial hold time (e.g. $\geq$10 min), results in a third peak which contains a significant percentage of aggregates, which are generated upon elution of the destabilized surface species gradually formed while adsorbed on the strong binding sites.

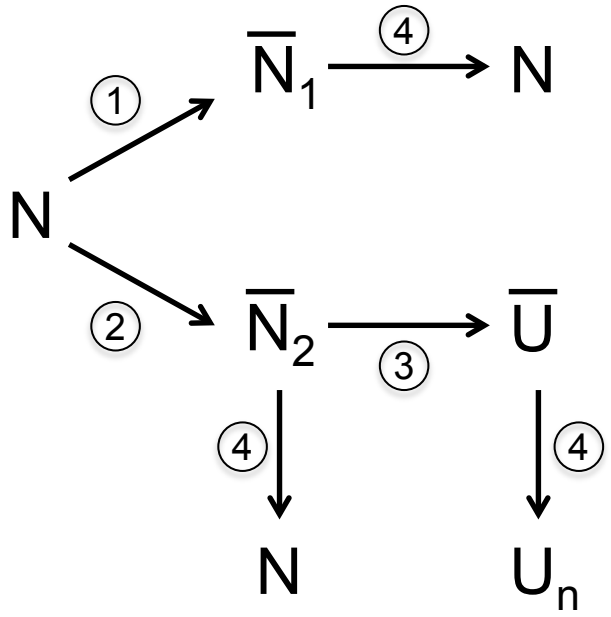

Figure 5.10. Mechanism leading to two and three-peak elution behavior on POROS XS. N, U, and U_n represent native, unfolded, and aggregated forms of the mAb. Overbars denote resin-bound species. $\overline{N_1}$ and $\overline{N_2}$ represent native protein bound to the weak but fast sites and to strong but slow binding sites, respectively. Step 1: binding to weak/fast binding site during load; step 2: binding to strong/slow binding sites during load; step 3: kinetically limited unfolding on strong binding sites during hold step; step 4: salt gradient elution. Two-peaks are eluted if the gradient (step 4) starts immediately after loading (steps 1 and 2) while three peaks are eluted at increasing salt concentrations if the gradient begins after a prolonged hold step (step 3).

5.4. Conclusions

A three-peak elution behavior has been observed when a mAb is loaded into a POROS XS resin column, held in the bound state for a period of time, and then eluted with a linear salt gradient. The percentage of protein eluting in each of the three peaks changes with hold time, with the first peak gradually decreasing, the second peak first increasing and then decreasing, and the third peak gradually increasing as the hold time is increased. We have determined that the first two peaks, which are also observed with zero old time, contain only monomeric species and likely result from the existence of different binding sites on the resin having both different binding strength and different binding kinetics. The third peak, observed even after a relatively short hold time, contains aggregated species that are formed as a result of protein conformational changes that increase in either magnitude or extent as the protein is held in the bound state for increasing lengths of time. Based on the changes in relative peak area as a function of hold time, it seems that the conformational changes are associated with binding to the strong, slow kinetics binding sites. From a more practical point of view, we have also verified some ways in which the three- and two-peak elution behaviors can be eliminated. Replacing sodium with arginine as a counterion in the acetate buffer is effective in essentially eliminating aggregate formation even after prolonged hold times. Based, in part, on prior observations [79], we believe that the effect of arginine is primarily to weaken protein-resin interactions that are responsible for generating destabilized surface intermediates. Arginine in the elution buffer, in fact, did not alter the amount of aggregates formed indicating that controlling the load buffer composition is critical. Arginine, however, does not remove the two-peak elution behavior observed for POROS XS without a hold time, as this behavior seems to be associated with the existence of multiple binding sites on the resin. On the other hand, replacing POROS XS with Nuvia HR-S and operating the column

under identical conditions completely removed both three- and two-peak elution behaviors, likely as a result of the more hydrophilic and more homogenous structure of this resin compared to POROS XS.

5.5. Supplementary Material

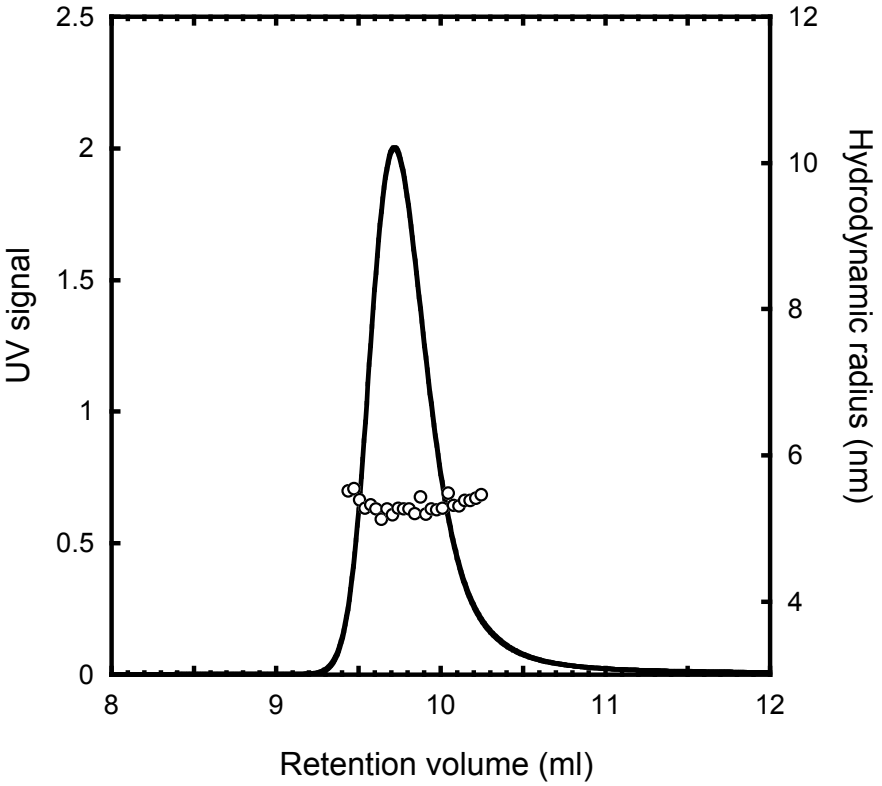

Figure 5.S1. Size exclusion chromatography with in-line dynamic light scattering analysis of a fresh mAb. SEC was conducted with a TSKgel 3000SWXL column (Tosoh Bioscience LLC, King of Prussia, PA, USA) in 40 mM sodium acetate at pH 5 and a flow rate of 0.5 ml/min.

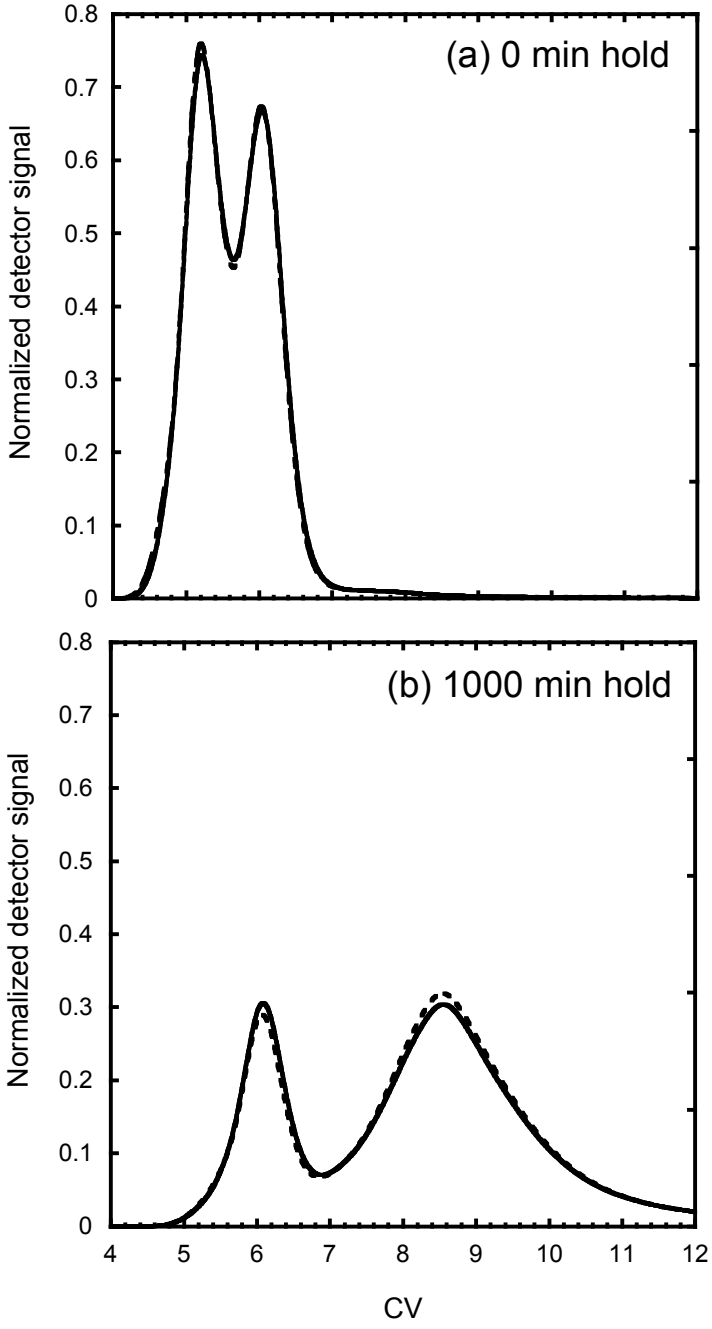

Figure 5.S2. Scaled UV detector signal (solid line) and fluorescence detector signals (dotted line) for elution form the POROS XS column with (a) 0 min and (b) 1000 min hold time followed by a 20 CV 0-1 M NaCl gradient in 40 mM sodium acetate at pH 5. The two detector signals are practically superimposed in (a).

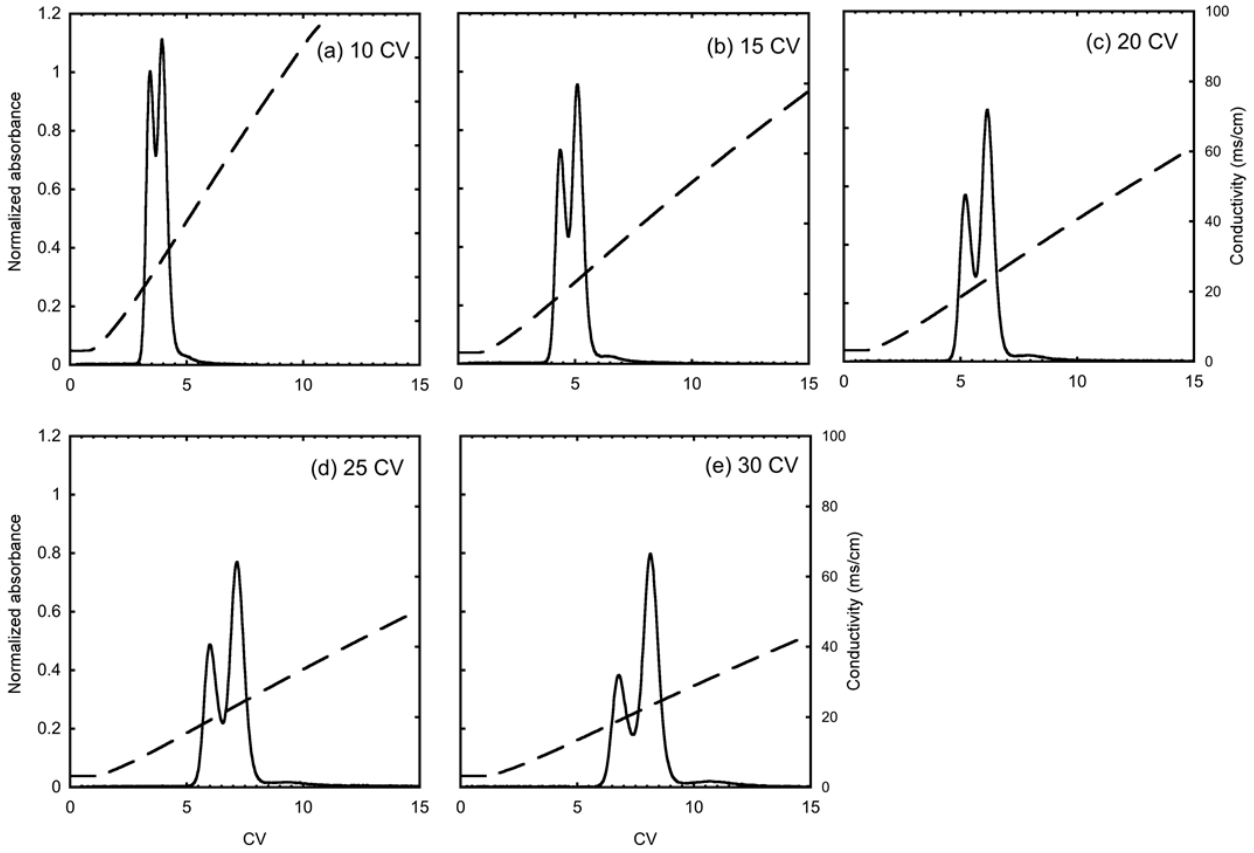

Figure 5.S3. Elution profiles obtained for the POROS XS column with 0 min hold followed by 0-1 M NaCl gradients with varying gradient durations at 0.5 ml/min in 40 mM sodium acetate at pH 5.

Chapter 6

Conclusions and Recommendations

6.1. Conclusions

The goal of this work was to elucidate protein conformational change and aggregation mechanism during cation exchange chromatography. Chapter 2 reports a two-peak elution behavior of a highly pure mAb during salt gradient elution on a chromatography column packed with the strong cation exchanger Fractogel SO3, whose backbone is grafted with polymers to enhance protein binding capacity and binding strength. SEC and DLS analysis show that while the early elution peak is consisted of pure monomer, the late elution peak is a mixture of monomer and higher molecular weight species. Further chromatography experiments suggest that the late elution peak becomes more prominent when the mAb stays bound to the resin for a longer time and when the mAb is loaded and held in the column at a lower pH and lower salt concentration. CLSM results reveal that the peak splitting behavior is related specifically to Fractogel's unique resin structure, backbone grafted with polymer extenders, which allow protein to retain some diffusional mobility to redistribute throughout resin particles during the hold time, finally reaching a low local bound protein concentration. The latter, in turn, facilitates protein conformational change. In Chapter 3, solution HXMS experiments prove that both the monomer in the early elution peak and the monomers in the late elution peak have the same protein conformation as that of the native mAb, while the components of the aggregates found in the late eluting peak show significant structural difference compared with the native mAb. Specifically, two peptides in the Fc region of the mAb exhibit significantly unfolding. Adsorbed

HXMS experiments further suggest that the mAb unfolds while bound to the resin, with the same two peptides in the Fc region of the mAb showing largest unfolding.

Based on the work of Chapter 2 and 3, a mechanism is proposed to describe what actually happens during protein binding, holding and elution on the cation exchange column. In the proposed mechanism, the protein first adsorbs on the resin through a diffusion-controlled mass transfer mechanism. While bound, the protein slowly and gradually unfolds, forming an unfolded intermediate on the resin. Finally, during salt gradient elution, a fraction of the unfolded species refolds to native monomers, while the rest form high molecular weight species in the late elution peak.

Chapter 4 extends the previous studies to other mAb molecules and to other resins with different structures. Among all of the six cation exchange resins tested with a same mAb under similar operating conditions, CEX resins with grafted polymers, including Fractogel SO3, Eshmuno S and Nuvia S, and CEX resin with a bimodal pore size distribution, POROS HS, are shown to result in a two-peak elution behavior. On the other hand, CEX resins with a macroporous structure and no polymeric surface extenders, such as UNOsphere S and Source S, show almost no evidence of a second peak. For three different mAbs tested on the Fractogel SO3 resin under the same operating conditions, one exhibits a prominent two-peak elution behavior, one shows a slight second peak, and the remaining one cannot be eluted even under very high salt (e.g. 1 M sodium chloride). A melting temperature study with Circular Dichroism suggests that the distinct elution behavior of the three mAbs could be correlated with their solution stability. Another interesting result in this Chapter is that replacing sodium with arginine as a counter-ion in the load buffer suppresses protein unfolding an aggregation on CEX resins. We

conclude that arginine reduces the protein binding strength on the resin preventing conformational changes that can ultimately lead to aggregate formation.

In Chapter 5, we report a three-peak elution behavior for a fourth mAb during salt gradient elution after a period of hold time (>10 min), on a column packed with the CEX resin POROS XS. This resin has a macroporous structure with bimodal pore size distribution. DLS results suggest that the first two peaks contain exclusively monomeric species while the third peak contains a mixture of monomeric and multimeric species. A set of biophysical methods, including CD, in-line fluorescence and HXMS, prove that the two early elution peaks are conformationally identical to the native mAb, while the aggregates in the third peak contain some unfolding regions, especially with two peptides in the Fc region of the mAb showing significant more solvent exposure. Based on the results of chromatography experiments under different operating conditions, such as different loading counter-ions, different CEX resins, different hold time and elution flow rates, together with a mechanistic modeling study, we conclude that the two early-eluting peaks form as a result of interactions with two different binding sites present in the resin, one with weak but fast binding, and the other with strong but slow binding. The protein bound to the strong site gradually unfold during the hold time, finally forming aggregates in the third peak during high salt elution.

6.2. Recommendations for Future Work

Several recommendations are given for future work based on evidence presented thus far on protein unfolding and aggregation behavior during cation exchange chromatography.

In Chapter 2 the grafted polymers on the backbone of Fractogel SO3 were shown to facilitate protein movement and redistribution inside the resin particles thus lowering the local bound protein concentration, and finally, leading to protein conformational change. From a microscopic point of view, polymer-protein interactions can be studied to de-couple the mass transfer and adsorption effects. The binding strength between polymers and protein can be measured by surface plasmon resonance (SPR) [85] and the effects of polymers on protein stability can be investigated by HXMS. Both techniques should yield some insight into designing polymer-grafted resins which eliminate or mitigate protein conformational change.

In Chapter 3 and 5, results from HXMS studies for two mAbs showed that during aggregates formation on CEX resins the largest local unfolding occurred in the Fc region of the mAbs. This evidence suggests the Fc region is a prime target for modification using protein engineering tools to improve the mAb stability when binding to CEX resins. As shown by Lee et al. [86] and Chennamsetty et al. [87], target mutation has been widely applied to enhance antibody resistance to aggregation.

In Chapter 4, the melting point by circular dichroism (CD) analysis of three mAbs were shown to correlate with the mAbs' elution behavior on cation exchange columns, which suggests the possibility of predicting the propensity of protein aggregation on chromatographic surface based on protein solution stability. For this purpose, a set of different biophysical methods can be applied to measure protein solution stability against a variety of stresses, such as protein

denaturation study in exposure to guanidine hydrochloride by CD, protein solvent exposure and flexibility at low pH by HXMS, and protein melting temperature study by Differential Scanning Calorimetry (DSC) and Differential Scanning Fluorimetry (DSF).

Antibody stability on other types of chromatography can also be studied in the future. For instance, Zhang et al. [88][89] and Gagnon et al. [90][91] showed that some mAbs exhibit conformational change upon binding and elution during protein affinity chromatography, a widely used capture step in the pharmaceutical industry. HXMS and some other biophysical methods can be applied to establish molecular details of protein global and local structural instability.

References

[1] J.M. Reichert, Monoclonal antibodies as innovative therapeutics, J. Curr. Pharm.Biotechnol. 9 (2008) 423–430.

[2] W. Wang, S. Singh, D.L. Zeng, Antibody structure, instability, and formulation, J. Pharm. Sci. 96 (2007) 1–26.

[3] A.S. Rosenberg, Effects of protein aggregates: an immunologic perspective, AAPS J. 8 (2006) E501–E507.

[4] J.L. Cleland, M.F. Powell, S.J. Shire, The development of stable protein formulations - a close look at protein aggregation, deamidation, and oxidation, Crit. Rev. Ther. Drug Carr. Syst. 10 (1993) 307–377.

[5] A. Shukla, B.B. Hubbard, T. Tressel, S. Guhan, D. Low, Downstream processing of monoclonal antibodies - Application of platform approaches, J. Chromatogr. B 848 (2007) 28–39.

[6] A. Stein, A. Kiesewetter, Cation exchange chromatography in antibody purification: pH screening for optimised binding and HCP removal, J. Chromatogr. B 848 (2007) 151–158.

[7] T. Ishihara, T. Kadoya, H. Yoshida, T. Tamada, S. Yamamoto, Rational methods for predicting human monoclonal antibodies retention in protein A affinity chromatography and cation exchange chromatography - Structure-based chromatography design for monoclonal antibodiesm, J. Chromatogr. A 1093 (2005) 126–138.

[8] A.M.-B. Staby, R.G.R.G. Hansen, J.H. Jacobsen, L.A. Andersen, M. Gerstenberg, I.H. Jensen, Comparison of chromatographic ion-exchange resins - IV. Strong and weak cation-exchange resins and heparin resins, J. Chromatogr. A 1069 (2005) 65–77.

[9] B.L. Karger, R. Blanco, The effect of on-column structural-changes of proteins on their hplc behavior, Talanta 36 (1989) 243–248.

[10] J.L. McNay, E.J. Fernandez, How does a protein unfold on a reversed-phase liquid chromatography surface? J. Chromatogr. A 849 (1999) 135–148.

[11] A. Jungbauer, C. Machold, R. Hahn, Hydrophobic interaction chromatography of proteins - III. Unfolding of proteins upon adsorption, J. Chromatogr. A 1079 (2005) 221–228.

[12] Y. Xiao, A.S. Freed, T.T. Jones, K. Makrodimitris, J.P. O'Connell, E.J. Fernandez, Protein instability during HIC: Describing the effects of mobile phase conditions on instability and chromatographic retention, Biotechnol. Bioeng. 93 (2006) 1177–1189.

[13] R. Muca, W. Marek, W. Piatkowski, D. Antos, Influence of the sample-solvent on protein retention, mass transfer and unfolding kinetics in hydrophobic interaction chromatography, J. Chromatogr. A 1217 (2010) 2812–2820.

[14] W. Marek, W. Piatkowski, D. Antos, Multiple-injection technique for isolating a target protein from multicomponent mixtures, J. Chromatogr. A 1218 (2011) 5423–5433.

[15] L. Zhang, G. Zhao, Y. Sun, Molecular insight into protein conformational transition in hydrophobic charge induction chromatography: a molecular dynamics simulation, J. Phys. Chem. B 113 (2009) 6873–6880.

[16] A. Voitl, A. Butté, M. Morbidelli, Behavior of human serum albumin on strong cation exchange resins: I. Experimental analysis, J. Chromatogr. A 1217 (2010) 5484–5500.

[17] R. Gillespie, T. Nguyen, S. Macneil, L. Jones, S. Crampton, S. Vunnum, Cation exchange surface-mediated denaturation of an aglycosylated immunoglobulin (IgG1), J. Chromatogr. A 1251 (2012) 101–110.

[18] H. Luo, N. Macapagal, K. Newell, A. Man, A. Parupudi, Y. Li, Y. Li, Effects of salt-induced reversible self-association on the elution behavior of a monoclonal antibody in cation exchange chromatography, J. Chromatogr. A 1362 (2014) 186–193.

[19] H. Luo, M. Cao, K. Newell, C. Afdahl, J. Wang, W.K. Wang, Y. Li, Double-peak elution profile of a monoclonal antibody in cation exchange chromatography is caused by histidine-protonation-based charge variants, J. Chromatogr. A, 1424 (2015) 92–101.

[20] W. Marek, R. Muca, S. Wos, W. Piatkowski, D. Antos, Isolation of monoclonal antibody from a Chinese hamster ovary supernatant. II: Dynamics of the integrated separation on ion exchange and hydrophobic interaction chromatography media, J. Chromatogr. A 1305 (2013) 64–75.

[21] F. He, S. Hogan, R.F. Latypov, L.O. Narhi, V.I. Razinkov, High throughput thermostability screening of monoclonal antibody formulations, J. Pharm. Sci. 99 (2010) 1707–1720.

[22] D. Houde, J. Arndt, W. Domeier, S. Berkowitz, J.R. Engen, Characterization of IgG1 conformation and conformational dynamics by hydrogen/deuterium exchange mass spectrometry, Anal. Chem. 81 (2009) 2644–2651.

[23] A.M. Lenhoff, Protein adsorption and transport in polymer-functionalized ion-exchangers, J. Chromatogr. A 1218 (2011) 8748–8759.

[24] M.C. Stone, Y. Tao, G. Carta, Protein adsorption and transport in agarose and dextran-grafted agarose media for ion exchange chromatography: Effect of ionic strength and protein characteristics, J. Chromatogr. A 1216 (2009) 4465–4474.

[25] Y. Tao, G. Carta, G. Ferreira, D. Robbins, Adsorption of deamidated antibody variants on macroporous and dextran-grafted cation exchangers: I. Adsorption equilibrium, J. Chromatogr. A 1218 (2011) 1519–1529.

[26] E.X. Perez-Almodovar, Y. Tao, G. Carta, Protein adsorption and transport in cation exchangers with a rigid backbone matrix with and without polymeric surface extenders, Biotechnol. Progr. 27 (2011) 1264–1272.

[27] T.M. Pabst, D. Antos, G. Carta, N. Ramasubramanyan, A.K. Hunter, Protein separations with induced pH gradients using cation-exchange chromatographic columns containing weak acid groups, J. Chromatogr. A 1181 (2008) 83–94.

[28] T.M. Pabst, Ph.D. Dissertation, University of Virginia, Charlottesville, VA, 2008.

[29] K. Mattison, A. Morfesis, M. Kaszuba, A primer on particle sizing using dynamic light scattering, Am. Biotechnol. Lab. 21 (2003) 20–22.

[30] G. Carta, A.R. Ubiera, T.M. Pabst, Protein mass transfer kinetics in ion exchange media: Measurements and interpretations, Chem. Eng. Technol. 28 (2005) 1252–1264.

[31] Y. Tao, E.X. Pérez Almodóvar, G. Carta, G. Ferreira, D.D. Robbins, Adsorption kinetics of deamidated antibody variants on macroporous and dextran-grafted cation exchangers. III. Microscopic studies, J. Chromatogr. A 1218 (2011) 8027–8035.

[32] K. Ahrer, A. Buchacher, G. Iberer, D. Josic, A. Jungbauer, Analysis of aggregates of human immunoglobulin G using size-exclusion chromatography, static and dynamic light scattering, J. Chromatogr. A 1009 (2003) 89–96.

[33] R.K. Brummitt, D.P. Nesta, L. Chang, A.M. Kroetsch, C.J. Roberts, Nonnative aggregation of an IgG1 antibody in acidic conditions, Part 2: nucleation and growth kinetics with competing growth mechanisms, J. Pharm. Sci. 100 (2011) 2104–2119.

[34] E.X. Perez Almodovar, B. Glatz, G. Carta, Counterion effects on protein adsorption equilibrium and kinetics in polymer-grafted cation exchangers, J. Chromatogr. A 1253 (2012) 83–93.

[35] C.B. Andersen, M. Manno, C. Rischel, M. Thorolfsson, V. Martorana, Aggregation of a multidomain protein: A coagulation mechanism governs aggregation of a model IgG1 antibody under weak thermal stress, Protein Sci. 19 (2010) 279–290.

[36] J. Feder, T. Jossang, Scaling behavior and cluster fractal dimension determined by light-scattering from aggregating proteins, Phys. Rev. Lett. 53 (1984) 1403–1406.

[37] T. Jossang, J. Feder, E. Rosemqvist, Heat aggregation kinetics of human IgG, J. Chem. Phys. 82 (1985) 574–589.

[38] M.C. Stone, G. Carta, Protein adsorption and transport in agarose and dextran-grafted agarose media for ion exchange chromatography, J. Chromatogr. A 1146 (2007) 202–215.

[39] J.L. Fogle, J.P. O'Connell, E.J. Fernandez, Loading, stationary phase, and salt effects during hydrophobic interaction chromatography: alpha-lactalbumin is stabilized at high loadings, J. Chromatogr. A 1121 (2006) 209–218.

[40] E. Haimer, A. Tscheliessnig, R. Hahn, A. Jungbauer, Hydrophobic interaction chromatography of proteins IV. Kinetics of protein spreading, J. Chromatogr. A 1139 (2007) 84–94.

[41] I. Lundstrom, Model of protein adsorption on solid surfaces, Prog. Colloid Polym. Sci. 70 (1985) 76–82.

[42] J.T. McCue, P.A.Ng. Engel, R. Mcniven, J. Thömmes, Modeling of protein monomer/aggregate purification and separation using hydrophobic interaction chromatography, Bioprocess. Biosyst. Eng. 31 (2008) 261–275.

[43] H. Yang, M.R. Etzel, Evaluation of three kinetic equations in models of protein purification using ion-exchange membranes, Ind. Eng. Chem. Res. 42 (2003) 890–896.

[44] S.U. Sane, S.M. Cramer, T.M. Przybycien, Protein structure perturbations on chromatographic surfaces, J. Chromatogr. A 849 (1999) 149–159.

[45] M.C. Stone, G. Carta, Patterns of protein adsorption in chromatographic particles visualized by optical microscopy, J. Chromatogr. A 1160 (2007) 206–214.

[46] T.W. Weber, R.K. Chakravorti, Pore and solid diffusion models for fixed-bed adsorbers, AIChE J. 20 (1974) 228–238.

[47] A. Brock, Fragmentation hydrogen exchange mass spectrometry: A review of methodology and applications, Protein Expr. Purif. 84 (2012) 19–37.

[48] R.E. Iacob, J.R. Engen, Hydrogen exchange mass spectrometry: are we out of the quicksand? J. Am. Soc. Mass Spectrom. 23 (2012) 1003–1010.

[49] W. Burkitt, P. Domann, G. O'Connor, Conformational changes in oxidatively stressed monoclonal antibodies studied by hydrogen exchange mass spectrometry, Protein Sci. 19 (2010) 826–835.

[50] A. Zhang, S.K. Singh, M.R. Shirts, S. Kumar, E.J. Fernandez, Distinct aggregation mechanisms of monoclonal antibody under thermal and freeze-thaw stresses revealed by hydrogen exchange, Pharm. Res. 29 (2012) 236–250.

[51] R. Majumdar, P. Manikwar, J.M. Hickey, H.S. Samra, H.A. Sathish, S.M. Bishop, C.R. Middaugh, D.D. Weis, D.B. Volkin, Effects of salts from the hofmeister series on the conformational stability, aggregation propensity, and local flexibility of an igg1 monoclonal antibody, Biochemistry 52 (2013) 3376–3389.

[52] P. Manikwar, R. Majumdar, J.M. Hickey, S.V. Thakkar, H.S. Samra, H.A. Sathish, S.M. Bishop, C.R. Middaugh, D.D. Weis, D.B. Volkin, Correlating excipient effects on conformational and storage stability of an IgG1 monoclonal antibody with local dynamics as measured by hydrogen/deuterium-exchange mass spectrometry, J. Pharm. Sci. 102 (2013) 2136–2151.

[53] J.L. Fogle, E.J. Fernandez, Amide hydrogen-deuterium exchange: A fast tool for screening protein stabilities in chromatography, LC-GC North Am. 24 (2006) 96–101.

[54] T.T. Jones, E.J. Fernandez, alpha-Lactalbumin tertiary structure changes on hydrophobic interaction chromatography surfaces, J. Colloid Interface Sci. 259 (2003) 27–35.

[55] Y. Xiao, T.T. Jones, A.H. Laurent, J.P. O'Connell, T.M. Przybycien, E.J. Fernan- dez, Protein instability during HIC: Hydrogen exchange labeling analysis and a framework for describing mobile and stationary phase effects, Biotechnol. Bioeng. 96 (2007) 80–93.

[56] R.W. Deitcher, J.P. O'Connell, E.J. Fernandez, Changes in solvent exposure reveal the kinetics and equilibria of adsorbed protein unfolding in hydrophobic interaction chromatography, J. Chromatogr. A 1217 (2010) 5571–5583.

[57] A.M. Gospodarek, M.E. Smatlak, J.P. O'Connell, E.J. Fernandez, Protein stability and structure in HIC: hydrogen exchange experiments and COREX calculations, Langmuir 27 (2011) 286–295.

[58] Y. Bai, J.S. Milne, L. Mayne, S.W. Englander, Primary structure effects on peptide group hydrogen-exchange, Proteins 17 (1993) 75–86.

[59] L. Wang, H. Pan, D.L. Smith, Hydrogen Exchange-Mass Spectrometry: Optimization of Digestion Conditions, Mol. Cell. Proteomics 1 (2001) 132–138.

[60] R. Jefferis, J. Lund, M. Goodall, Recognition sites on human-IgG for Fc-gamma receptors - the role of glycosylation, Immunol. Lett. 44 (1995) 111–117.

[61] D. Ejima, K. Tsumoto, H. Fukada, R. Yumioka, K. Nagase, T. Arakawa, J.S. Philo, Effects of acid exposure on the conformation, stability, and aggregation of monoclonal antibodies, Prot. Struct. Func. Bioinf. 66 (2007) 954–962.

[62] J. Buchner, M. Renner, H. Lilie, H.J. Hinz, R. Jaenicke, T. Kiefhabel, R. Rudolph, Alternatively folded states of an immunoglobulin, Biochem. 30 (1991) 6922–6929.

[63] A.W.P. Vermeer, W. Norde, The thermal stability of immunoglobulin: Unfolding and aggregation of a multi-domain protein, Biophys. J. 78 (2000) 394–404.

[64] D. Ejima, R. Yumioka, K. Tsumoto, T. Arakawa, Effective elution of antibodies by arginine and arginine derivatives in affinity column chromatography, Anal. Biochem. 345 (2005) 250–257.

[65] T. Arakawa, K. Tsumoto, K. Nagase, D. Ejima, The effects of arginine on protein binding and elution in hydrophobic interaction and ion-exchange chromatography, Protein Expr. Purif. 54 (2007) 110–116.

[66] A. Hirano, T. Arakawa, T. Kameda, Interaction of arginine with Capto MMC in multimodal chromatography, J. Chromatogr. A 1338 (2014) 58–66.

[67] T. Arakawa, D. Ejima, K. Tsumoto, N. Obeyama, Y. Tanaka, Y. Kita, S.N. Timasheff, Suppression of protein interactions by arginine: a proposed mechanism of the arginine effects, Biophys. Chem. 127 (2007) 1–8.

[68] U. Das, G. Hariprasad, A.S. Ethayathulla, P. Manral, T.K. Das, S. Pasha, A. Mann, M. Ganguli, A.K. Verma, R. Bhat, S.K. Chandrayan, S. Ahmed, S. Sharma, P. Kaur, T.P. Singh, A. Srinivasan, Inhibition of protein aggregation: supramolecular assemblies of arginine hold the key, PLoS One 2 (2007) e1176.

[69] A.M. Gospodarek, D.E. Hiser, J.P. O'Connell, E.J. Fernandez, Unfolding of a model protein on ion exchange and mixed mode chromatography surfaces, J. Chromatogr. A 1355 (2014) 238–252.

[70] S.M. Kelly, T.J. Jess, N.C. Price, How to study proteins by circular dichroism, Biochim. Biophys. Acta 1751 (2005) 119–139.

[71] N. Harn, C. Allan, C. Oliver, C.R. Middaugh, Highly Concentrated Monoclonal Antibody Solutions: Direct Analysis of Physical Structure and Thermal Stability, J. Pharm. Sci. 96 (2007) 532–546.

[72] T. Wang, O.S. Kumru, L.I. Yi, Y.J. Wang, J. Zhang, J.A.E.H. Kim, S.B. Joshi, C.R. Middaugh, D.B. Volkin, Effect of Ionic Strength and pH on the Physical and Chemical Stability of a Monoclonal Antibody Antigen-Binding Fragment, J. Pharm. Sci. 102 (2013) 2520–2537.

[73] Y. Wu, J. Simons, S. Hooson, D. Abraham, G. Carta, Protein and virus-like particle adsorption on perfusion chromatography media, J. Chromatogr. A 1297 (2013) 96–105.

[74] J. Guo, S. Zhang, G. Carta, Unfolding and aggregation of a glycosylated monoclonal antibody on a cation exchange column Part I Chromatographic elution and batch adsorption behavior, J. Chromatogr. A 1356 (2014) 117–128.

[75] J. Guo, G. Carta, Unfolding and aggregation of a glycosylated monoclonal antibody on a cation exchange column Part II Protein structure effects by hydrogen deuterium exchange mass spectrometry, J. Chromatogr. A 1356 (2014) 129–137.

[76] M. Urmann, H. Graalfs, M. Joehnck, L.R. Jacob, C. Frech, Characterization of a novel stationary phase designed for production-scale purification Cation-exchange chromatography of monoclonal antibodies, Landes Bioscience mAbs 2 (2010) 395–404.

[77] E.X. Perez-Almodovar, Y. Wu, G. Carta, Multicomponent adsorption of monoclonal antibodies on macroporous and polymer grafted cation exchangers, J. Chromatogr. A 1264 (2012) 48–56.

[78] T.M. Pabst, E.J. Suda, K.E. Thomas, P. Mensah, N. Ramasubramanyan, M.E. Gustafson, A.K. Hunter, Binding and elution behavior of proteins on strong cation exchangers, J. Chromatogr. A 1216 (2009) 7950-7956.

[79] J. Guo, G. Carta, Unfolding and aggregation of monoclonal antibodies on cation exchange columns: Effects of resin type, load buffer, and protein stability, J. Chromatogr. A, 1388 (2015) 184–194.

[80] J.M. Reck. T.M. Pabst, A.K. Hunter, G. Carta, Adsorption equilibrium and kinetics of monomer-dimer monoclonal antibody mixtures on a cation exchange resin, J. Chromatogr. A, 1402 (2015) 46-59.

[81] POROS Strong Cation Exchange Resins: XS and HS 50, Applied Biosystems, Publication No. 100031321, 2015.

[82] N. Afeyan, N.F. Gordon, I. Mazsaroff, L. Varady, S.P. Fulton, Y.B. Yang, F.E. Regnier, Flow-through particles for the high-performance liquid chromatographic separation of biomolecules: perfusion chromatography, J. Chromatogr. A 519 (1990) 1-29.

[83] Yamamoto, S., Nakanishi, K., Mastuno, R., Ion exchange chromatography of proteins. Dekker, New York, NY 1988.

[84] G. Carta, A. Jungbauer, Protein Chromatography – Process Development and Design, Wiley-VCH, 2010.

[85] D.A. Barrett, G.M. Power, M.A. Hussain, I.D. Pitfield, P.N. Shaw, M.C. Davies, Protein interactions with model chromatographic stationary phases constructed using self-assembled monolayers, J. Sep. Sci., 28 (2005) 483–491.

[86] C.C. Lee, J.M. Perchiacca, P.M. Tessier, Toward aggregation-resistant antibodies by design, Trends Biotechnol., 31 (2013) 612–620.

[87] N. Chennamsetty, V. Voynov, V. Kayser, B. Helk, B.L. Trout, Design of therapeutic proteins with enhanced stability, PNAS, 106 (2009) 11937–11942.

[88] S. Zhang, K. Xu, W. Daniels, J. Salm, J. Glynn, J. Martin, C. Gallo, R. Godavarti, G. Carta, Structural and functional characteristics of virgin and fouled protein A MabSelect resin cycled in a monoclonal antibody purification process, Biotechnol. Bioeng., 113 (2015) 367–375.

[89] S. Zhang, W. Daniels, J. Salm, J. Glynn, J. Martin, C. Gallo, R. Godavarti, G. Carta, Nature of foulants and fouling mechanism in the Protein A MabSelect resin cycled in a monoclonal antibody purification process, Biotechnol. Bioeng., 113 (2016) 141–149.

[90] P. Gagnon, R. Nian, D. Leong, A. Hoi, Transient conformational modification of immunoglobulin G during purification by protein A affinity chromatography, J. Chromatogr. A, 1395 (2015) 136–142.

[91] P. Gagnon, R. Nian, Y. Yang, Q. Yang, C.L. Lim, Non-immunospecific association of immunoglobulin G with chromatin during elution from protein A inflates host contamination, aggregate content, and antibody loss, J. Chromatogr. A, 1408 (2015) 151–160.